4

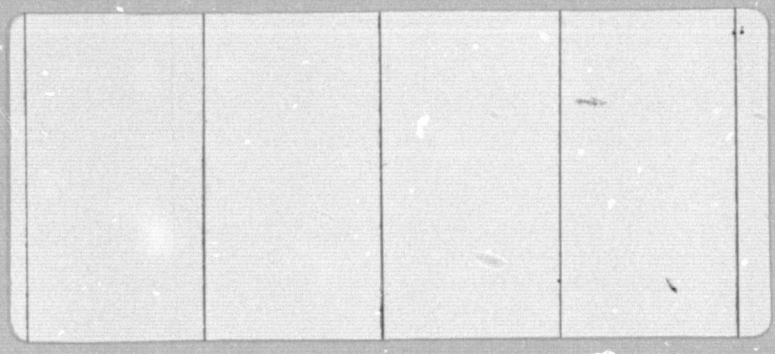

NAVAL
RESEARCH
LABORATORY

WASHINGTON, D.C.

FINAL REPORT ON

SKYLAB ALTIMETER OBSERVATIONS

OVER TERRAIN

September 1975

Principal Investigator
A. Shapiro

Co-Investigators
J. Thormodsgard and J. Okada

NASA/JSC Technical Monitor
L. York TF6

The research reported in this document was sponsored by the National Aeronautics and Space Administration, Lyndon B. Johnson Space Center, Houston, Texas 77058, under contract T-4716B, EPN 363

Space Science Division
Naval Research Laboratory
Washington, D. C. 20375

Unclassified
SECURITY CLASSIFICATION OF THIS PAGE *(When Data Entered)*

REPORT DOCUMENTATION PAGE		READ INSTRUCTIONS BEFORE COMPLETING FORM
1. REPORT NUMBER	2. GOVT ACCESSION NO.	3. RECIPIENT'S CATALOG NUMBER
4. TITLE *(and Subtitle)* Skylab Altimeter Observations Over Terrain		5. TYPE OF REPORT & PERIOD COVERED FINAL Report
		6. PERFORMING ORG. REPORT NUMBER
7. AUTHOR(s) Allan Shapiro, June M. Thormodsgard, and J. M. Okada		8. CONTRACT OR GRANT NUMBER(s) T-4716B, EPN 363
9. PERFORMING ORGANIZATION NAME AND ADDRESS Naval Research Laboratory Washington, D. C. 20375		10. PROGRAM ELEMENT, PROJECT, TASK AREA & WORK UNIT NUMBERS 71G01-13
11. CONTROLLING OFFICE NAME AND ADDRESS National Aeronautics and Space Adminstration L. B. Johnson Space Center Houston, Texas 77058		12. REPORT DATE September 1975
		13. NUMBER OF PAGES 156
14. MONITORING AGENCY NAME & ADDRESS*(if different from Controlling Office)*		15. SECURITY CLASS. *(of this report)* Unclassified
		15a. DECLASSIFICATION/DOWNGRADING SCHEDULE

16. DISTRIBUTION STATEMENT *(of this Report)*
General

17. DISTRIBUTION STATEMENT *(of the abstract entered in Block 20, if different from Report)*

18. SUPPLEMENTARY NOTES

19. KEY WORDS *(Continue on reverse side if necessary and identify by block number)*
Skylab
Radar
Altimeter
Radar Altimetry
Topography

20. ABSTRACT *(Continue on reverse side if necessary and identify by block number)*

Data obtained by the Skylab radar altimeter (S-193) over the Continental USA for Pass 1 of SL-2 and Passes 16, 17, 18, and 28 of SL-3 were analyzed by the Naval Research Laboratory to relate radar return signal parameters such as range, power, and waveform to ground track terrain features. The altimeter, which was originally designed for ocean observations, performed predictably well over terrain with moderate to low relief. The

DD FORM 1 JAN 73 1473 EDITION OF 1 NOV 65 IS OBSOLETE
S/N 0102-014-6601

Unclassified
SECURITY CLASSIFICATION OF THIS PAGE *(When Data Entered)*

maximum radar return from more complex areas corresponded usually to the lower flatter regions within the 7-kilometer diameter footprint.

The altimeter-measured heights correlated with map topography with an rms deviation of ±30 meters for terrain topography with large height dispersion (Passes 1 and 28) and ±5 meters for slowly varying terrain (Passes 16, 17, and 18). The received power varied with specific terrain features and it ranged from a radar cross-section of 100 dB-above-one-square-meter (dBsm) for the Utah Salt Flats to 60 dBsm for mountains with forests. The ocean radar cross-section was located approximately at the mid-point of these extremes (80 dBsm).

The analysis of the waveform and statistical characteristics of the individual signals indicated that larger signal power was usually related to dominantly specular reflections from patches 100 meters or larger.

The results established the capability of a spacecraft altimeter system to observe characteristic radar signatures for different types of terrain within the bandwidth restrictions of the AGC and range-tracker loops. Improved reliability of operation and more complete height information on complex regions can be attained by a dedicated altimeter system with extended dynamic range in both power and altitude.

ACKNOWLEDGMENTS

The author would like to thank B. Yaplee of NRL for the initial suggestion of utilizing the Skylab altimeter over terrain. He also expresses his appreciation to L. York of NASA-Johnson Space Center, who helped to obtain the various data sources, J. McGoogan and C. Leitao of NASA-Wallops Flight Center who provided the improved Skylab ephemeris, and A. Uliana and D. Hammond of NRL for helpful discussions on special programming problems and altimeter concept.

ABSTRACT

Data obtained by the Skylab radar altimeter (S-193) over the Continental USA for Pass 1 of SL-2 and Passes 16, 17, 18, and 28 of SL-3 were analyzed by the Naval Research Laboratory to relate radar return signal parameters such as range, power, and waveform to ground track terrain features. The altimeter, which was originally designed for ocean observations, performed predictably well over terrain with moderate to low relief. The maximum radar return from more complex areas corresponded usually to the lower flatter regions within the 7-kilometer diameter footprint.

The altimeter-measured heights correlated with map topography with an rms deviation of ±30 meters for terrain topography with large height dispersion (Passes 1 and 28) and ±5 meters for slowly varying terrain (Passes 16, 17, and 18). The received power varied with specific terrain features and it ranged from a radar cross-section of 100 dB-above-one-square-meter (dBsm) for the Utah Salt Flats to 60 dBsm for mountains with forests. The ocean radar cross-section was located approximately at the mid-point of these extremes (80 dBsm).

The analysis of the waveform and statistical characteristics of the individual signals indicated that larger signal power was usually related to dominantly specular reflections from patches 100 meters or larger.

The results established the capability of a spacecraft altimeter system to observe characteristic radar signatures for different types of terrain within the bandwidth restrictions of the AGC and range-tracker loops. Improved reliability of operation and more complete height information on complex regions can be attained by a dedicated altimeter system with extended dynamic range in both power and altitude.

SLYLAB ALTIMETER OBERVATIONS OVER TERRAIN

TABLE OF CONTENTS

LIST OF ILLUSTRATIONS

LIST OF TABLES

SKYLAB ALTIMETER OBSERVATIONS OVER TERRAIN

INTRODUCTION

The narrow-pulse radar altimeter of the Skylab EREP package (S-193) was operated over land areas to determine from satellite heights the radar reflection characteristics of the terrain at nadir, and to evaluate the ability of a satellite radar altimeter to sense the topographic and physical properties of terrain reflecting surfaces. Observations were made over different types of terrain of the continental USA and the range, received power, waveform, and statistical properties of the radar return signal as a function of the sub-satellite area were analyzed. Although the skylab altimeter was originally designed to operate over the ocean surface where relatively homogeneous reflection conditions prevail, it performed predictably well over terrain with moderate to low relief, with range-tracker loss only over land areas with large variations and complex reflection properties.

In this report are described pertinent technical parameters of the Skylab (S-193) radar altimeter system and its operational modes, which determine the types and the character of the data obtained (Section 1), the data processing and analysis undertaken at the Naval Research Laboratory (Section 2), error analysis (Section 3), the results of and the conclusions drawn from the data analysis (Sections 4 and 5), and consideration of parameters for a

dedicated radar altimeter system with improved response and data handling capability (Section 5).

1. ALTIMETER DESIGN AND OPERATION

In this section are given the basic engineering parameters of the Skylab (S-193) radar altimeter system, the general operational geometry of radar altimetry, the details of operation of the automatic gain control (AGC), the range acquisition, the range tracker, and the sample-and-hold (S&H) gate wave-sampling subsystems of the altimeter, and also information concerning the pre-programmed format used for data acquisition and calibration. Emphasized are the design and operational capabilities and some of the limitations of the altimeter to determine land relief and associated terrain features suitable for cartographic applications.

1.1 Geometry of Terrain Observations

The basic Skylab altimeter system parameters are given in Table 1. These parameters determine the operating geometry shown in Figures 1 and 2. Two basically different types of terrain can be considered, each with its characteristic radar signal return. In Figure 1, a flat area is assumed and the resulting radar return may consist of either a specular or diffuse reflection or a combination of both. If the diffuse reflection is dominant, the return will be similar to that obtained from the ocean, as shown in the lower right. In this case, the mean radar return consists of a rise-time of about 100 ns, corresponding to the 100-ns transmitted pulse, and a trailing edge of about 500 ns produced by the antenna drop-off as the incident angle increases. The radar illuminated footprint in the first 100 ns is of the order of 7 km and will increase to about 10 km in the trailing edge. For specular reflection, the radar return waveform is approximately the same as that of

TABLE 1

NOMINAL SKYLAB ALTIMETER SYSTEM PARAMETERS
FOR TERRAIN OBSERVATIONS

Transmitter	
TWT Power Output	2 kW
Frequency	13.9 GHz
Pulse Width	100 ns
Pulse Repetition Frequency	250 pps
Antenna	
Paraboloid Diameter	1.12 m
Aperture Efficiency	50%
Gain (λ = 2.16 cm)	41.3 dB
3 dB beamwidth	1.6° (measured)
Receiver	
Pre-Amplifier (Tunnel Diode)	33 dB
IF Center Frequency	350 MHz
Bandwidth	10 and 100 MHz
Derived Radar Footprint Diameter for Skylab Height (4.3×10^5m)	
Specular Return	100 m
Pulse Width	7.3 km
Beamwidth (3 dB)	8.5 km

the transmitted pulse as shown in the upper right of Figure 2. The reflecting area in this case may correspond to the maximum area that allows a phase coherent return, and which, at the satellite height and the RF wavelength used by the radar, has a diameter of the order of 100 m. In general, the radar return will be composed of both diffuse and specular reflections. If more than one smooth area within the radar footprint contributes to specular reflection, a fluctuating signal with a pulse shape similar to that of the transmitted pulse is produced.

In mountainous regions where the vertical height structure of the observed terrain may extend over several hundred meters within the footprint, the waveform of the radar return may appear as shown in Figure 2. Specular reflection may be present at different heights in a rough area such that return delay times from such reflections will extend over several microseconds and will also vary due to different scattering characteristics. It will be shown later that the AGC operation of the altimeter system will favor the larger signals for range lock operation, and that only a small portion (250 ns) of the return is utilized for the radar output measurements. In mountainous regions the spot size will be limited by the antenna beamwidth rather than by the pulse width and it will thus be of the order of 10 km.

1.2 Basic Skylab Altimeter Operation

The Skylab radar altimeter is designed to measure the amplitude and range of a received signal with high precision. The basic signal operations performed by the receiver system, shown in Figure 3, include the following functions:

1. Automatic gain control (AGC) of the receiver,
2. Range acquisition,

3. Determination and tracking of range by the range tracker,

4. Reproduction of a portion of the received waveform by eight 25-ns sample-and-hold (S&H) gates.

The dynamic range of the detector is about 6 dB, and since the dynamic range of the received signal is expected to be considerably larger, the AGC establishes the proper power level at the detector so that the other three functions can be performed with a signal level that is within the linear range of the detector. The acquisition process narrows the range uncertainty so that the range tracker is able to lock and track within a small time delay region of the radar return. Once range lock is verified, the AGC gate is matched to the expected received waveform, the S&H gates are positioned in a fixed time sequence relative to the range reference output of the range tracker, and the system initiates the pre-programmed sequence of data acquisition. The data outputs of the altimeter are recorded at fixed time intervals and include the AGC (received power), the time delay of the transmitted radar pulse (range), and the eight S&H gated amplitudes (waveform and statistical amplitude fluctuations).

The signal processing characteristics are summarized in Table 2 and will be considered in more detail in the following sections.

1.3 AGC Operations

The automatic-gain-control (AGC) circuit senses the power level of the radar return signal within a pre-positioned time gate in which the signal is expected, and it then utilizes the mean of 64 peak signal amplitudes to control the gain of the receiver. Before acquisition an 800-microsecond wide sampling gate and following acquisition and

TABLE 2

SIGNAL PROCESSING SYSTEM PARAMETERS

AGC

Acquisition Window	800 μs
Tracking Window	600 ns
Closed Loop Time Constant	.2 sec
Dynamic Range	45 dB
AGC Output	Peak of 64 pulse average
AGC Granularity	.1 dB
Steady State Tracking Error	1/2 dB

Altitude Tracking Loop

Type	Digital, 200 MHz logic
Loop Bandwidth	2 Hz
Altitude Output	32 pulse average
Altitude Granularity	2.5 ns

Waveform Sampling

Number of S&H Gates	8
Sampling Gate Width	25 ns
Gate Spacing	25 ns

during tracking a 600-nanosecond wide gate positioned at the tracked range are used to gate the return signal for the AGC.

To allow for the normalized cross-section σ_o of different sea states, the height variations of the spacecraft, attitude changes, and different altimeter mode operations, a large dynamic range for the AGC is provided as shown in Figure 4, which extends from about -10 dBm to -60 dBm. The noise threshold, which is also shown, is approximately -50 dBm for the 100 MHz receiver bandwidth sub-mode and -60 dBm for the 10 MHz sub-mode.

The large dynamic range of about 50 dB permits the altimeter to operate over a variety of terrain. However, since the relatively rapid changes in received power level encountered in observations over solid terrain are attenuated by the AGC smoothing filter, which was designed for the gradual changes in ocean reflections, rapid changes in received power will cause loss of range lock, as well as reduce the acquisition capability of the altimeter.

1.4 Range Acquisition

Range acquisition is achieved by performing two threshold decisions respectively in (1) the coarse-search mode and (2) the fine-search mode. A graphic description of the two search modes is given in Figure 5. In the coarse-search, a one-microsecond gate scans in 320-ns steps at a rate of 4 ms/step for an interval of 82 microseconds (12,300 m) which is centered about an a priori estimated time delay T_o. The received signal from the sub-satellite area, which is shown to the left of the estimated arrival time, is nominally a non-symmetrical pulse with about a 100-ns rise-time and a 500-ns trailing edge. Since the maximum rate of change in the delay time of the received

signal, due to orbital vertical motion and ocean surface deviations from a sphere, is of the order of a few nanoseconds per 4 ms, the received signal is essentially frozen relative to the 320-ns shifts of the one-microsecond gate. Thus, as the search gate scans across the signal, there are at least 2 to 3 gates that will contain the received signal. When the signal is detected more than once, as indicated by a threshold decision, the acquisition process switches to the fine-search mode. This mode uses a 200-ns gate in 50-ns shifts at the 4-ms/step rate, which scans a 3.2-microsecond time interval that is centered at the detected coarse-search time delay. The same decision threshold process is repeated and when the signal is located more than once in the fine-search mode, the range tracker operation is initiated. If the signal is missed in the acquisition process, the operation reverts back to the coarse-search mode and the scan is repeated. The maximum time of acquisition, assuming no miss, is 1.04 seconds in the coarse-search mode, 0.256 seconds in the fine-search mode, and about 0.5 seconds for range verification for a total of 1.8 seconds.

The acquisition process over the ocean is based on the assumption that the received signal has a unique and narrow pulse shape, constant mean power, and is located at an approximately fixed time delay inside the a priori time delay uncertainty. The acquisition process over terrain may be considerably altered because:

1. the pulse shape will, in general, be extended in time and vary with different types of reflection characteristics and terrain topography,
2. the mean power may change relatively rapidly at different portions of the return, and

3. the location of the ramp portion of the return, on which the acquisition system operates, may shift rapidly during the time of detection.

A possible radar return from a mountainous area is shown in Figure 2. Acquisition here is possible at several points where the signal amplitude increases over a few hundred nanoseconds. However, the earlier larger signals are favored because the AGC is controlled by the peak amplitude of the return and the scan is from left to right. Thus, several possibilities exist which could prevent efficient range acquisition. For example:

1. The coarse-search may detect a signal at an early point in time that does not coincide with the peak signal detected by the AGC. The fine-search may not be able to detect the signal at the same location with AGC loop control overly reducing appropriate receiver gain, or on the other hand, the fine-search can detect the signal but during pull-in the range tracker is not able to lock in because of the small available signal. In either case, the acquisition reverts to the coarse-search mode and a new attempt is made to locate a signal ramp.

2. The coarse-search may detect a signal that is the peak signal, but the mean amplitude of the signal may decrease rapidly due to variations in the reflection mechanism. The slowly responding AGC is not able to follow the drop in the signal level and neither the fine-search nor range tracker will be able to locate the signal.

3. The coarse-search detects a signal as in paragraph 2 above, but the signal moves rapidly in range in

a direction opposite to that of the scanning operation. Again either the fine-search will miss the signal location or the range tracker will not be able to follow the rapid range change.

Any combination of the above conditions may increase the acquisition time and thus, it is not surprising that in areas of complex relief, acquisition times of the order of 10 seconds or more actually occur. For some extremely complex terrain, the signal is not acquired at all.

1.5 Range Tracker Operation

Once range acquisition is achieved, the three main operations of the receiver system, namely, AGC, range tracking, and S&H gate sampling, are performed on a few hundred nanosecond segments of the acquired signal. Thus, for complex topographic terrain observations, the receiver system ignores any radar return whose time delay falls outside the narrow time interval for range tracker processing. The range tracker operation is controlled by three 100-nanosecond gates, as shown in Figure 6. The noise gate is placed 150 ns before the expected ramp of the radar return, and the plateau gate is placed 50-ns after the ramp gate. The range is tracked in a feedback loop that utilizes in a split gate configuration the difference between the amplitude of the ramp and 1/2 the amplitude of the plateau gate to establish the position of the radar return relative to the position of the split gates as shown in Figure 7. This voltage difference is applied to the time discriminator control curve in the feedback loop, which shifts the split gates to a position that minimizes the output voltage. Since the radar return is both pulse and beamwidth limited as indicated by the return pulse wave shape in Figure 7, the null of the time discriminator curve does not occur at the origin.

For terrain observations, range tracker operation may be modified and complicated by several factors. First, loss of range verification may be produced by energy in the noise gate reflected from higher elevations. Second, the waveform of the radar return, because of the different reflection mechanisms that may be encountered, may be considerably different from that assumed for ocean returns. This will introduce both an error in the range measurements as well as affect the range tracking capability. Finally, rapid changes in amplitude or range of the sampled radar return that cannot be followed by the AGC or range tracker loops respectively will cause either marginal operation or loss of range lock.

1.6 S&H Gate Operation

Portions of the radar return waveform used in the split gate configuration are sampled by eight 25-ns contiguous gates that are shifted at about 20-second intervals across the nominal noise, ramp, and plateau regions to cover 600-ns of the waveform shape, as shown in Figure 6. The gate outputs, recorded at a rate of 100 amplitudes per second, can be used to study the statistical characteristics of the radar return as a function of time delay, assuming a range jitter of less than 25 ns.

Over terrain, it is not possible, in general, to obtain the complete waveform of the received signal, since the waveform may extend over several microseconds. In addition, the noise, ramp and plateau portions of the waveform cannot be combined, since the terrain and reflection characteristics of the observed areas may change considerably during the one-minute interval required to sample the 600-ns portion of the received waveform. However, an estimate of a small segment of the waveform can be made over uniform

terrain by combining the noise-and-ramp, or ramp-and-plateau portions of the waveform when the position of the sampling gates changes. This changeover occurs three times in each run, as will be shown in the next section.

1.7 Pre-Programmed Sequence of Data Acquisition

The altimeter measurements are grouped in a sequence of frames, with each frame containing data for a 1.04-second interval, corresponding to 7.5 kilometers of ground track distance or covering an extended footprint area roughly 7.5 x 15 kilometers. The sub-satellite area is probed with a 100-ns pulse 256 times during each frame and the radar system processes the received signals to produce 4 AGC outputs, 8 range outputs and 104 amplitude outputs for each of the 8 S&H gates.

The programmed sequence for mode 1, which was exclusively used for terrain observations, is shown in Table 3. The mode is divided into six sub-modes (SM). The first three sub-modes are used for data acquisition with the first sub-mode operating with a 10-MHz receiver bandwidth, the second sub-mode using a 100-MHz bandwidth and the antenna being tilted by about 0.5° in pitch angle in the final sub-mode. The length of each sub-mode in terms of number of frames and actual time duration is also given.

In the second set of three sub-modes, the conditions of the first two sub-modes are simulated, and the transmitted pulse shape, transmitted power and internal system delay are calibrated. The total run time for mode 1 is about 3.5 minutes.

Each of the data acquisition sub-modes is further divided into three sub-sub-modes (SSM) to shift the time position of the S&H gates across the noise, ramp, and

plateau regions of the received waveform. These shifts occur, as indicated in Table 3, at about 15 or 20 second intervals, which correspond to 112 and 149 kilometers of ground track distance respectively. Geographic areas covered in the different sub-modes are listed in Tables A-1 through A-5 in the Appendix.

For runs over complex terrain where frequent range tracker loss occurred not all sub-modes were activated. In general, sub-modes 1 and 2 were completed but the correct number of available data points was not obtained, due to improper operation of the frame counter.

TABLE 3

MODE 1 PRE-PROGRAMMED SEQUENCE

SM	Antenna Pointing	BW	Signal Processing	Number of Frames[a]	Running Time (sec)	Data Mode
0	Sub-Sat	10 MHz	Range Tracker	15, 15, 15,[b]	46.8	DAS
1	Sub-Sat	100 MHz	Range Tracker	20, 20, 20,[b]	62.4	DAS
2	1/2° pitch	100 MHz	Range Tracker	20, 20, 20,[b]	62.4	DAS
3	NA	100 MHz	Alt. Counter	3, 2	5.2	CDS
4	NA	10 MHz	Alt. Counter	2, 2	4.16	CDS
5	NA	10 MHz	Range Tracker	2, 2	4.16	CDS
TOTAL				178	185.12	

Note: [a]15 frames = 15.6 sec. = 112 Kms groundtrack distance.
20 frames = 20.8 sec. = 149 Kms groundtrack distance.

[b]15- or 20-frame series represent three sub-sub-modes (SSM), where S&H gates are positioned sequentially at noise, ramp, and plateau sections of signal.

2. DATA FLOW, REDUCTION, AND ANALYSIS

In this section are outlined the overall organization of Skylab altimeter data flow, and the methods of data reduction and analyses applied to these data at NRL to evaluate altimeter performance and capabilities. The analysis is basically a comparison of reduced altimeter data and ground truth, the latter mainly pertinent topographic information from 1:250,000 scale maps (AMS edition), supplemented by some Skylab photography and weather data. Appropriate references are made to detailed descriptions and discussions of typical cases appearing later in Sections 4 and 5.

2.1 Overall Data Flow

The overall data flow from Skylab altimeter output to NRL is shown in Figure 8. The altimeter output was recorded in the spacecraft in Pulse Code Modulation (PCM) counts on raw data tape. The format of the altimeter output on the raw data tape was prescribed for a data frame, covering 1.04 seconds in spacecraft time, 7.5 kilometers in ground track distance, or a footprint area roughly 7.5 by 15 kilometers, with 1,040 ten-bit words read out at a rate of 10 kilobits/sec, giving frame time, four AGC values, eight range delay times, 104 sets of eight S&H gate outputs, averaged noise, ramp, and plateau gate outputs and associated housekeeping data. Details of this format are available in reference 1.

The raw data tape was brought back after each Skylab mission to the Johnson Space Center (JSC) where all data, except the S&H gate outputs, were converted to engineering units. In addition, the Airlock Module Time (AMT) was converted to GMT, and the spacecraft position and height were computed from the Skybet Orbit Program. The modified

data stream was recorded on pre-processed tape in computer compatible format and transmitted to NRL with a header record which contained the required algorithms for read out of altimeter data. The data format for the pre-processed tape is given in references 2 and 3.

The altimeter data on the pre-processed tape was further processed at NRL, where a geodyne orbit was used to refine spacecraft position and to convert altimeter range measurements to ground heights. The results were then compared with Skylab photography and ground truth data.

2.2 Data Reduction

The scheme of data reduction and analysis performed at NRL on the pre-processed tape is shown in Figure 9. The data reduction consisted of a primary evaluation of the data on the pre-processed tape, followed by the application of corrections and time tags to AGC and ALT data, and finally the conversion of ALT to ground height.

2.2.1 Primary Evaluation

The following data were read out directly for each frame from the pre-processed tape for primary evaluation of data and cross indexing of frame number and spacecraft location:

1. Frame or data block number
2. Operating mode, sub-mode (SM) and sub-sub-mode (SSM)
3. Frame counter
4. Altimeter lock status
5. Average altitude for each frame
6. Standard deviation of altitude within frame

7. Residual height relative to Skybet height estimate

8. Average AGC for given frame

9, 10,11. Average noise, ramp, and plateau gate outputs for given frame

12. Frame time (GMT)

13, 14. Longitude and latitude of sub-satellite position from Skybet orbit.

The first criterion to be met was a check of range tracker lock. Because of the complex reflection characteristics of the terrain, three separate conditions had to be satisfied simultaneously before range lock was considered acceptable.

1. The altimeter lock status word was present (digit 0)

2. The ratio of ramp-to-noise gate output was larger than two.

3. The difference between adjacent range readings did not exceed 500 m.

In addition, estimates of the quality of data could be obtained from the AGC values and changes in the standard deviation of the altitude readings. All data satisfying these range lock conditions were then subjected to further corrections, analysis, and evaluation.

2.2.2 Altitude Corrections

Each altitude value was corrected for the following:

1. A 40-ns delay introduced by JSC during conversion to engineering units

2. The instrument system delay

3. A decrease in bandwidth delay for the 100-MHz sub-mode

4. The propagation delay in the atmosphere.

For SL-3 and SL-4 data, the corrections for the 40-ns delay and the instrument system delay were already made by JSC on the pre-processed tape, and only the two remaining corrections had to be applied. The instrument system and bandwidth delay times were derived from pre-flight and in-flight calibration.

The instrument delay was derived in the following manner:

In-flight calibration system delay (Mode 1, SM5 (CDS 3), 10 MHz bandwidth)	2,624,085 ns
Pre-flight calibration (digital delay generator offset, 10 MHz bandwidth) (reference 4)	2,624,000 ns
System delay in calibration mode (10 MHz)	+85 ns
Antenna hardware delay (reference 4)	10 ns
Correction for Data Acquisition (triangular Pulse) minus calibration mode (square pulse)	85 ns
Total system delay (10 MHz bandwidth)	180 ns
Pre-flight calibration correction for 100 MHz bandwidth (SM 2) (reference 4)	-90 ns
Total system delay (100 MHz)	90 ns

For SL-2, the 40-ns delay introduced by JSC was added to produce a total delay correction of 220 ns for the 10 MHz sub-mode.

Finally, an atmospheric correction of 17 ns (Reference 8) was applied to account for the mean delay of the signal through the troposphere and ionosphere. Thus the basic range corrections applied to the measured value t_m are given by

$$t_c = t_m - t_{id} - t_{bias} - t_{atm} + t(100\ \text{MHz})$$

where

t_{id} = 180 ns (system delay at 10 MHz)

t_{bias} = 40 ns (bias introduced by JSC)

t_{atm} = 17 ns (atmospheric correction)

and

$t(100\ \text{MHz}) = 90$ ns.

The net effective corrections applied to the measured time delay in SL-2, 3, and 4 are summarized in Table 4.

TABLE 4

EFFECTIVE TIME DELAY CORRECTIONS AT NRL

	10 MHz	100 MHz
SL-2	-237 ns	-147 ns
SL-3,4	-17 ns	73 ns

2.2.3 Time Tag of Output Data

A unique time tag for each altitude and AGC measurement cannot be defined, since each altitude and AGC value depends on the non-uniform weighting of past values by the range tracker and the AGC loops, and also on the input characteristics of the signal. It is possible however, to estimate the time of each measurement from the known time

characteristics of the range tracker and AGC processing loops. If a uniform input signal and uniform weighting are assumed, a unique measurement time, which on the average will correspond to the true measurement time of each output value, is obtained.

Range Time Tags

The nominal measurement times of the eight altitude readings in each frame relative to frame time are listed in Table 5 (reference 5).

TABLE 5

TIME TAG FOR RANGE MEASUREMENTS RELATIVE TO FRAME TIME (FT)

Altitude Position in Frame	Time of Readout Relative to FT in ms	Measurement Time Relative to FT in ms	Time Separation in ms	Averaging Time for each altitude in ms
1	66	-80	146	128
2	192.5	66	126.5	125
3	320.5	192.5	128	128
4	448.5	320.5	128	128
5	576	448.5	127.5	128
6	704.5	576	128.5	127
7	832.5	704.5	128	129
8	960	832.5	127.5	128

The table also gives the time of readout for each altitude, the time separation between sampled altitudes, and the time interval over which each altitude output is averaged. It is seen that the altitudes are not read uniformly and that there is an interval of 19 ms near the beginning of each frame where altitude is not measured. The interval in which

32 range-tracker-processed altitude measurements are averaged is about 128 ms in time or 919 m in ground track distance.

Based on the time distribution shown in Table 5, the time tag for the averaged altitude for each frame is given by

$$t_{av\ alt/frame} = FT + 383\ ms\ .$$

AGC Time Tag

Similar time tags can be assigned to the AGC measurements. Using the AGC loop time-constant of 200 ms, the AGC measurement times are advanced by 200 ms as shown in Table 6.

TABLE 6

AGC TIME TAG

AGC Value Position in Frame	Time of Readout Relative to FT in ms	Measurement Time Relative to FT in ms	Time Separation in ms
1	61	-139	320
2	381	181	280
3	661	461	240
4	901	701	200

The measurement time for the averaged AGC value for one frame is

$$t_{av\ AGC/frame} = FT + 301\ ms.$$

S&H Gate Time Tag

The measurement times for the S&H gate values have been assumed to correspond to the times of readout which occur at 10-ms intervals starting with the FT.

The measurement times of all of these values are decreased by about 1.6 ms to account for the one-way time delay of the radar signal.

2.2.4 Conversion of Altimeter Altitudes to Ground Heights

The measured altimeter altitudes were converted to ground heights relative to the geoid along the Skylab ground track as shown in Figure 10.

The ground height values were obtained from

$$h_t = (h_c + \Delta h - h_g) - h_m$$

where h_c is the computed spacecraft height relative to the SAO reference surface used in the Geodyne orbit,

Δh is a correction for shifting the reference surface (SAO) used in Geodyne orbit computation to the reference surface of the Marsh-Vincent Geoid (1973),

h_g is the geodetic deviation obtained from the Marsh-Vincent Geoid (1973),

and

h_m is the measured altitude.

Since the same flattening is used in both reference surfaces, the value of Δh is a constant and equal to the difference between the SAO equatorial radius of 6,378,155 m and the Marsh-Vincent equatorial radius of 6,378,142 m, or 13 m.

2.3 Data Analysis

Analyses of the reduced data performed at NRL to evaluate Skylab altimeter performance consisted of the following:

a. Comparison of fine-structure AGC output and fine-structure ground heights,

b. Comparison of altimetry ground height and map topography,

c. Comparison of AGC signal level and height residual,

d. Sample-and-hold (S&H) gate output calibration and analysis, and

e. Correlation of AGC, radar altimetry, and topographic map profiles.

Fine-structure data, consisting of four AGC and eight range-delay times per data block, were used for comparative analysis only in the first and last cases. In the last case, (e), running averages of fine-structure data, including map elevation readings every one-fourth of a data block, were compared.

In the second and third types of analyses conducted, AGC and altimetry ground height data, averaged per data block, were compared with ground-truth, that is, corresponding terrain elevations and other features extracted from 1;250,000 scale (AMS edition) topographic maps of the U.S. The data frame or data block (DB), equivalent to 1.04 seconds of real Skylab transit time or 7.5 kilometers in ground track distance, was a convenient unit for production processing of the data stream, and also for averaging out large fluctuations in range and AGC data, whether due to the real terrain or due to tracking and AGC loop error. It was also noted that some average terrain feature could be

identified with a data block. The details of topographic map use are described in Section 2.3.2.

The sample-and-hold gate output calibration and analysis was performed to statistically evaluate target reflection characteristics, namely the type of reflection, specular or diffuse, and the size of reflecting patches.

All of the reduced altimeter data averaged per data block, topographic map data per data block, and pertinent geographical descriptions are collected into a set of tables, "Catalogue of Terrain Radar Signatures," appendixed to this report.

2.3.1 Fine-Structure AGC and Ground Height

Fine-structure AGC signal levels and the reduced ground heights as a function of measurement time were plotted for selected portions of each pass to obtain an understanding of the interaction between the range tracker and AGC loops resulting from changing topography and reflection mechanism of the terrain. Skylab photography, available for Pass 28, was also included to aid in the interpretation of terrain influence on altimeter function. The data are discussed in Section 4.2 and illustrated in Figures 13 through 20.

2.3.2 Comparison of Altimetry Ground Heights and Map Topography

As previously mentioned, the fine-structure radar altimetry ground heights were averaged over a data block for the purposes of this comparison. This averaging was applied to all good ground height data to generate a large data base for the detailed evaluation of overall altimeter performance.

With respect to identifying corresponding map topography, different approaches in the selection and the use of map elevations within a footprint were used. An initial attempt to generate detailed two-dimensional profiles of the ground track by combining a series of profiles of the terrain along lines parallel to the ground track was found to be laborious and unproductive because of large errors in the altimetry and map reading. Another attempt considered the identification of a "dominant" area within a footprint, but this failed because the largest areas within a footprint of a uniform terrain type were not necessarily the most reflecting. This procedure was used only for Passes 1 and 28, where the elevation of the dominant area is identified as "expected height from map reading" in Figures 21 and 25.

The procedure finally adopted for general evaluation of the relation between altimetry and map elevations by data block was to determine maximum-minimum elevation bounds within a footprint from the topographic maps as shown in Figure 10, and then observing whether the altimetry ground heights fell within these bounds or not. This relation is discussed in Section 4.3 and illustrated in Figures 21 through 25. The maximum-minimum bounds for each data block are given by calculating ($h_{mid} \pm \Delta h/2$) from the data tabulated in the appendixed Catalogue of Terrain Radar Signatures.

2.3.3 AGC and Height Residuals

The deviations of the derived altimetry ground heights from the map height bounds derived previously are tabulated and also plotted separately as height residuals and compared with the AGC outputs. This plot relates apparent height errors to received power variations and it permits the evaluation of the instrument reponse of the range tracker to changes in AGC. The data are discussed in Section 4.4 and illustrated in Figures 26 through 30.

2.3.4 Sample-and-Hold Gate Output Calibrations and Analysis

The S&H gate outputs were recorded in PCM counts on pre-processed tape with two bits used to signify proper acquisition (reference 6). These values were converted to voltage by using calibration curves for receiver temperature for each gate given in reference 7. The S&H gate calibration curves were actually averaged for the temperature range -20°C to +25°C to obtain a response for the relatively constant receiver temperature of 0°C. In addition, the amplitudes of each gate were corrected for AGC changes within a frame with the maximum AGC value normalized to unity.

The corrected S&H gate outputs were analyzed in data blocks of one frame each and the following operations were performed.

1. Plot of selected individual waveforms.
2. Computation and plot of the average value and standard deviation of each gate output for selected frames to obtain the pulse shape of the radar return.
3. Calculation of the amplitude distribution for each gate within a frame to statistically evaluate the amplitude fluctuations.
4. Computation of the amplitude auto-correlation for each gate for shifts of several pulse periods to determine the coherence of the radar return signal in each gate.

This analysis is discussed in Section 4.5 and illustrated by Figures 31 through 41.

Selected information concerning the ramp or rise time part of the return signal can be found in the appendixed Catalogue of Terrain Radar Signatures.

2.3.5 Correlation of AGC, Radar Altimetry, and topographic Map Profiles

The cross-correlation between sets of smoothed altimetry and map elevation data was calculated to obtain a quantitative evaluation of altimeter performance in measuring terrain elevations. Running averages of the data were used not only to smooth out the data, but also to match resolution scales for meaningful comparisons to be made. Details of these calculations and results are described in Section 5.1 and illustrated in Figures 44 through 47.

A correlation of the fine topography with AGC signal level was also attempted, but the results were inconclusive based on a simple terrain reflection model. However different mean received power levels could be associated with specific types of terrain.

3. IDENTIFICATION OF ERROR SOURCES

There are a number of systematic and random errors affecting the accuracy of the final altimeter-derived ground height, ranging from various spacecraft position and time errors, which are summarized in Table 7, to errors in the measurement of range and AGC signal power, and the sampling of radar return signal waveform. The measurement errors are of the order of 100 to 200 meters in range, and they are mainly due to poorer tracking performance over terrain with high complex relief.

Errors in reading topographic map elevations were of the order of 10 to 30 meters, assuming that the correct corresponding ground track was known.

3.1 Position Uncertainty of Altimeter Measurements

The accuracy of the location of the reflecting area associated with a given altitude output measurement is limited by the factors given below.

3.1.1 Timing Uncertainty

The conversion from AMT to GMT produced a residual bias and random error of about 15 ms and $\pm$13 ms respectively. After a correction for the bias error was applied to the SL-3 and SL-4 data, there still remained a random error in the emphemeris time corresponding to a position error of $\pm$100 m.

3.1.2 Orbit Uncertainty

Errors in the Skybet orbit are $\pm$700 m along-track, $\pm$270 m cross-track, and $\pm$200 m in height [Note 1]. These errors produce an uncertainty of about 1 km in position and the displacement is mainly along the ground track of the spacecraft.

---

[1] Skylab EREP PI Data Mtg. at JSC, 16-18 July 1973

A refined orbit computed by the Geodyne program at Wolf Research Corporation for NASA/Wallops is estimated to reduce this position error to about $\pm$100 m. A comparison between the Skybet and Geodyne orbit position values for Pass 28 data show a position bias for the Skybet orbit of +1500 m with an rms spread of $\pm$460.

3.1.3 Range Tracker Data Smoothing

Over terrain where the measured heights from individual radar returns may be assumed to vary randomly, the smoothing operation of the range tracker on the individual range estimates from each radar return produces an additional time delay in range readout. For the 2 Hz nominal bandwidth of the range tracker, this means an additional time delay of 1/4 sec to the time tag for the measured height value. This time delay could further increase if the antenna angle is off nadir, since the slope of the received waveform is reduced, with a corresponding reduction of the range tracker bandwidth. Thus, for typical cases, the position of the observed measured height as indicated by the time tag may be shifted by anywhere between 2 km and 8 km due to the range smoothing by the range tracker. Examples of this shift will be further discussed in Section 5.

3.1.4 Radar Footprint

The position of the reflecting area for which a height measurement is obtained may be located anywhere within the radar footprint. The uncertainty of this position is estimated to be of the order of $\pm$2.0 km, and it is present either in the case of dominantly specular returns in flat areas, or in the case of diffuse returns in complex terrain.

3.1.5 Antenna Off-Nadir Angle

The altimeter antenna is normally directed to the nadir position. However, in operation the antenna pointing is anywhere between 1/2 and 1° from nadir, which can produce position shifts between 4 and 8 km.

A summary of the individual position errors is given in Table 7.

TABLE 7

POSITION ERRORS

Timing	$\pm$100 m rms
Orbit	$\pm$100 m rms
Range Tracker	-4 km $\pm$4 km peak
Footprint	$\pm$2 km rms
Antenna Angle	$\pm$8 km peak

3.2 Height Error

The height measured by the range tracker of the radar altimeter over terrain is determined from a small portion of the radar return where a proper waveform is present. Any changes in amplitude, pulse shape, and range will increase the range jitter and reduce the precision of the height measurement.

3.2.1 Amplitude Variations

There are often large rapid amplitude fluctuations observed over rough terrain, which cannot be fully controlled by the AGC. In the case of sudden drops in signal strength, the range tracker may operate for short intervals on just the receiver noise, while it searches for a signal of the proper waveform to preserve lock. This search can produce peak height errors of the order of 100 m, until the AGC

increases receiver gain sufficiently for the detection of signal. In some cases where the ramp is displaced, the recovered signal will be outside the split-gate of the range tracker, and range lock is lost.

3.2.2 Pulse Shape Variations

Large changes of pulse shape due to a change in reflection mechanism will also increase height jitter. In addition, the smaller amplitude and less-defined waveform for a diffuse return may further increase range jitter. The magnitude of such errors will be similar to those caused by amplitude variations.

3.2.3 Range Rate

When very rapid and large changes in height cannot be followed by the range tracker, large height residuals may be produced. These errors, depending on the rate and magnitude of the height changes in the topography, may produce errors up to 200 m.

3.3 AGC Error

The variation in AGC output is proportional to the mean of the peak received power. However, the readout values may be in error by several dB due to improper calibration of the AGC system. An uncertainty of a few dB is inherent in the AGC measurement, but since only relative values were used in the interpretation of the results, no additional effort to reprocess data, including a correction for this error, was considered necessary.

3.4 Errors in Waveform Analysis and Statistical Distribution

The errors in S&H gate output are mainly due to range-tracker jitter, which causes a displacement between the return signal and the S&H gate positions and consequently a "displaced" sampling of the waveform. The jitter, which reflects the attempt of the range-tracker loop to track the

noisy signal will increase as the signal-to-noise ratio (SNR) decreases, and the errors in S&H gate output will vary accordingly. Individual gate bias levels will also contribute to gate output error for small SNR.

3.5 Topographic Map Height Errors

The precision of height measurements from topographic maps is usually considered to be about one-half of the contour intervals on the map, which varied from ± 30 to ± 10 m depending on the complexity of the terrain.

4. DESCRIPTION OF ALTIMETRY DATA AND TERRAIN CHARACTERISTICS

4.1 General Description of Observations

Data on a total of 13 Skylab altimeter passes over terrain were received by NRL. A quick survey showed that 6 of the 13 passes contained useful data, and five of these were analyzed in detail. A list of the pass numbers for each of the Skylab missions received by NRL is given in Table 8.

TABLE 8

SL-2	P1,	P11				
SL-3	P16,	P17,	P18,	P23,	P28,	P31
SL-3	P4,	P6,	P11,	P37,	P49	

The 6 passes which acquired relatively reliable terrain data are underlined. Pass 11 of SL-2 and Pass 31 of SL-3 contained only calibration data. All SL-4 passes were marginal due to a large drop in received power (-24 dB) caused by apparent antenna gain deterioration.

The most reliable operation was achieved in passes 16, 17 and 18 of SL-3 where all 3 sub-modes were activated. For the remaining passes (1 of SL-2, and 23 and 28 of SL-3) only the first 2 sub-modes were employed, due to a large number of frames where range tracker loss occurred. Table 9 provides a summary of the number of frames acquired in each pass and the approximate location of the ground track for each sub-mode. The ground tracks of the 5 passes which were processed by NRL are shown in Figure 12 and a general description of the terrain observed on each pass is given in the following paragraphs.

Pass 1 (SL-2) 5/30/73

The first pass of SL-2, travelling southeastward, acquired range lock over the Pacific Ocean and crossed the West Coast of the United States at Coos Bay, Oregon. The ground track traversed a variety of terrain with complex topography, which included large mountain ranges, forests, canyons, and some valleys and small mountain lakes. The observations covered portions of Oregon, California, Nevada, and Utah and were terminated over the Marble Canyons in Arizona. As indicated in Table 9, only 25 percent of the available frames (data blocks) had range lock. This pass is typical of the Skylab altimeter performance over complex terrain, where a narrow pulse range tracker could not accommodate large changes in both topographic height and received power.

Pass 16 (SL-3) 9/6/74

The observations of Pass 16 started over Baja California in Mexico, and continued over the Gulf of California, and the Desierto del Altar. The ground track then entered the United States near Ajo in Arizona, where it covered some valleys and mountains. It then continued over the highlands of Arizona and New Mexico which are mostly covered by ranchlands, and over large mountains in Colorado. The pass terminated over a flat area near Pueblo, Colorado. This was the best run as a result of a combination of reliable instrument performance and gradually changing terrain features. More than 90 percent of the frames had range lock.

Pass 17 (SL-3) 9/7/73

The ground track of Pass 17 traversed mostly smooth areas and in spite of poor antenna pointing range lock was achieved for more than 90 percent of the available frames.

TABLE 9

Summary of Skylab Terrain Observations

Identification	Mode	No. Good Data Blocks	Total No. Data Blocks	Type	Location
Pass 1, SL-2	100	12	13	Bay	Coos Bay, Ore.
Date: 5/30/73	101	9	27	Mts. & Forest	Roseburg, Medford & Klamath Falls, Ore.
Beginning	102	10	23	Forests & Lakes	Klamath Falls, Ore. Alturas, Calif.
Time 20:37:57					
Long. -125.1					
Lat. 43.7					
End	110	9	54	Mts, Valleys, Forests	Long Valley, Buena Vista Valley, Toiyabe Range, Nev.
Time 20:41:33					
Long. -110.7					
Lat. 36.2	111	10	56	Mts, Valleys, Forests	Ely & Lund., Nev. Cedar City, Utah
	112	5	31	Plateaus, Canyons, Cliffs, Terraces	Marble City, Ariz.
	TOTALS:	55	204		
Pass 16, SL-3	100	15	15	Gulf of California	Mexico
Date: 9/6/73	101	15	15	Desert	Mexico
Beginning	102	15	15	Valley & Mountains	Ajo, Arizona
Time 21:23:54					
Long. -115.1	110	18	18	Valley & Mountains	Pheonix, Arizona
Lat. 30.9	111	18	28	Ranches	Holbrook, Arizona
End					
Time 21:27:11	112	20	21	Ranches	Holbrook, Arizona & New Mexico
Long. -103.8					
Lat. 38.8	120	14	15	Ranches	Gallup, New Mexico
	121	19	41	Mountains, Valleys, Forests	Gallup, New Mexico Pueblo, Colorado
	122	10	10	Ranchland	Pueblo, Colorado
	TOTALS:	116	128		

Table 9 (continued)

Identification	Mode	No. Good Data Blocks	Total No. Data Blocks	Type	Location
Pass 17, SL-3	100	15	15	Farmland	Des Moines, Iowa
Date 9/7/73	101	15	15	Rivers and Farmland	Waterloo & Dubuque Iowa
Beginning Time 20:45:31 Long. -94.2 Lat. 41.3	102	16	25	Rivers and Farmland	Dubuque, Iowa LaCrosse, Wis.
End Time 20:49:06 Long. -77.6 Lat. 47.3	110	20	20	Lakes & Swamps	Madison, Wisc.
	111	20	20	Lake Michigan	Manitowoc, Wisc.
	112	20	23	Lakes & State Parks	Traverse City and Cheboy, Mich.
	120	17	17	Forests & Lake Huron	Cheboygan, Mich. & Alpena, U. S.
	121	16	16	Forests & Lakes	Blind River, Ont., Canada
	122	20	20	No map available	Canada
	TOTALS:	159	171		
Pass 18, SL-3	100	15	15	Flat, ranches	Sonora & San Angelo, Texas
Date: 9/9/73	101	15	15	Flat, ranches	Brownwood, Texas
Beginning Time 19:15:16 Long. -100.8 Lat. 30.8	102	15	15	Flat, ranches	Abilene, Texas
	110	20	20	Flat, ranches, Brazos R.	Sherman, Texas and Oklahoma
	111	19	23	Flat, Lake Texoma	Ardmore, Oklahoma
End Time 19:18:47 Long. -88.5 Lat. 39.2	112	14	15	Hills	McAlester, Okla. & Fort Smith, Ark.
	120	14	29	Forests & Arkansas R.	Ozark Nat'l Forest, Arkansas
	121	20	23	Ozark Mts.	Springfield & Rolla, Missouri
	122	20	21	Flat, Mississippi R.	St. Louis, Missouri and Illinois
	TOTALS	152	176		

Table 9 (continued)

Identification	Mode	No. Good Data Blocks	Total No. Data Blocks	Type	Location
Pass 23, SL-3	100	14	38		
Date: 9/11/73	101	15	23		
Beginning	102	16	19		
Time 21:02:25					
Long. -112.9	110	24	35		
Lat. 45.2	111	20	27		
End:					
Time 21:05:22	112	20	20		
Long. -97.8					
Lat 48.9	120	2	7		
	TOTALS	111	169		
PASS 28, SL-3	100	11	22	Mts. & Forests	Millet & Ely, Nevada
Date: 9/13/73	101	13	20	Mts. & Salt Flats	Elko, Nevada
Beginning	102	15	15	Great Salt Lake and Desert	Bringham City, utah
Time 19:33:31					
Long. -116.5	110	15	39	Mts., Plateau, Ridges & Rivers	Preston, Idaho
Lat 39.3					
	111	2	24	Ranges	Lander, Wyo.
End					
Time 19:35:48	TOTALS	56	120		
Long -107.9					
Lat 43.5					

The outstanding terrain features included farmlands in Iowa, swamps in Wisconsin, and two large lakes, Lake Michigan and Lake Huron.

Pass 18 (SL-3) 9/9/73

The ground track of Pass 18 is similar to that of Pass 17 in terms of relief. Large areas of flats and ranchlands in Texas, gently sloping hills in Oklahoma, Arkansas and Missouri are typical terrain features. There was range lock on about 90 percent of the frames.

Pass 23 (SL-3) 9/11/73

The Skylab altimeter in this pass was operated over Idaho, Montana and North Dakota. About 75 percent of the pass had range lock.

Pass 28 (SL-3) 9/13/73

The ground track of Pass 28 includes a combination of the type of terrain observed in Pass 1 of SL-2 and Passes 16, 17 and 18. The run started in the mountains and forests of Nevada, then passed over the Salt Flats and desert areas of Utah, and finished over a mixture of mountains, plateaus and ridges in Idaho and Wyoming. About 50 percent of available frames had range lock.

4.2 Fine-Structure AGC and Ground height

The fine-structure Skylab altimeter AGC output, as defined in paragraph 2.2, represents the combined effects of complexity of terrain and reflectivity along the ground track. Low relief, valley floors, and specular reflection will enhance AGC signal level, while high complex relief and low reflectivity or signal scattering terrain types, including vegetation, will produce low AGC signal levels. In other words, AGC signal level will generally vary with the particular type of terrain in this prescribed manner. Low

signal levels will also increase range noise, and in extreme cases will result in loss-of-lock by the range tracker. Typical examples of such relations for various types of terrain are shown in Figures 13 through 19.

Pass 16

In Figure 13 is shown the altimeter output for the first part of Pass 16. The upper curve is the AGC response to the observed terrain, and the lower curve is the corresponding altimeter tracking profile. The ground track, starting in the Valle Chico in Mexico (DB 180), passes over the Sierra San Felipe mountains (DB 183), and then descends to the Gulf of California (DB 184, 185). The spacecraft is over the Gulf of California for about nine seconds (DB 186-195) and it then remains over the Desierto del Altar for the remainder of the plot (to DB 204). It is apparent that the presence of the San Felipe mountains reduces the receiver power by about 25 dB. The initial sudden drop in AGC signal level results in a loss of range lock for one frame (DB 181), but because of good antenna pointing, range is recovered in DB 182, and the tracker even follows the relatively large descent of about 500 meters to the coastal flats of the Gulf. The same altimeter behavior can also be better observed in Figure 22 which includes a topographic map profile for the same ground track.

Over the Gulf, the AGC signal level increases to and remains a constant value of -30 dB until the Desierto del Altar is reached. The altimeter-measured ground height remains stable over the Gulf and then increases smoothly with the topographic map land elevations as can be seen in Figure 22.

The above case is a good example of the potential performance of the instrument over land and water areas of moderate relief.

Pass 17

Another example of fine-structure altimeter output is shown in Figure 14 for Pass 17 over Wisconsin. The terrain consists mostly of swamps and small lakes, but here there is a large fluctuation of the AGC signal of 10 to 20 dB, which, together with the lower signal level, is due to a large off-nadir antenna pointing angle as will be explained later in Section 4.4. A correspondence between the AGC signal level and the altimetry profile is less evident in this case. However, strong signals usually reflect flat or valley terrain, while a drop in signal power means steeper relief, with the magnitude of the fluctuation being enhanced by poor antenna pointing. In spite of poor performance at such angles, the range tracker remained locked in over the relatively even terrain, and range jitter, while larger than that in Pass 16, was still relatively small (Note increase of elevation scale by a factor of 4.)

Another sample of Pass 17 over the Lake Michigan region is shown in Figure 15. In this case, the spacecraft approached the lake from the west over farmland in Wisconsin. The altimeter profiles the approach to the lake, but the high frequency variations in height represent range tracker jitter due to high range rates. The high AGC values over the western portion of the lake and the later decrease are probably due to an initially smooth water surface which is subsequently disturbed by prevailing westerly winds as the eastern coast of the lake is approached (NOAA Daily Weather Maps, 3-9 September 1973).

In Figure 16 the altimeter output for the Lake Huron region is shown. Here, again the altimeter follows the descending elevation to the lake. However, in this case, the AGC signal level over the lake is about 15 dB below that of Lake Michigan. This is produced by a sub-mode change

which tilts the antenna by about 1/2 degree in pitch, but as will be shown later, the pointing is actually off by 1 degree due to an initial offset in the pointing of the antenna beam. The large off-nadir angle also results in large range jitter over the lake region.

Pass 28

Other examples of fine-structure altimeter outputs are shown in Figures 17 through 20, where cloudless Skylab photography taken over the ground track is also included. In Figure 17 the terrain consists of alternating mountain ranges and valleys in Nevada and several range-lock losses are observed. The generally low AGC signal and the large change in AGC over the Cherry Creek Mountains are apparent. It is seen that even for a constant AGC signal level, the range acquisition is delayed if the value falls below -50 dBm. The run is continued in Figure 18 and reliable operation is attained only after large AGC signal is regained over the Bonneville Salt Flats in Utah.

Figure 19 again shows the potential performance of the altimeter for large and constant AGC. The first drop in AGC due to the Newfoundland mountains has no adverse effect on range measurement since the change in AGC is less than 5 dB and the AGC signal is quite strong. A later drop in AGC signal over the lakeside mountains near the Great Salt Lake is much larger (20 dB) and there is a corresponding large jitter in measured height before the AGC and the range tracker restabilized. In Figure 20 an increase in jitter as well as occasional range tracker loss are indicated as the Skylab passes over complex relief in Wyoming. Reliable operation is again achieved over flats and the Fork River.

4.3 Comparison of Radar Altimetry with Map Topography

Altimeter-measured and topographic map elevations along the ground track were compared by the following method, which was finally adopted after a few trial and error attempts. This consisted of estimating maximum and minimum map elevations in a footprint in order to establish bounds, and then comparing altimeter-determined ground heights with these bounds. Height residual is defined here as the value by which the altimetry ground height exceeds these bounds. The height residual could then be positive or negative. The relation of the altimeter-determined elevations to the maximum-minimum bounds is depicted in Figure 21 through 25, while the height residuals are shown in Figures 26 through 30 and also tabulated in Tables A-1 through A-5 for each data block. In this instance, fine-structure altimetry data was averaged over a data block or 1.04 seconds in time to reduce AGC and range jitter, and then compared with the map data for the corresponding block.

This method of analysis showed that large height residuals existed for several data blocks prior to and following range lock loss and also when large off-nadir antenna angles existed. In retrospect, this technique provided a general means of evaluating altimeter performance in terms of accuracy, response and reliability. The following sections show the results of this operation and the possible causes of any anomalies observed.

Pass 1

In Figure 21 the topographic heights for Pass 1 are shown plotted vs. time. As has been indicated previously, this pass scanned a region of very complex relief and range lock was lost over many areas. In general, however, the altimeter-measured heights closely followed the topographic map profile. There are a few major discrepancies which will

be discussed later. It is seen that range lock is lost initially as the Skylab ground track crosses the West Coast of the United States at Coos Bay, Oregon. However, as the relief becomes more uniform, range is again acquired, but it is lost again as the height increases rapidly. Only for more or less uniform relief can the range tracker follow the height changes. Large height residuals are often observed near large changes in height, and the range tracker tends to remain inertially locked-in to a previous elevation. This can be clearly seen near Alturas, California where altimeter-measured height is radically below map height for the case of rapidly rising elevation. Here, the altimeter-measured heights correspond to the lower map elevations within a footprint. Contrarily, when the height is decreasing as near Cedar City, Utah, the range tracker tends to lock into the preceding, in this case, higher elevation. This action is equivalent to a low pass filter in the system which produces a slight lag of about one footprint in altimeter height measurement for rapid range rates.

Pass 16 (Figure 22)

The performance of the altimeter in Pass 16 shows the high accuracy and reliability which can be attained for terrain of moderate relief in conjunction with accurate nadir pointing. The decrease in height as the Gulf of California is approached as well as the gradual increase in height of the Desierto del Altar area are clearly seen. The tracking of the plateau region in Arizona is evident and range lock is lost only when a rapid and large increase in height at Mesa, Arizona occurs. Reliable operation is obtained over the highlands in New Mexico, but the steep relief near Durango, Colorado cannot be followed by the altimeter and range is lost for a considerable distance. In spite of the occasional range loss, this pass represents the

best of the height observations made by the Skylab and it also had the smallest rms error.

Pass 17 (Figure 23)

The ground track of this pass covered low areas of low relief and operation was relatively reliable in spite of a known off-nadir pointing angle. The early part of the pass was over farmlands in Iowa and Wisconsin and there is good correlation with map topography. Some residual errors are observed, however, near large vertical structures such as those near Dubuque, Iowa and Lacrosse, Wisconsin. The lag effect in altimeter ranging is again evident near the decrease in height as Lake Winnebago, Lake Michigan and Lake Huron are approached. The constant bias over Lake Huron is due to off-nadir pointing and will be more fully explained in the next section on height residuals.

Pass 18 (Figure 24)

Pass 18 is similar to Pass 17 in terms of observed topography and again the altimeter height profile follows the map elevations. Surprisingly, there was reliable tracking of the large height changes over Texas, but this is because of moderate relief and range rate manageable by the altimeter. Range lock is lost near Russellville, Arkansas, where steep relief persists over several frames. Small deviations near Ardmore, Oklahoma are not due to height changes but are caused by a sudden decrease in reflectivity as will be shown later in Figure 29.

Pass 28 (Figure 24)

The ground track of Pass 28 covers complex terrain in the early and late portions of the observations and homogeneous terrain in the middle portion. Range lock is lost over mountains near Ogden, Utah, and recovered reliably only in a dry basin near Landon, Wyoming. Major discrepancies

were observed near Ely, Nevada, due to a "lag" effect, and near Great Salt Lake and Preston, Idaho where large AGC changes were recorded. In general, the altimeter again measures the lowest elevations within the observed footprint.

4.4 AGC and Height Residuals

In Figure 26 through 30 are shown smoothed AGC values and associated minimum height residuals. The upper curve in Figure 26 represents the AGC values for Pass 1. It is seen that, in general, AGC values are below -35 dBm except over Klamath Falls, Oregon, and the Black Rock Desert, Nevada. The lowest values are from forests and mountains, with intermediate values for valleys and hills. The AGC values also show considerable fluctuations even after smoothing. This produces frequent range lock loss as seen in the lower curve. The larger negative residuals are always associated with a large drop in AGC values as seen for the plot near the Madoc National Forest, also after the Black Rock Desert, and for the valleys and hills in Nevada (DB 220). The AGC value for the Pacific Ocean (-35 dBm), shown at the beginning of the plot, is slightly lower than the average for the ocean indicating some off-nadir pointing, since relatively smooth sea-states were present.

In Figure 27 are given the results for Pass 16. The fluctuations of the AGC values are considerably reduced and a reference value of -30 dBm for the Gulf of California is obtained. While mountains and forests still produce small AGC values (-50 dBm), the small fluctuations in level allow the range tracker to follow the changes in height without range lock loss. The few failures in range tracker operation include one due to a drop in AGC (DB 242) and one due to a large vertical structure in DB 315 as indicated previously. The large height residuals over ranchland (DB 270 - 290) are caused by a combination of low AGC signal

levels and 100 MHz bandwidth operation in sub-mode 1.

The height residuals and the corresponding AGC values for Pass 17 are shown in Figure 28. The residual values have been generally greatly reduced, but again some of the larger negative residuals are associated with a decrease in received power. The case of the large positive residual (45 m) is probably due to a combination of the large elevation in the adjacent footprint and the low AGC value, which permits the weaker but earlier signal received from an off-nadir angle to dominate the range tracker operation. The low AGC causes the residual to reverse direction in the next frame which is then followed by a loss in range tracker lock. Another significant height difference is found over Lake Huron where a height bias of about -10 m relative to Lake Michigan is indicated. According to the map, the two lakes should be at the same elevation. Investigating the performance of the altimeter during this interval, it was discovered that (1) the AGC level for Lake Huron is about -15 dB below that for Lake Michigan, and (2), a sub-mode change occurred over Michigan that shifted the antenna pitch angle by 1/2 degree. If it is assumed that before change of sub-mode, the antenna angle was offset from nadir, a situation that occurred frequently over the ocean and which was later confirmed from waveform analysis over Lake Michigan, and also that the sub-mode change increased the off-nadir antenna angle to one degree, then an increase of about 10 m in satellite height would occur. This bias is obtained from a plot of height bias vs. antenna angle in a G.E. Report Skylab Altimeter, March 19, 1971, Figure 7, p. III-52. The initial off-nadir angle also accounts for the large AGC jitter over the farm areas in Iowa.

The AGC values and height residuals for Pass 18 are shown in Figure 29. The AGC jitter is greatly reduced due

to better nadir pointing and less relief. High AGC values indicate water surfaces over Lake Texoma, the White River in Missouri and the Mississippi River in Illinois. The Ozark Mountains in Missouri, forests in Arkansas and small mountains in the Northern part of Texas coincide with low AGC values, and the ranchlands in Texas provide intermediate values of about -35 dBm. The height residuals are primarily due to rapid height changes which cause preceding height values to be measured by the range tracker.

The values of the height residuals compared with the AGC values for Pass 28 in Figure 30 again show the correlation between large negative height residuals and received power. The large negative height residuals are almost always followed by a loss of range track. Figure 30 shows the considerable AGC fluctuations that occur over complex terrain. The large variations are partly caused by significant contributions from specular reflections which produce strong signal returns over short intervals and which just as quickly disappear. Typical of the large returns that are possible from specular reflections is the received power for the Great Salt Desert which saturated the receiver.

4.5 Waveform Analysis

The results of waveform analysis are described in Figures 31 through 41. The first two figures give the expected and measured waveform for returns from the ocean surface as a function of off-nadir angle. The other diagrams give plots of signal waveforms for different types of terrain, averaged for 100 pulses, and also the normalized auto-correlation functions for 100 samples of No. 4 sample-and-hold gate output. The jump or lag index in the latter is in units of 0.01 seconds of time, which is equivalent to 72 meters in ground track distance. The criterion for correlation distance or the size of a land

patch which gives a coherent signal return is a normalized correlation value larger than about 0.2 to 0.25. A steep correlation curve dropping to zero indicates a short correlation distance and a randomly scattered signal. On the other hand, a stretched out curve indicates a long correlation distance and large specular reflecting areas.

The theoretical ocean radar return consists of a triangular pulse whose rise time is about 100 ns and which decreases gradually to about 20 percent of the maximum value over the next 300 ns. As the off-nadir angle increases, there is a small decrease of rise time, but the trailing edge decreases to only about 35 percent of maximum for a 0.5 degree and 75 percent of maximum for a 0.75 degree off-nadir angle. The measured waveform for the three sub-modes of mode 1 for the ocean surface (Pass 11) shows that (1) there appears to be an off-nadir angle even for sub-modes 0 and 1 which is about 0.5 degree, (2) as sub-mode 2 is initiated, the 0.5 degree pitch angle further increases off-nadir operation to about 0.75 degrees, as determined from the trailing edge, (3) there is a shift in the range tracker position as is apparent from the shift in the rise time for 0.5 degree pitch angle change, and (4) there are considerable fluctuations in the radar return particularly in the trailing edge of the waveform, which is due to intrinsic signal noise since only 100 radar returns were averaged. These waveforms are used as a reference for comparison with waveforms obtained from terrain reflections.

Figure 33 shows the noise- and ramp-position gate outputs of Pass 1 for two adjacent frames, as sub-sub-mode 0 is changed to 1, over a relatively complex mountainous terrain in Nevada. When compared to an ocean return, it is apparent that there is some structure in the rise time which consists of both scatter and large-body reflection. The

large-body reflection is indicated by the spatial auto-correlation function shown on the right which shows that horizontal smooth areas of the order of about 150 m are present.

Similar radar returns are shown in Figures 33 and 34 for Pass 16. Note that noise- and ramp-gate outputs are shown as before in Figure 34, but that ramp- and plateau-gate outputs are shown in Figure 35.

The radar return in Figure 34 is from the Gulf of California and the rapid decrease in signal strength after the peak indicates reliable nadir pointing, which was also observed from other data for this pass. Furthermore, the auto-correlation curve shows that pure scattering dominates.

Figure 35 shows two returns for the 10 and 100 MHz submodes, which respectively reflect from mountains and ranchland in Arizona. In this case, the valleys in the mountains give a dominantly specular return as indicated by the rapid drop-off of the plateau region of the return waveform and the correlation distance of about 100 m. On the other hand, the ranchland appears to be a more diffuse target.

In Figure 36 the high correlation indicates that areas of over several hundred meters length contribute to specular return in passing over farmland in Iowa and swamps in Wisconsin. Another waveform for returns from farmland in Iowa is compared with the dominantly diffuse return from Lake Michigan in Figure 37. The high trailing edge of the Lake Michigan return indicates a large off-nadir angle as was indicated previously for Pass 17 observations. Another difference between a terrain and a water return is the much larger fluctuations in the trailing edge of the water return compared to large-body reflection from terrain.

Waveforms for Pass 18 observations are shown in Figures 38 and 39. While in Figure 38 both returns are from ranchlands in Texas, the presence of brushwood in one area has considerably increased the scattering component. Large body reflections of at least 300 m extent are indicated in the other return. In Figure 39 a strong specular return is noted over flats in Oklahoma.

The wavefrom results of Pass 28 are given in Figures 40 and 41. The mountain return in Figure 40 shows both scattering and large body reflections, with scattering apparently the dominant mechanism. In the following figure, the pulse shape indicates an almost purely specular return from the salt flats in Utah but the relatively low auto-correlation value also seems to show that large area reflections can fluctuate rapidly.

4.6 Catalogue of Terrain Signatures

The radar signatures of the Skylab ground tracks for Passes 1, 16, 17, 18, and 28 are listed in Tables A-1 through A-5 in the Appendix. Here, the AGC signal level, the reduced altimetry ground height, and some waveform analysis data are tabulated against topographic map elevations accompanied by a brief geographical description. An explanation of the column headings is given in the Appendix.

4.7 Available Data Base

For the reference of those who may be interested in further analysis of the data or a more detailed description of a particular area, a set of five volumes is available at NRL that contains all the computations performed by NRL on the five Skylab altimeter passes. Each volume is divided into three parts. The first part contains the initial evaluation data described previously in Section 2. The second part lists the following outputs for each data block:

(a) 4 AGC values and mean

(b) 8 measured range values

(c) 8 corrected range values and mean

(d) 8 corrected spacecraft heights and mean relative to geoid

(e) 8 height residuals and mean

(f) Geoid height.

In the third part, the S&H gate outputs and related statistical analyses are recorded. For each data block and S&H gate output, the following information is available:

(a) 104 S&H gate amplitudes after correction

(b) the mean and standard deviation of these amplitudes

(c) the amplitude distribution

(d) the auto-correlation of the amplitudes.

5. DISCUSSION OF RESULTS AND CONCLUSIONS

5.1. Radar Return Characteristics of Terrain at Normal Incidence

An evaluation of the Skylab radar altimeter terrain data indicates that certain radar return characteristics are associated with certain geometrical and physical properties of the observed terrain. The more significant of these characteristics and relations for normal incidence obtained from the Skylab altimeter observations are discussed below.

5.1.1 Equivalent Radar Cross-section of Terrain at Normal Incidence

For the radar altimetry data used in this particular analysis, a distribution of radar cross-sections such as shown in Figure 42 was obtained. This distribution simply reflects the relative occurrence of the different types of terrain sampled and it is therefore a signature of regional geography or terrain types along a particular ground track or tracks. On the other hand, however, this distribution and the data in Table 10 are indicative of the range of cross-sections to be expected over mixed land-and-water areas. It should be noted that the loss of range-tracker lock and data over steep mountainous relief with vegetative cover which often have small cross-sections of the order of 60 dB-above-one-square-meter (dBsm), account partly for the small number of data samples taken over such terrain, whereas in reality, mountainous terrain could be the dominant terrain type in some region. This means that careful interpretation of radar cross-section signatures is necessary.

The actual equivalent normalized radar cross-section for a terrain type may be considerably larger than shown since the effective scattering area at a given height is

smaller than the footprint in areas of complex relief. The upper and lower bounds of the radar cross-section are limited by the saturation and noise levels of the receiver respectively, but an extrapolation of the data base indicates that about 70 percent of the terrain radar returns would be included in the distribution. The saturation level of the receiver, that is, 110 dBsm, was only exceeded over the salt flats in Utah. The relatively large radar cross section over many complex terrain areas confirms the results of the waveform analysis, which had indicated that the radar return was produced by a dominantly smooth-area reflection at normal incidence, even at the short wavelength of 2.15 cm. While the indicated values of the radar cross section correspond to the maximum returns for the observed areas due to the power-level selecting mechanism of the AGC loop in the radar receiver, there may be additional significant power contributions from other height levels within an observed footprint, which signals are outside of the AGC gate and therefore not recorded.

5.1.2 Relation of Received Power to Terrain Features

The relative received power as a function of the observed geometric and physical terrain features is listed in Table 10. It is seen that only in flat desert areas and for smooth water surface does the received power exceed that from ocean return, while for ridges and dry lakes, it is about 10 dB below that for the ocean. The presence of vegetation, such as farmland or brushwood reduces this value by about 5 dB. The relatively lower values for areas with vegetation indicates that the vegetation reduces the specular component of the radar return. The smallest values of received power are obtained over mountains and forests. There is considerable scatter in these values since the received power varies with both terrain geometry, soil moisture, and vegetation.

TABLE 10

Dynamic Range of Peak Terrain Radar Return
Relative to Ocean Return

	dB
Salt Flats	20
Lakes	10
Ocean, Deserts	0
Valleys, Plains, Cities, Swamps	- 5
Ridges, Canyons, Dry Lakes	-10
Hills, Ranges, Mountains	-12
Cliffs, Forest	-16

Although off-nadir antenna pointing degrades both the power and the quality of the return signal, the effect of the pointing angle on return power can be generally quantified only in the case of returns from continuously uniform surfaces such as posed by bodies of water (Section 4.5 and Figures 31 and 32). Over terrain, the effect is less clearly defined because of the combined influence of relief and reflectivity.

5.1.3 Range Measurement Characteristics

It has already been indicated in Section 4 that the height measured by the Skylab altimeter corresponds to the bright spots of the illuminated footprint along the spacecraft ground track. These bright spots are usually found at heights which have the highest probability of normal reflecting areas. The bright spots can range in size from those of about 100 meters, corresponding to valley bottoms in mountainous terrain (Figure 33) to larger areas of a few hundred meters dimension in grasslands, swamplands, and similar uniform flat expanses (Figure 36). From this standpoint, the radar profiles the height variations of

generally the lowest areas within a footprint, and the finer undulations of the terrain are smoothed out. The altimeter therefore acts as a low-pass filter whose bandwidth is considerably smaller than that obtained from the basic footprint.

To show this more clearly, a section of Pass 16 has been analyzed in more detail. Figure 43 shows the profile obtained from topographic maps along the spacecraft ground track with elevations read every one-fourth of a footprint step. The bottom curve in Figure 44 represents a five-point running average of the former, which filters out wavelengths shorter than one-half footprint. When this is compared with the middle curve, which represents the height measured by the altimeter, it is seen that the high frequency content of the altimetry profile has been effectively suppressed in the radar measurements. Correlation studies of the two profiles indicate that the low frequency components of both profiles produce a relatively large correlation of 0.63. However, when the spacecraft position is shifted by about -7 km along the ground track, the correlation increases to 0.92. That such a shift may be necessary is further born out by analyzing the differential heights between the mean topographic profile and the altimeter measurements. For the same shift, the mean difference is decreased from 33 m to 17 m and the spread in the height difference is reduced from ± 50 to ± 38 m. These results are plotted in Figure 45. This apparent shift would indicate that either a time or position error in the ephemeris, which was not corrected, exists. A part of the shift is due to the range-tracker time-delay lag discussed in Section 2. To check the consistency of this result, a second section of P16 was analyzed similarly, and the results are shown in Figures 46 and 47. In this case the average profile from the topographic maps was relatively smooth, and the altimetry profile almost coincided with the

former. The correlation in this case increased from 0.94 to 0.98 and the mean difference and spread decreased from 27 m to 2 m, and ±51 m to ±7 m respectively for the same shift. Thus it appears that if the topographic map height is known, the position of the satellite over complex terrain could be obtained independently with an accuracy of the order of 100 m, by comparing short sections of the map profile over the ground track. An analysis of the gross characteristics of the differential height given in Section 4 showed that a shift in position of -7 km reduced the height differences and spread considerably also for P16, 17, and 18. The results are summarized in Table 11.

That the high frequency components of the altimetry profile affect the power measurements can be seen by comparing the top and bottom curves of Figures 44 and 46. However as previously mentioned in Section 2.3.5, no simple relation between terrain geometry and power variation could be established, since the latter is affected by a combination of factors such as relief, soil moisture, vegetation, and surface roughness.

5.1.4 Waveform and Statistical Characteristics of Radar

It has been shown in Section 4 that the pulse shape of the radar return indicates a dominant large body reflection. The drop-off of the correlation as shown in Figure 38 indicates that the flat areas are of the order of a few hundred meters length. This is shown more clearly in Figure 48 where the amplitude for each pulse return is plotted for different sample-and-hold gates in the ramp region. The coherent return over several pulses is evident, and the fluctuations in amplitude are due to the varying size of smooth normal areas. The second half of the plot shows the corresponding plateau region and the absence of a signal implies that no scattering effects are observed.

TABLE 11

DIFFERENTIAL HEIGHT AND SPREAD ANALYSIS

PASS			Points Removed Before Range Tracker Loss		Shift by 1 Frame	
	μ (m)	σ (m)	μ (m)	σ (m)	μ (m)	σ (m)
Pass 1	-36	±80	-14	±33	no improvement	
Pass 16	- 2	±16	- 1	±15	0	±5
Pass 17	0	± 8	1	± 7	-1	±4
Pass 18	1	± 6	1	± 6	1	±5
Pass 28	-24	±54	-14	±26	no improvement	

Previous terrain radar observations from aircraft platforms near nadir indicate that the radar return even at lower frequencies (480 MHz, 3800 MHz) appears to be predominantly diffuse (Reference 9). The dominant specular return from orbital heights may be due to the large platform height and small pulse width which emphasize the coherent component. It has been shown (Reference 10) that if smooth patches of the order of 100 m exist, the ratio between the specular and diffuse component is given by

$$\frac{P_{sp}}{P_d} = \frac{k}{\sigma_o} \frac{h}{c\tau}$$

where k = the reflection coefficient,

h = the height of the observation platform,

σ_o = normalized radar cross section,

c = velocity of light,

and τ = pulse width.

Thus as the platform height increases, and the radar pulse width decreases, the specular component will become dominant.

When the coherent return is reduced sufficiently, the range tracker loses lock. An example is given in Figure 49 for DB 243 of F16 where the amplitude in ramp gate 7 is shown. The drop in amplitude is due to the loss of significant signal from smooth areas due to rapidly increasing height and large increases in slope. Before the range tracker loses lock, the altimetry ground height is less than the map height, since the tracker persists in searching near the same height level.

5.2 Radar Altimeter Performance

While the radar altimeter lost range lock about 30 percent of the time in the five analyzed passes, the remaining 70 percent of the data showed reliable altimeter

performance over many complex terrain features. The flexibility and high sensitivity of the Skylab altimeter made it possible to obtain height data that reasonably closely profiled the low frequency characteristics of the relief along the spacecraft ground track as already discussed in Section 5.1.3. The limitations to its performance were primarily due to the range tracker and the AGC loop responses and interaction between the two. A combination of off-nadir antenna pointing and the time-delay truncation of the radar return by the range tracker and AGC processor degraded return signal amplitude and quality. The situation worsened with increasing relief of the observed terrain, and in extreme cases, resulted in loss of range locks.

The off-nadir pointing angle of the antenna can be obtained from the radar return characteristics from water surfaces by measuring either the rate of drop-off of the trailing edge in the plateau region or the amplitude and bandwidth of the range jitter. Since normally over terrain only small water surfaces are present, the signal plateau region usually could not be used. An exception was the observation over Lake Michigan in Pass 17, and as has already been indicated in Section 4, the drop-off of the trailing edge indicated that the antenna pointed off-nadir by about 0.75 degrees. The alternate method (Ref. 11) of height-jitter characteristics can be used, if the plateau region for signal returns from large water surfaces is not available. While this method is only strictly valid for large off-nadir angles (> 1°), it has been applied to a sample of each pass for estimating system performance. The results are given in Table 12. It is seen that the largest bandwidth is obtained for the Gulf of California, which implies an off-nadir angle of less than 0.5 degree. The reduced bandwidth over Lake Huron of 1.8 Hz would indicate an off-nadir angle of about one degree. This agrees with

other factors, such as the low received power from Lake Huron as compared with that from Lake Michigan and the Gulf of California, and it is further confirmation of the height error of about 10 m discussed previously in Section 4.4. Similar analysis, applied to homogeneous terrain areas, are shown for small sections of ranchland in Texas (Pass 18) and the Salt Flats in Utah (Pass 28). The improvement in jitter (0.8 m) for large specular return is apparent over the Salt Flats.

In spite of the above limitations, the Skylab altimeter accommodated large range and AGC rates and became inoperative only over the larger vertical height dispersions.

TABLE 12

Range Tracker Jitter and Bandwidth

	Jitter (m)	Bandwidth (Hz)
P1, Pacific Ocean	2.9	2.0
P 16, Gulf of California	2	2.3
P 17, Lake Michigan	2.8	2.3
Lake Huron	3.25	1.8
P 18 Ranchland, Texas	1.9	2.2
P 28, Salt Flats, Utah	.8	2.3

5.3 Design Considerations for a Dedicated Terrain Altimeter

Terrain observations at nadir require a radar altimeter system different from one used exclusively for ocean observations. Significant differences in the nature of the target are:

1. The terrain represents a complex radar target where range variations within a practical-size footprint may amount to several hundred meters.

2. Range fluctuations are rapid and frequent within a footprint, and their pattern can vary from one footprint to another.

3. Reflection will be both specular and diffuse, with the former being favored since it returns a stronger coherent signal.

4. A number of factors, such as slope, rate of slope change (sharp or gentle relief), dielectric constant, surface roughness, and vegetation, affect terrain reflectivity, which is in contrast to a relatively simple scattering mechanism for ocean surface returns.

5. Range and reflected power variations within a footprint, due to the causes described, could be of the order of 1,000 m and 30 dB respectively.

A full description of the radar return would consist of a three-dimensional representation such as shown in Figure 50, where received power could be shown as a function of height z, ground track distance x, and track displacement y. The signal sampled by a specific narrow range gate would yield the reflected power for a particular terrain elevation. This would provide information on both the relief and the radar reflection characteristics for each elevation of the terrain along the sub-satellite ground track. By combining a series of measurements along parallel tracks, a two-dimensional reflectivity profile for each elevation is obtained.

The design parameters required of a satellite altimeter which would provide such an output are:

1. A maximum sampling rate which will yield independent

data samples. This would make it possible to identify and to describe the extent of specular-return regions and to locate reflecting areas with height and horizontal resolutions of the order of one and 100 meters respectively for satellite altitudes.

2. The use of beamwidth-limited operation, by either decreasing antenna size or increasing pulsewidth, so that a footprint can be uniquely associated with a given land area.

3. A threshold range tracker which detects the earliest return and responds to range rates of about 1,000 m/s.

4. An adaptive S&H gate with response time of the order of one second, where the width of the operating sampling gate can be varied to accommodate the maximum height range of the observed terrain. For this purpose, about 20 S&H gates would be needed to sample the radar

5. A dynamic IF range of 30 dB, so that both small signals from small scattering areas and large signals from specular or larger scattering areas can be measured simultaneously.

6. Refined antenna-pointing calibration, which can be obtained from the radar return over the ocean or other water surfaces for which reflection or scattering characteristics can be assumed to be known.

A possible set of system parameters required to produce such a performance for a minimum radar cross section of 53 dBsm (200-ns pulsewidth) is given in Table 13.

A data-processing scheme for such a system is shown in Figure 51. Three parallel detector circuits, different in power levels through 10dB attenuator inputs, cover an instantaneous dynamic signal power range of 30 dB. The AGC is controlled by the peak signal as in the Skylab altimeter, but the first detector is also allowed to sense signals 30-dB below the peak level.

TABLE 13

System parameters for a dedicated terrain satellite radar altimeter with a satellite height $h_s = 4 \times 10^5$m.

Transmitter	
TWT power output	2kW
Wavelength	2 cm
Pulse-width	200 ns
Pulse Repetition Frequency with burst of 10 pulses separated by 200 μs	100
Average transmitted power	0.4 W
System loss	6 dB
Antenna	
Paraboloid diameter	1.5 m
Aperture efficiency	50%
Gain	43 dB
3 dB beamwidth	1°
Receiver	
System temperature	500°K
Bandwidth	5 MHz
SNR (σ = 53 dBsm)	10
Data Processing	
Type of acquisition and track	Threshold
Tracking bandwidth	10 Hz
(Tracking used to position S&H gate #5)	
Number of S&H gates	20
S&H gate #1 precedes S&H gate #5 by 10 μs and is used as a noise gate	
S&H gates #2 - 20 are contiguous	
S&H gate pulsewidths	200, 400, 800 ns
Increase of pulsewidth is controlled by comparison of outputs of S&H gates #1 and #20	

TABLE 13 (cont.)

Decrease of pulsewidth is controlled by comparison of outputs of S&H gates #1 and #10	
Bandwidth of pulsewidth decision	1 Hz
Number of 10-dB channels	3
AGC bandwidth	10 Hz
Instantaneous dynamic range of received power	30 dB
Total dynamic range	60 dB
Footprint	
Fresnel Zone	90 m
Diffuse return (max.)	7 km

The initial range of the radar return is acquired and tracked by a comparison of the signal with a delayed version of the waveform in a threshold device, which also provides a timing pulse for positioning S&H gate #5. The 20 S&H gates are spaced as indicated in Table 13. Gate #1 is used to monitor the noise level of the return signal and to provide a reference for the other S&H gates so that the full return signal is always captured. The outputs consist of those of the three sets of 20 S&H gates, which correspond to three power levels, plus that of the initial threshold detector.

This satellite terrain radar system should be basically used to construct a radar topographic map of the earth, which would also include other terrain intelligence such as vegetative cover and dielectric constants from calibrated specular-reflection data. Accurate height measurements over flat areas can provide continental networks of reference points, which can be used to connect intercontinental systems and derive for the first time relative orthometric heights on a global scale. A base map of this type, once established, can then be used to determine future changes in terrain features caused by climate, weather, or man-made effects.

5.4 Conclusions

A large data base for terrain radar altimetry was obtained by the altimeter aboard the Skylab mission. Although there was considerable latitude in the quality of the data due to complexities of the terrain and limitations in instrument performance, the latter consisting primarily of antenna pointing error and bandwidth restriction, the available data base showed the existence of a distinct radar signature of the low-frequency profile of the elevations along the ground track. Different levels of return signal

strength and different signal wave forms were identifiable with gross terrain features. Loss of lock in range tracking and consequently loss of significant terrain intelligence over land areas of complex relief indicated the need for larger dynamic power range and range rate capability in a dedicated terrain altimeter, and the specifications for such a system have been outlined.

REFERENCES

1. "Earth Resources Data Format Control Book PHO-TR543," Vol. 1, NASA JSC, March 1973, p. 2.1.5-27.

2. Ibid., p. 2.1.5-24 to 45.

3. "S193 Altimeter Program Design Document," ERS-100, 6 Feb 1973, Appendix A-1.

4. "Skylab Program EREP, " Sensor Performance Report, Vol. V (S193 ALT), NASA JSC, 31 July 1973, p. 6-9.

5. "Earth Res. Prod. Processing Recs. for EREP Electr. Sensors," PHO-TR524 Rev A, Ch. 1, Philco-Ford Corp., 10 May 1973, p. 7-17a.

6. "Earth Resources Data Format Control Book," op. cit., p. 2.1-25.

7. "S-193 Microwave Radiometer/Scatterometer Altimeter," Vol. 1b, General Electric Corp., 27 Oct. 1972, p. 6-36.

8. "Sea Surface Topography from Space," NOAA Technical Report ERL 228-AOML 7 (Feb. 1972), Vol. 1, p. 1-3.

9. "Radar Terrain Return Measured at Near Vertical Incidence," Edison, A. R., Moore, R. K., and Warner, B. D. , Transactions IRE, AP-8, 1960, pp. 246-254.

10. "Anomalous Radar Backscattering from Terrain at High Altitudes," Shapiro, A. and Yaplee, B. S., Proc. IEEE, Vol. 63, No. 4, April 1975, p. 717.

11. Private Communication, Miller, L. S., Applied Science Associates, Apex, N. C.

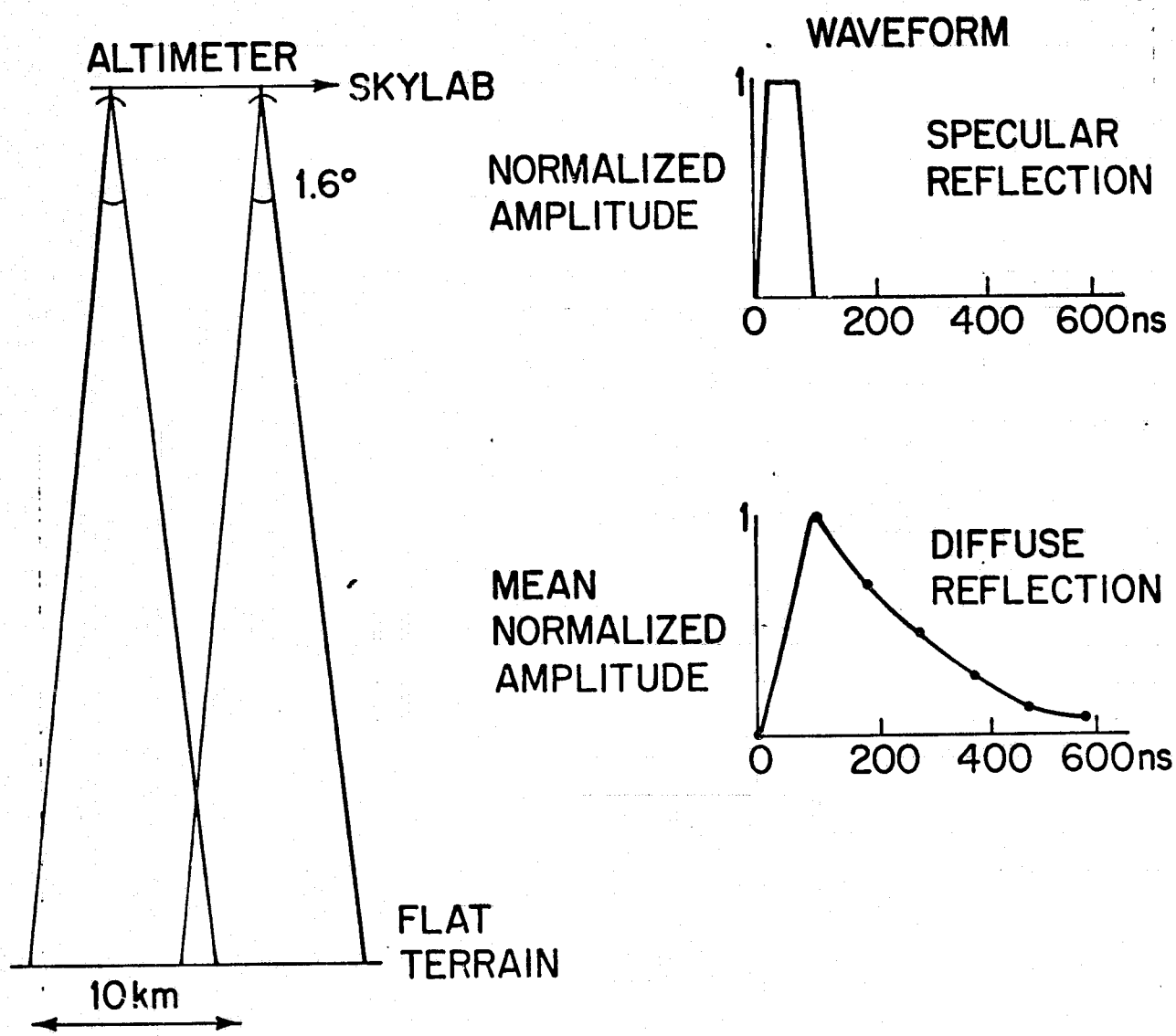

FIGURE 1. GEOMETRY OF FLAT TERRAIN OBSERVATIONS.

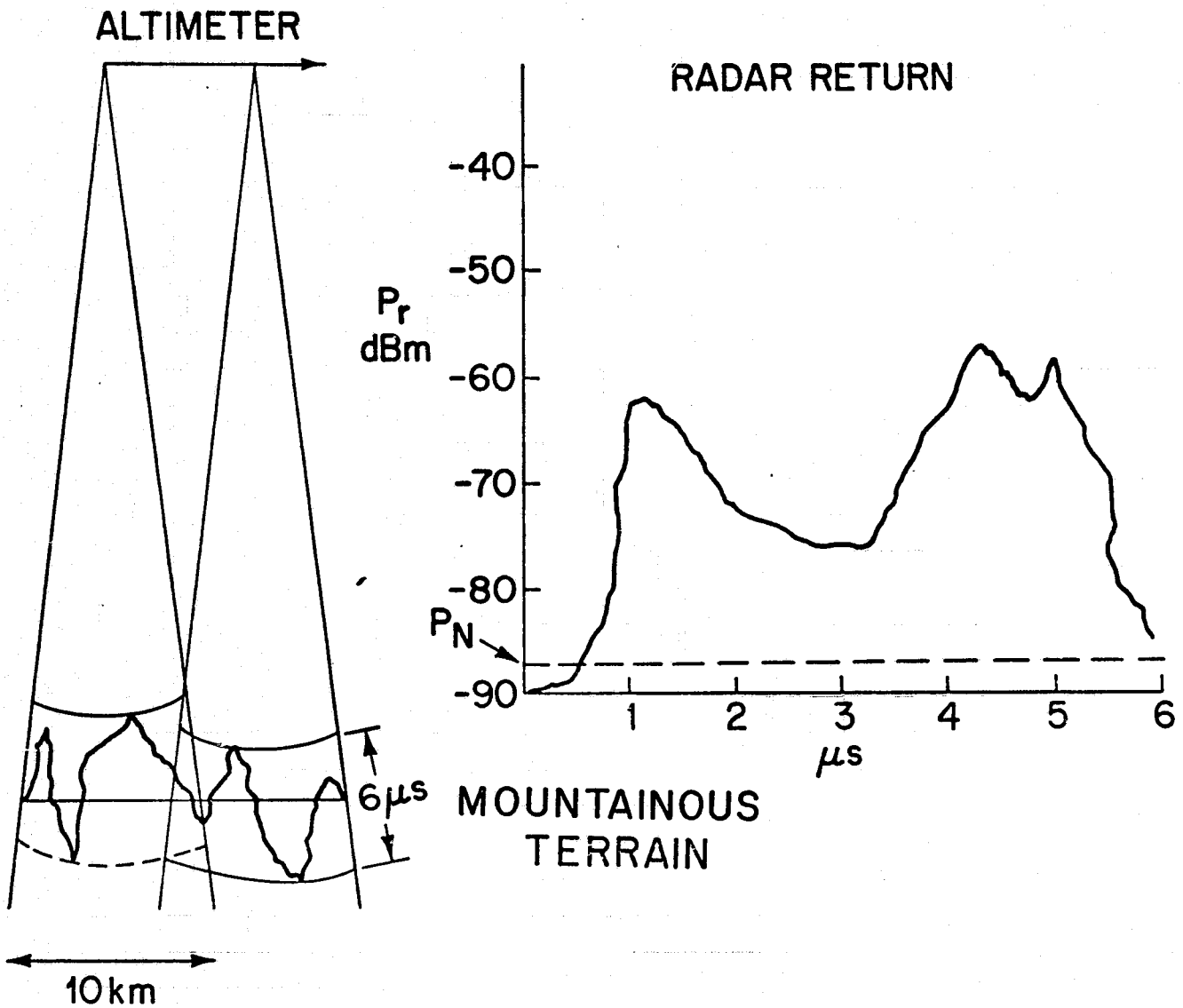

FIGURE 2. GEOMETRY OF COMPLEX TERRAIN OBSERVATIONS.

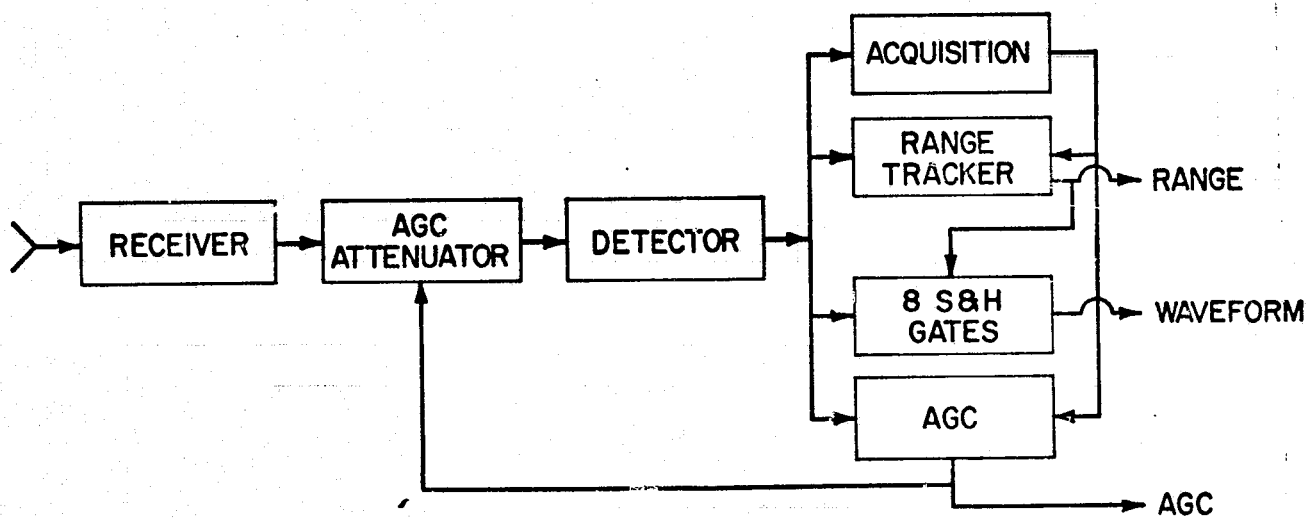

FUNCTIONS:

1. ACQUISITION - (a) COARSE SEARCH, (b) FINE SEARCH
2. AGC - (a) RECEIVER GAIN CONTROL, (b) RECEIVE POWER MEASUREMENTS
3. RANGE TRACKER - (a) S&H GATE POSITION, (b) DELAY MEASUREMENT
4. WAVEFORM - (a) RADAR RETURN PULSE SHAPE, (b) TEMPORAL AMPLITUDE CHARACTERISTICS

FIGURE 3. FUNCTIONAL BLOCK DIAGRAM OF SKYLAB ALTIMETER RECEIVER.

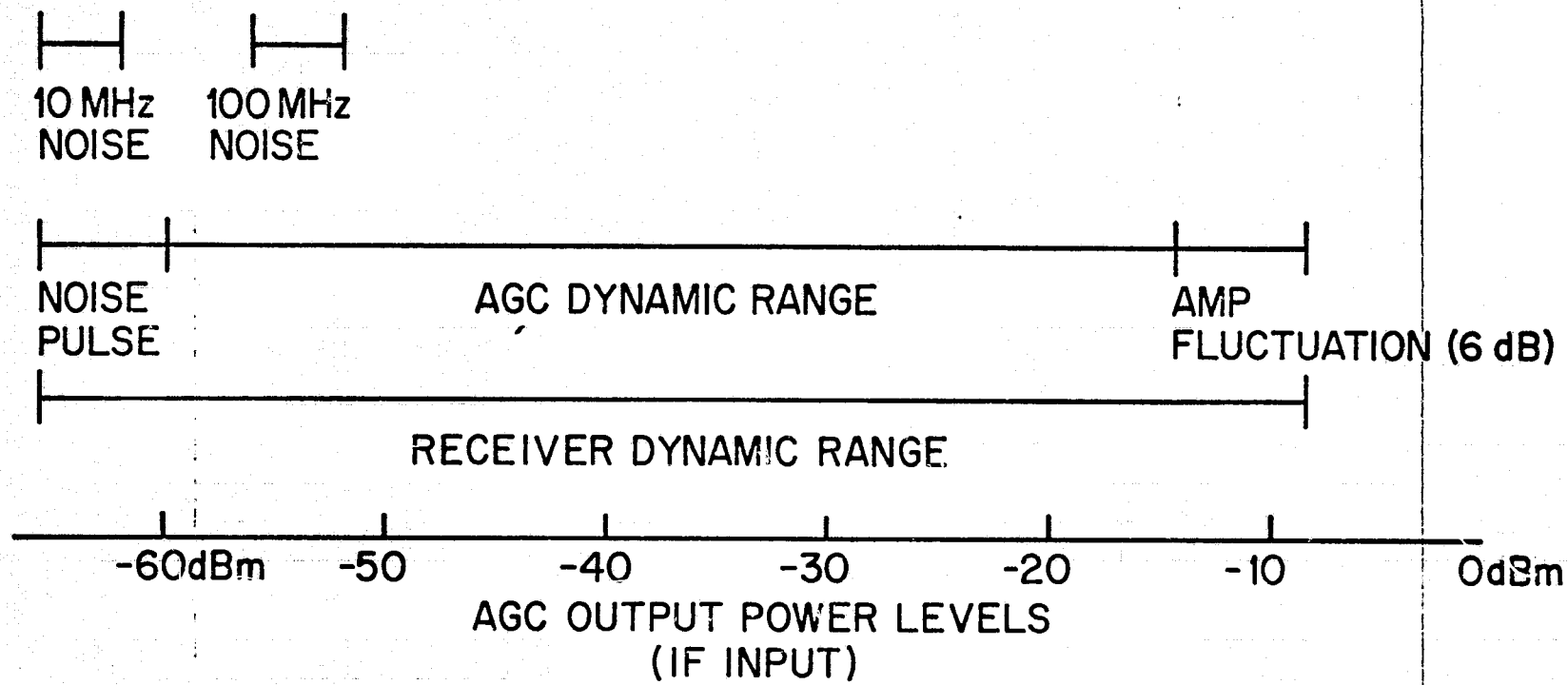

FIGURE 4. RANGE OF PEAK VALUES OF AVERAGE RECEIVED POWER AT AGC OUTPUT.

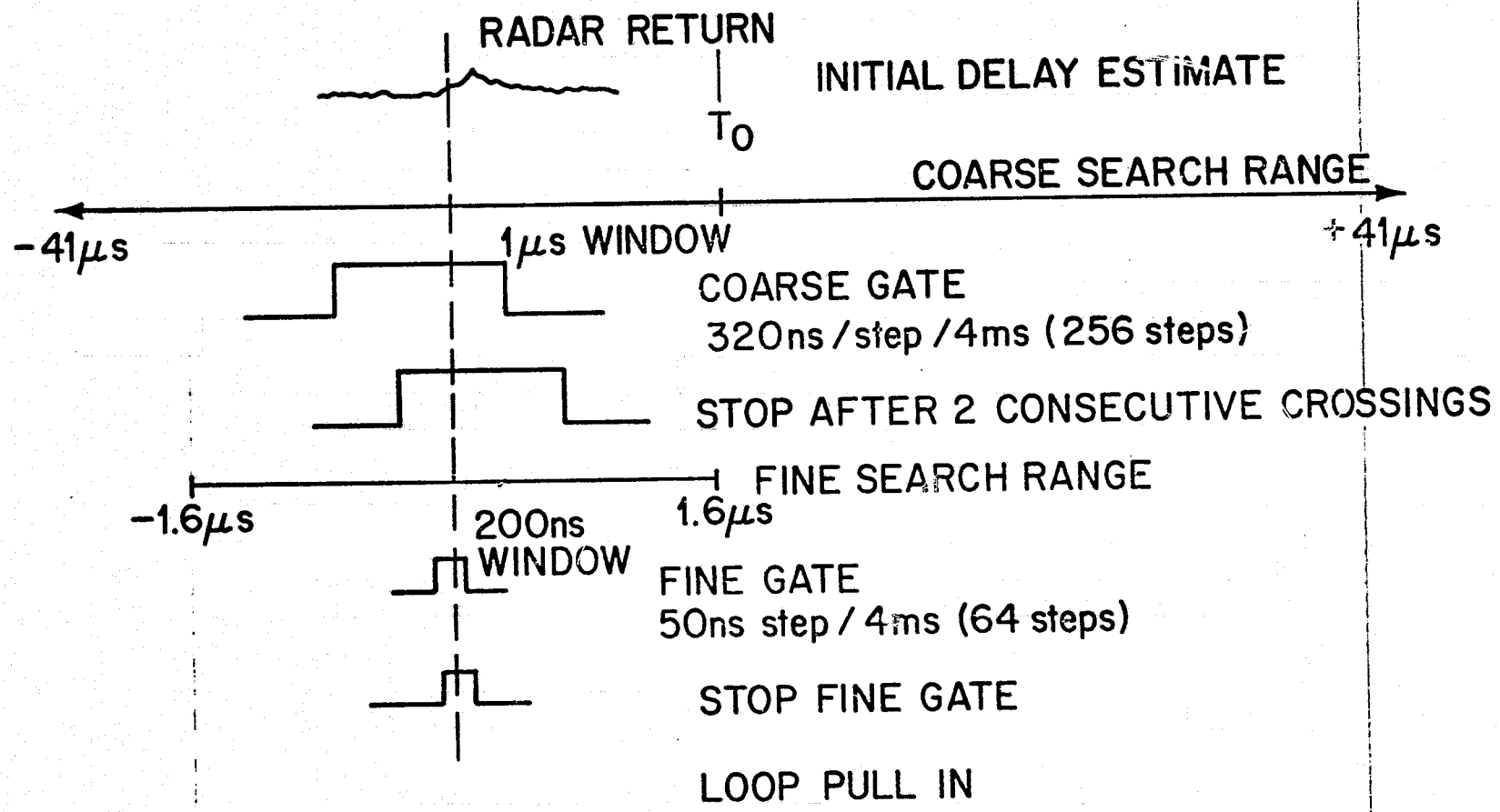

FIGURE 5. ACQUISITION MODE.

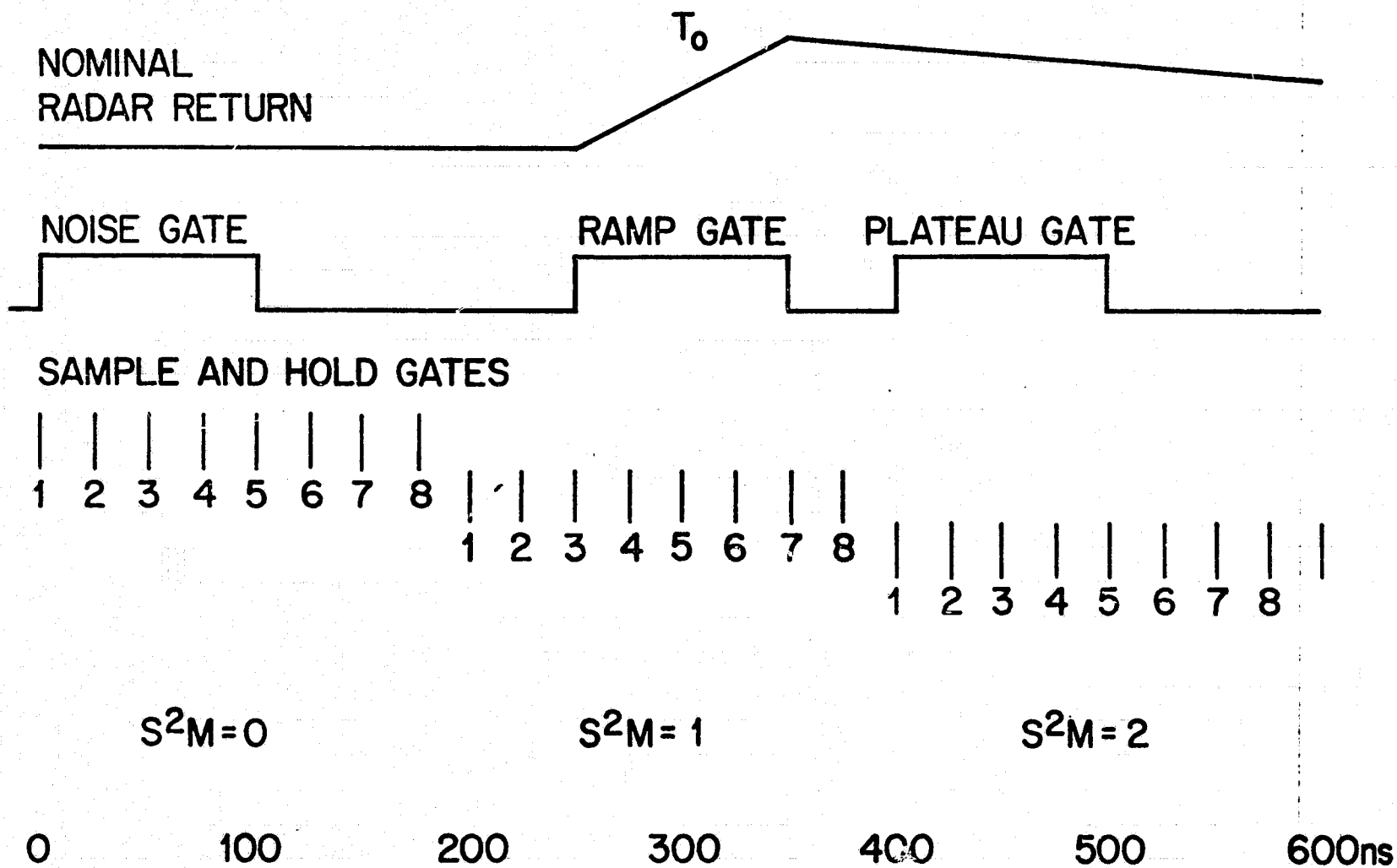

FIGURE 6. SAMPLING GATES FOR RANGE-TRACKER AND WAVEFORM.

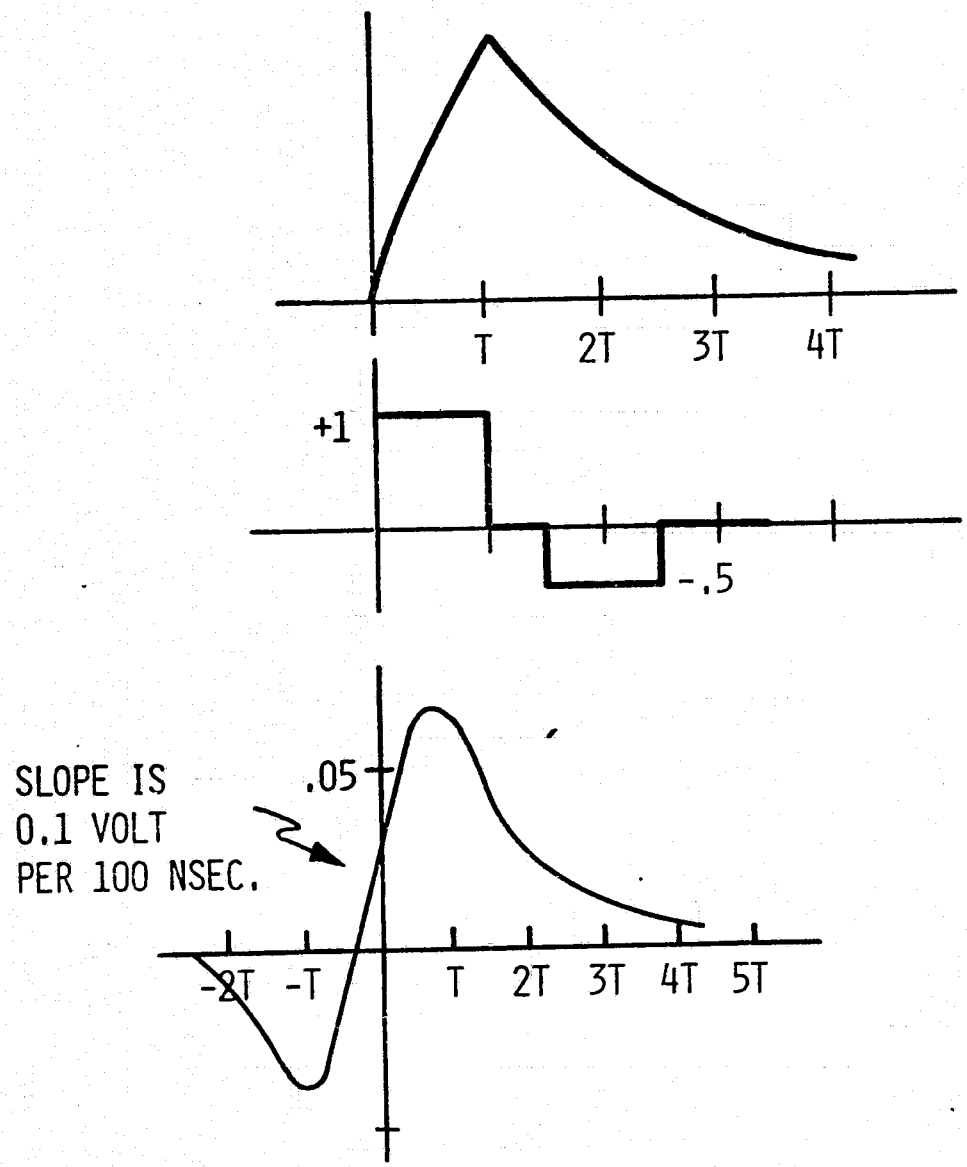

RETURN WAVESHAPE FOR 100 NSEC. PULSE AT NADIR WITH 1.5° ANTENNA BEAMWIDTH.

TRACKING GATE CONFIGURATION.

TIME DISCRIMINATOR CONTROL CURVE FOR THE WAVESHAPE AND TRACKING GATES SHOWN ABOVE.

FIGURE 7. RANGE-TRACKER GATE AND CONTROL CURVE.

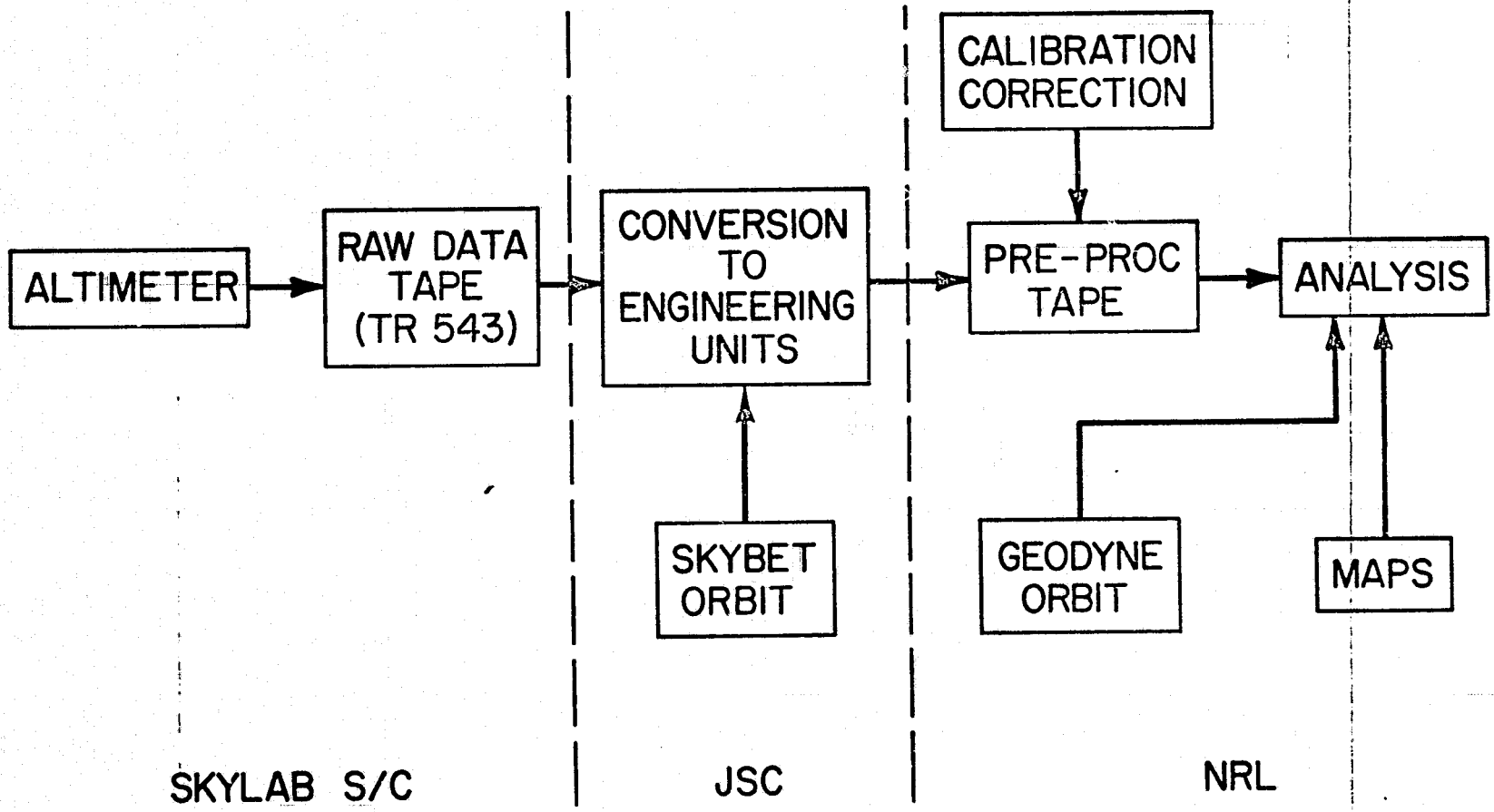

FIGURE 8. DATA FLOW DIAGRAM.

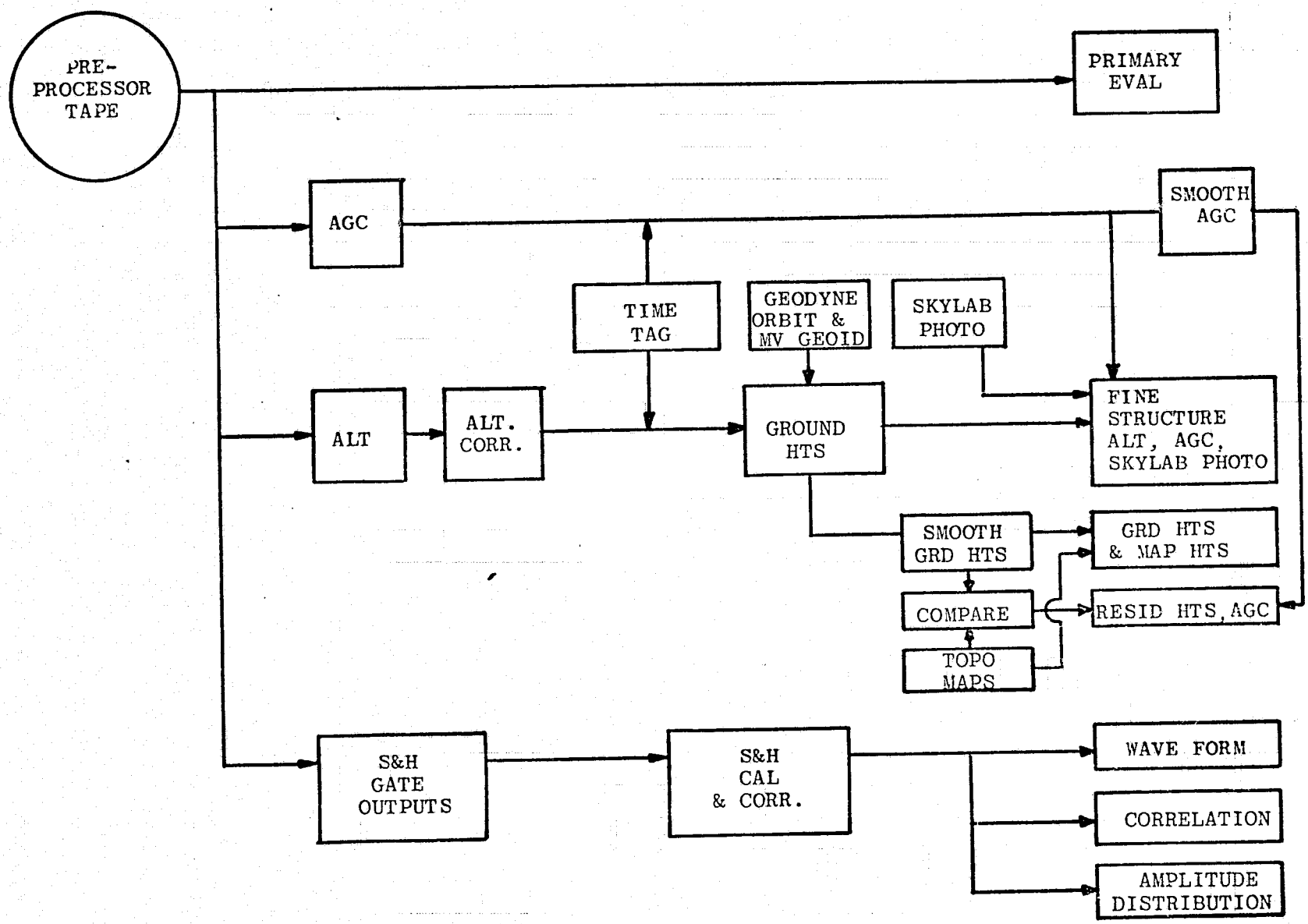

FIGURE 9. NRL DATA REDUCTION AND ANALYSIS

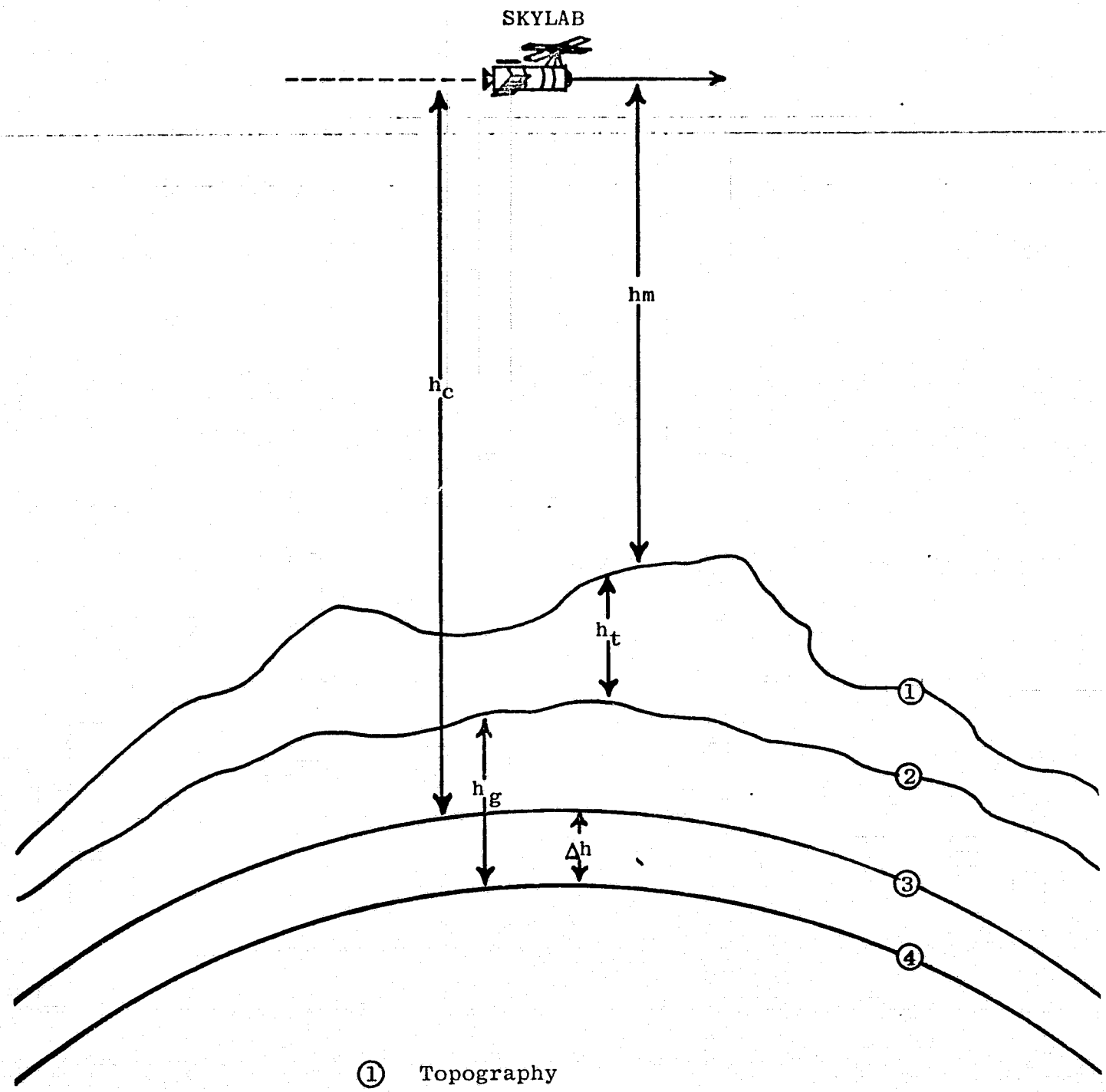

① Topography

② Geoid

③ SAO Ref. Spheroid ($r_{eq.}$ = 6,378,155)

④ Marsh Vincent Reference Spheroid ($r_{eq.}$ = 6,378,142)

FIGURE 10. SKYLAB ALTIMETRY GEOMETRY.

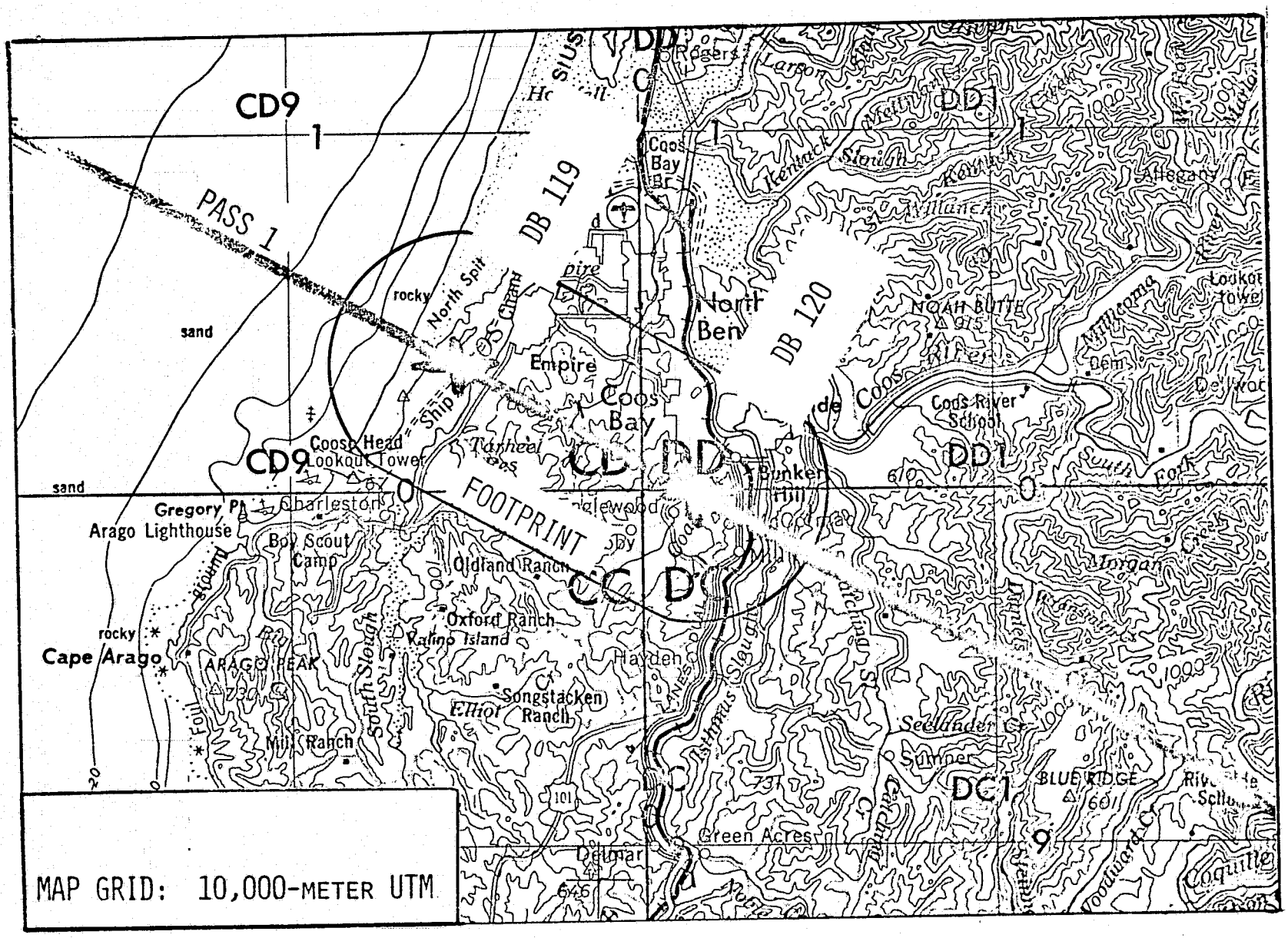

FIGURE 11. SKYLAB ALTIMETER FOOTPRINT.

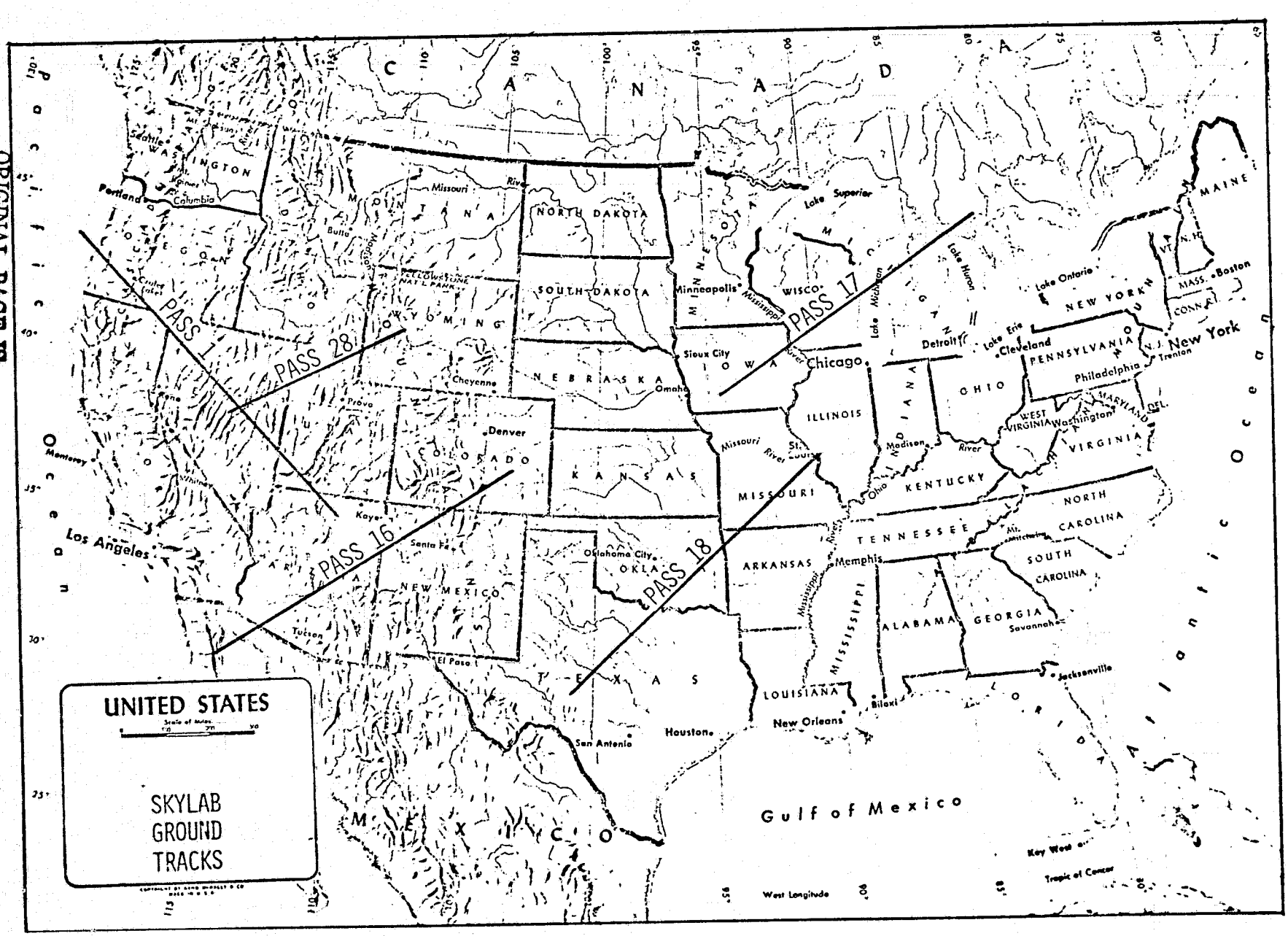

FIGURE 12. SKYLAB GROUNDTRACKS

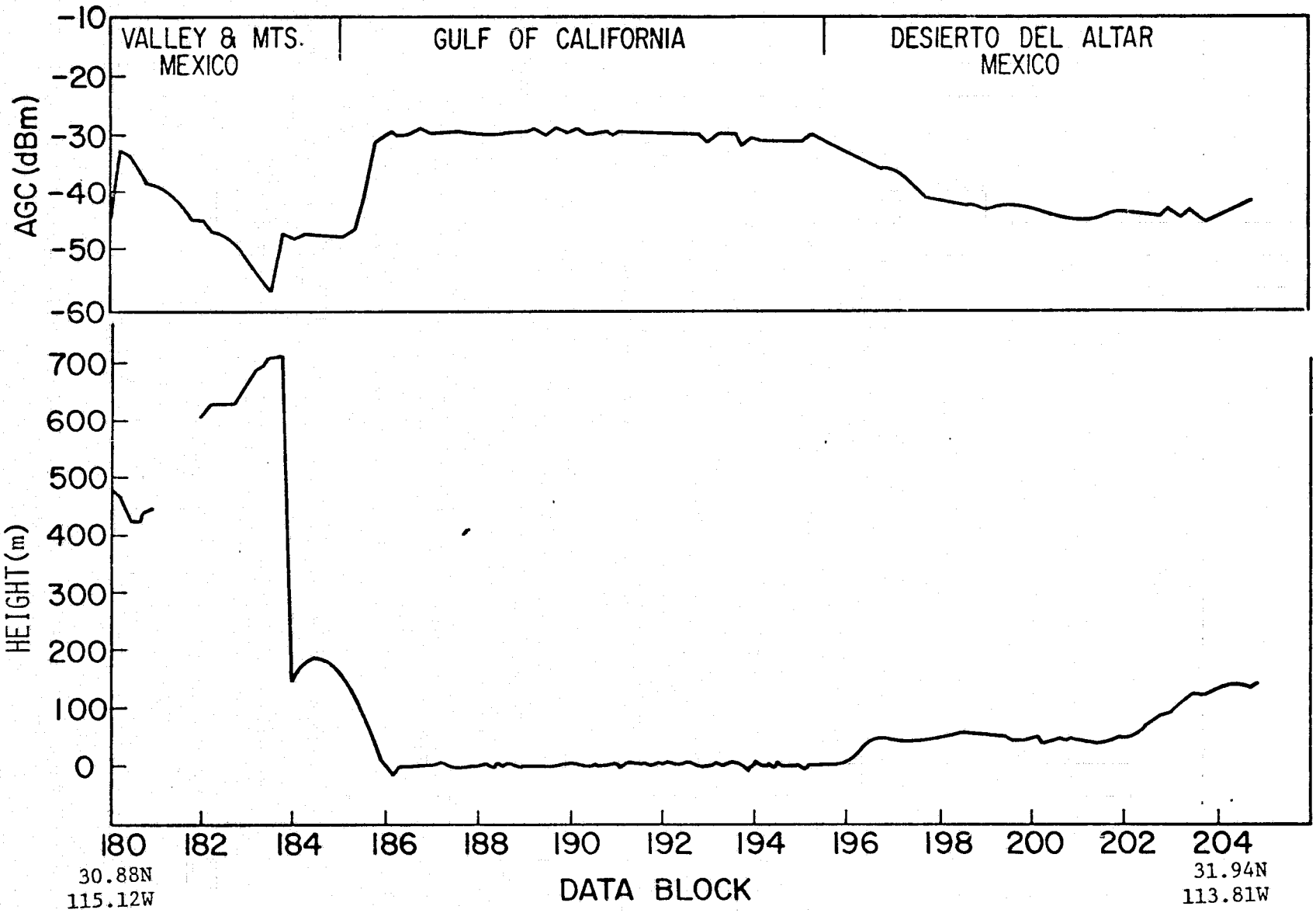

FIGURE 13. FINE-STRUCTURE AGC AND ALTIMETRY GROUND HEIGHT (PASS 16).

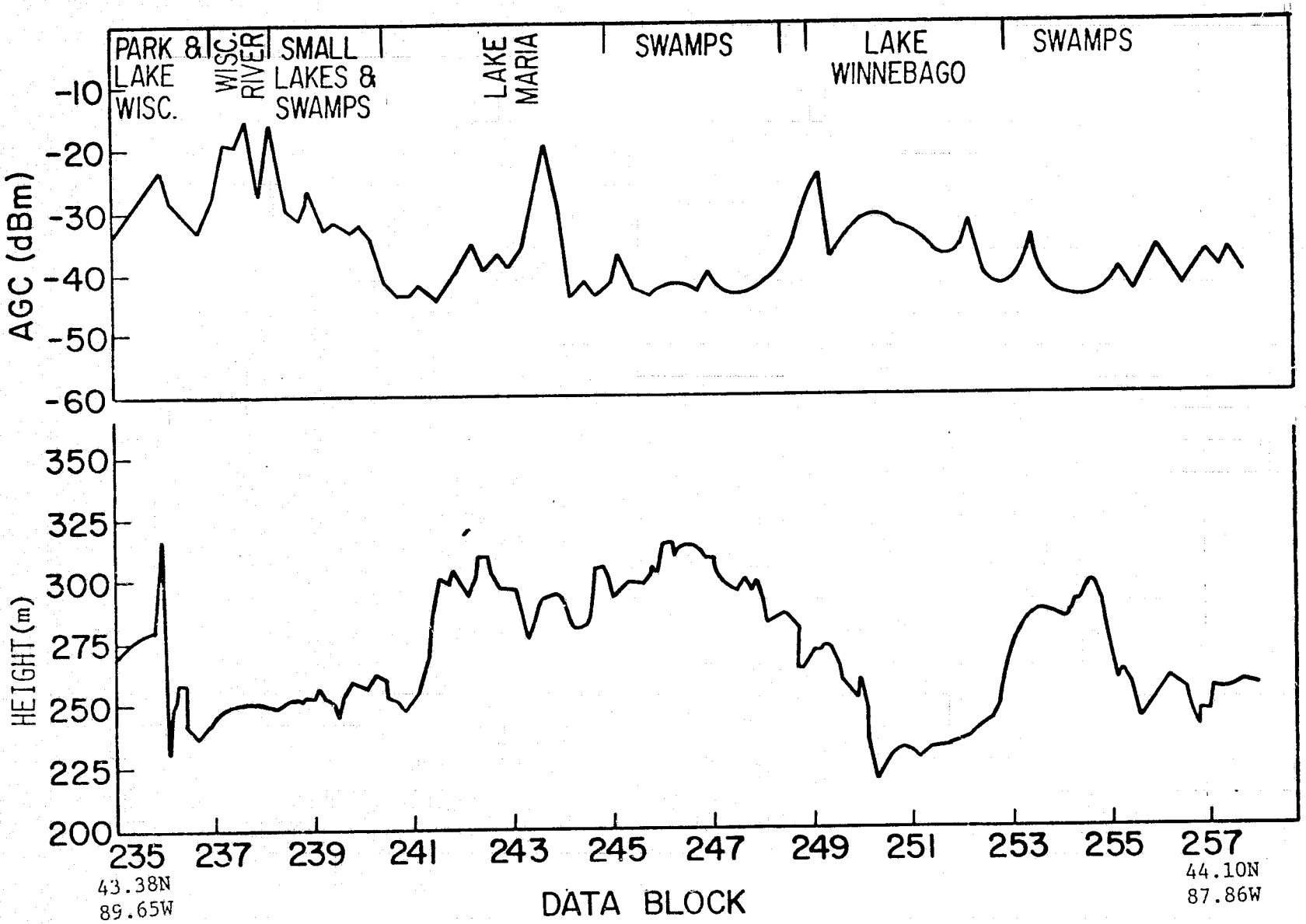

FIGURE 14. FINE-STRUCTURE AGC AND ALTIMETRY GROUND HEIGHT (PASS 17, DB235-257).

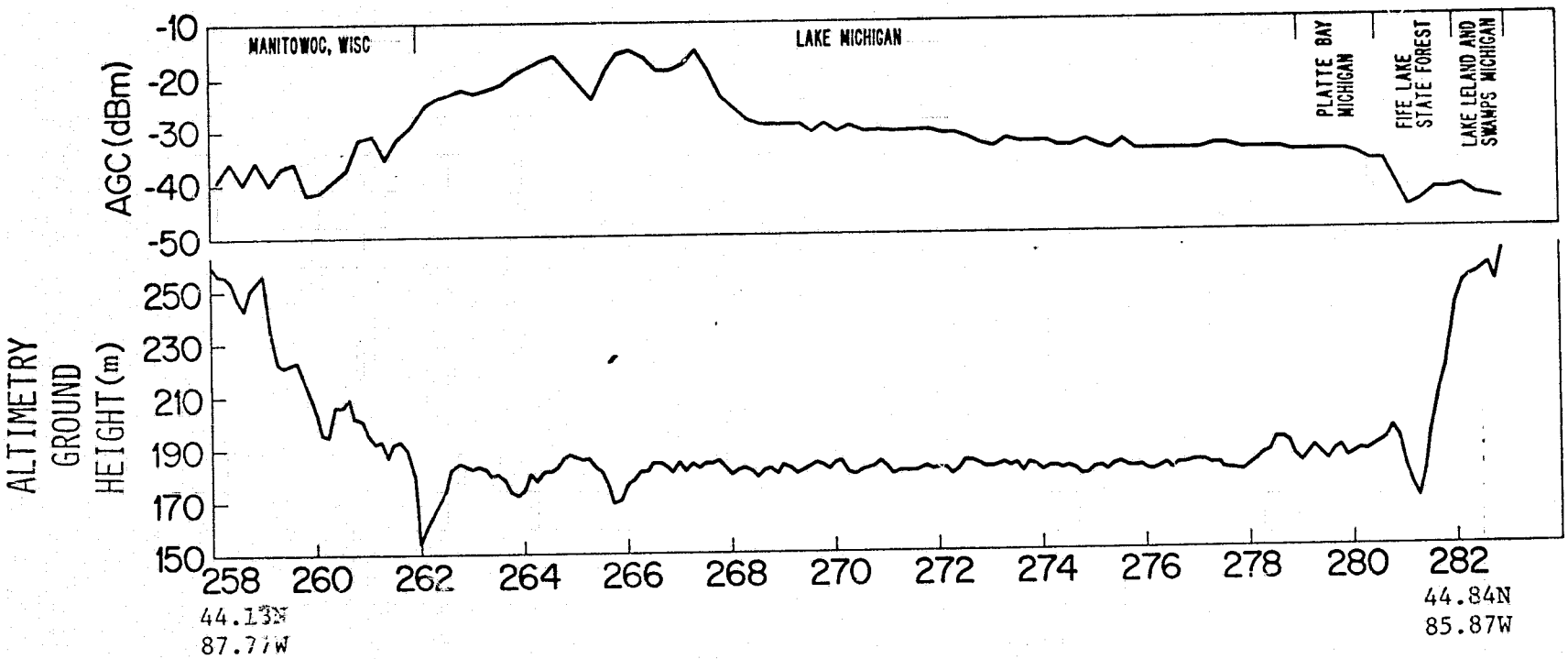

FIGURE 15. FINE-STRUCTURE AGC AND ALTIMETRY GROUND HEIGHT (PASS 17, DB258-282).

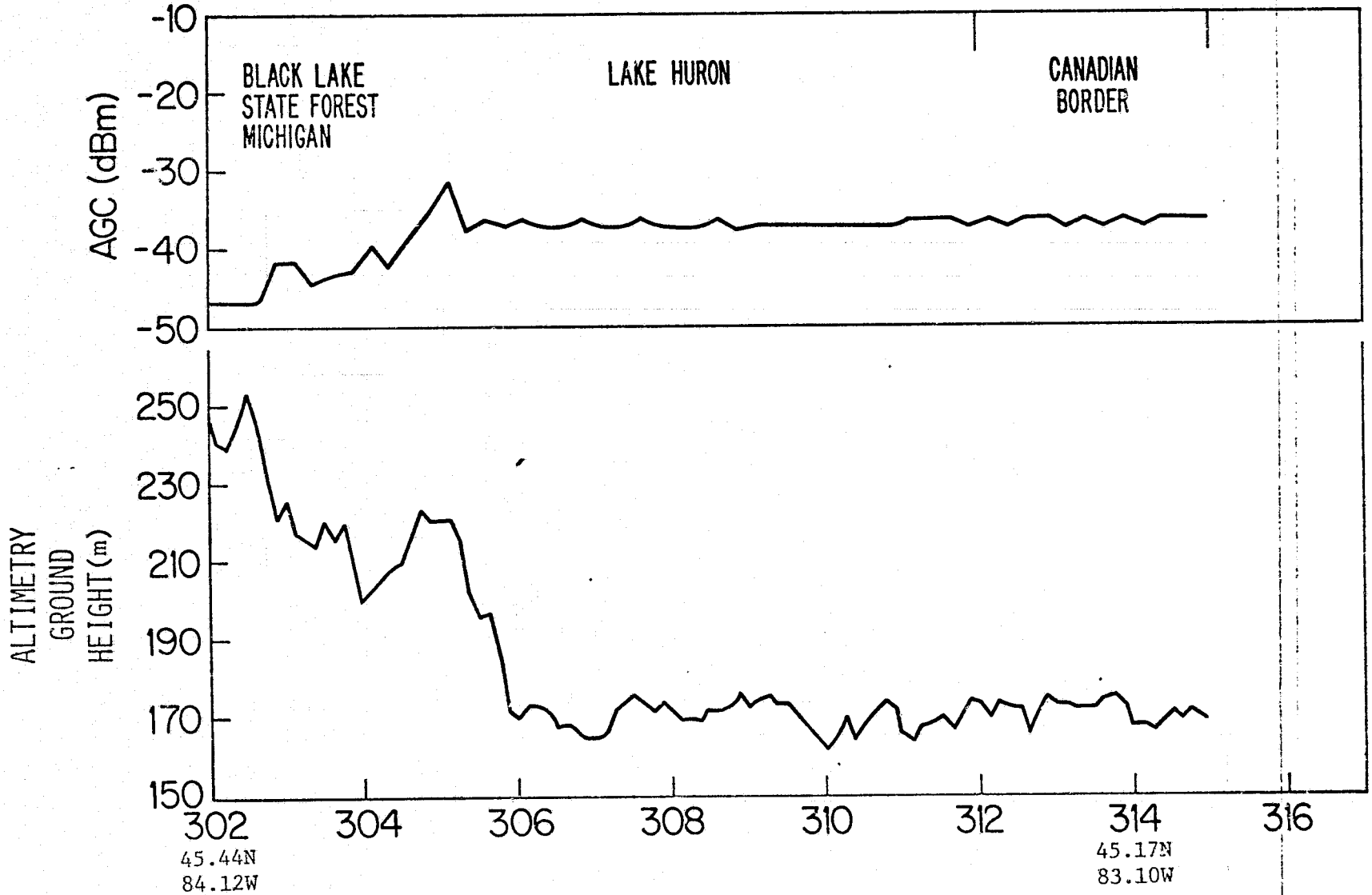

FIGURE 16. FINE-STRUCTURE AGC AND ALTIMETRY GROUND HEIGHT (PASS 17, DB302-316).

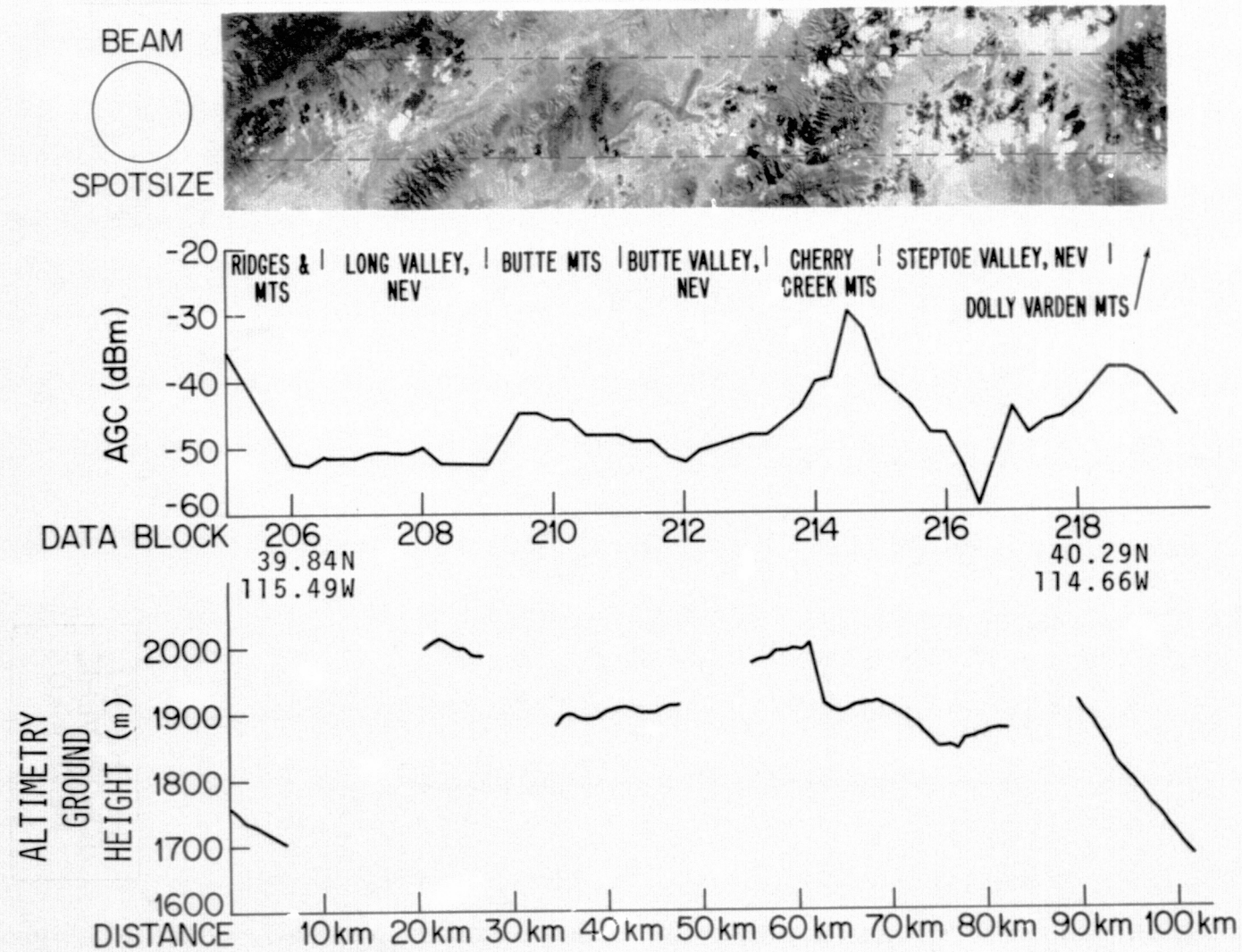

FIGURE 17. SKYLAB PHOTOGRAPHY, ALTIMETRY GROUND HEIGHTS, AND AGC (SL-3, PASS 28).

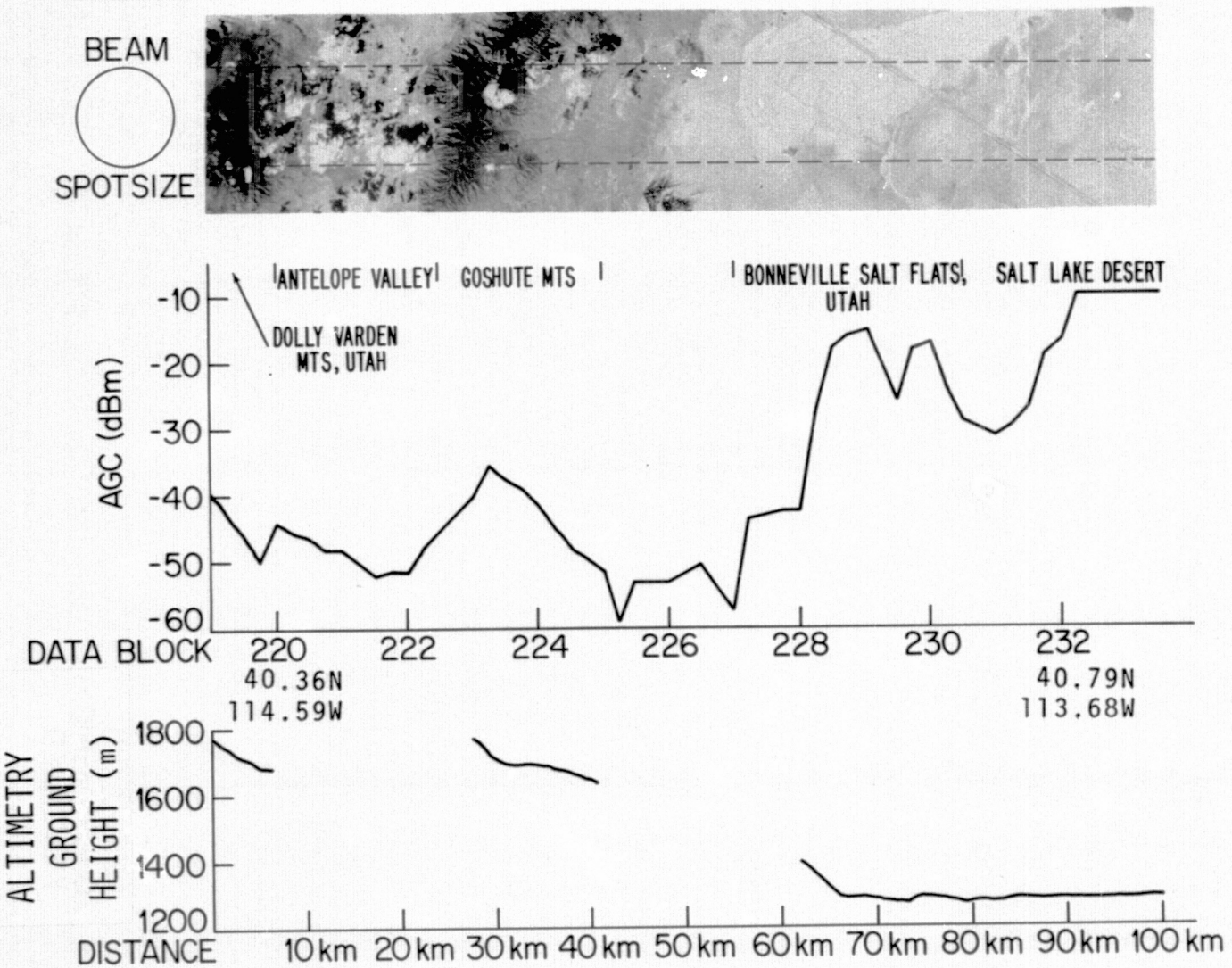

FIGURE 18. SKYLAB PHOTOGRAPHY, ALTIMETRY GROUND HEIGHTS, AND AGC (SL-3, PASS 28).

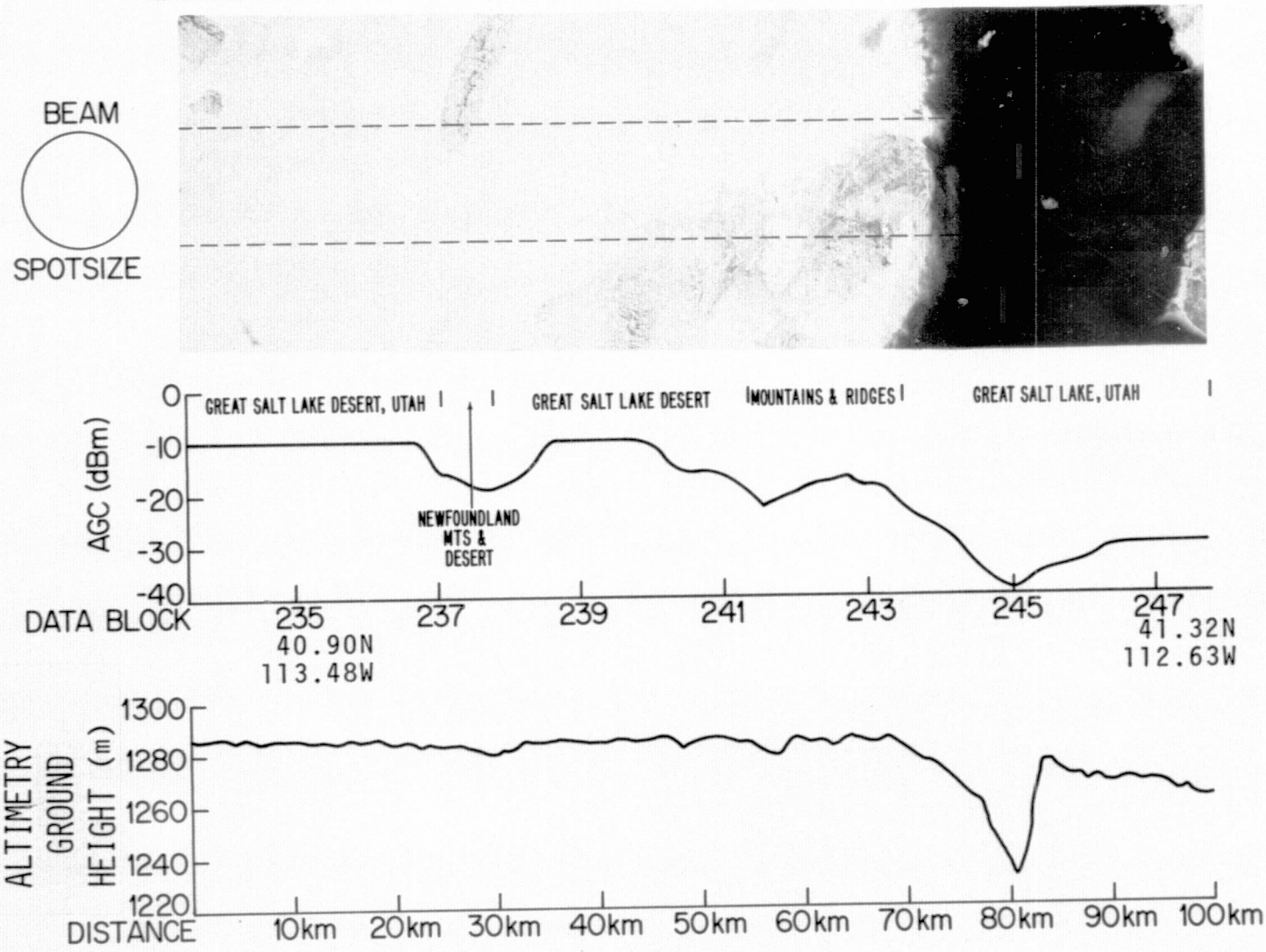

FIGURE 19. SKYLAB PHOTOGRAPHY, ALTIMETRY GROUND HEIGHTS, AND AGC (SL-3, PASS 28).

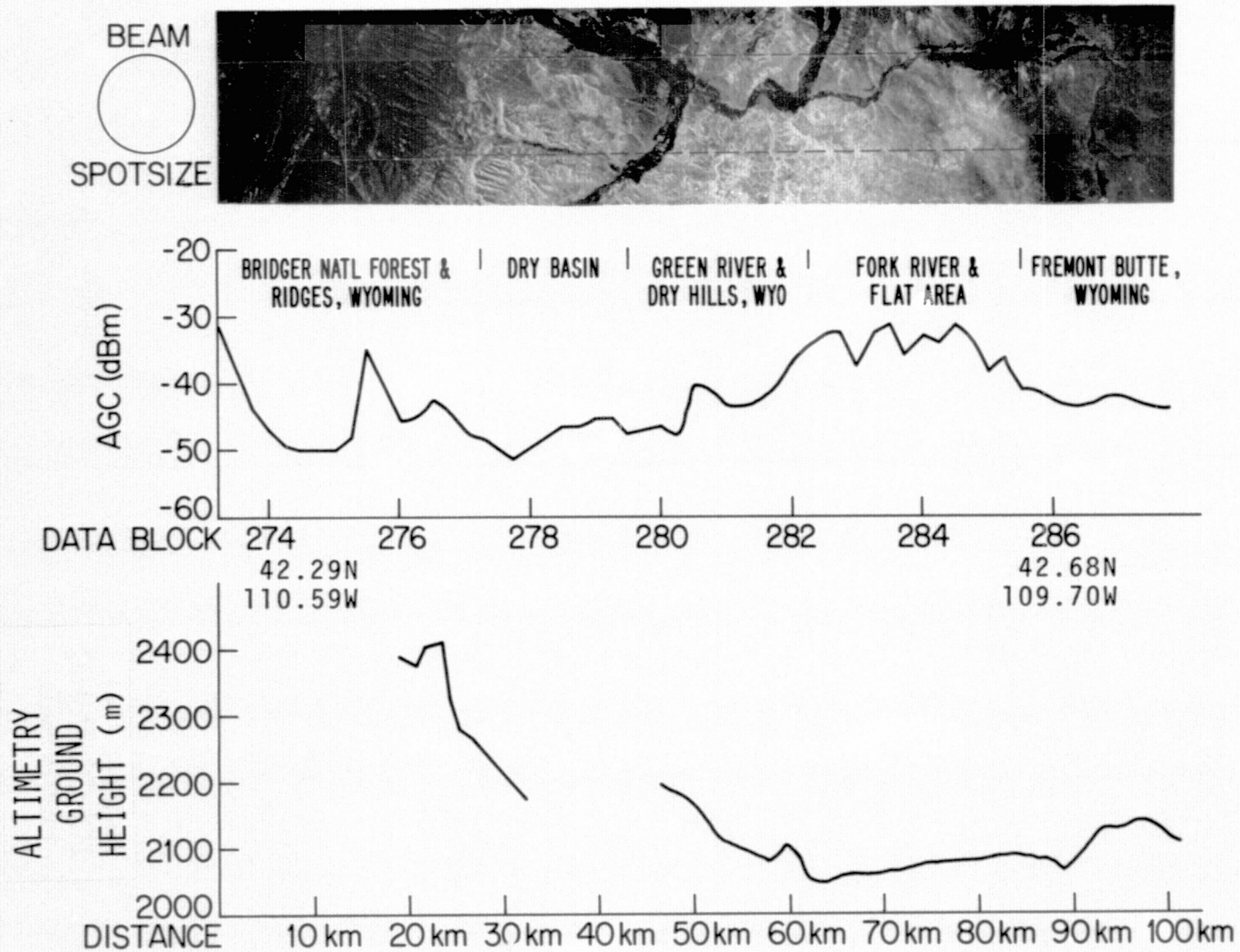

FIGURE 20. SKYLAB PHOTOGRAPHY, ALTIMETRY GROUND HEIGHTS, AND AGC (SL-3, PASS 28).

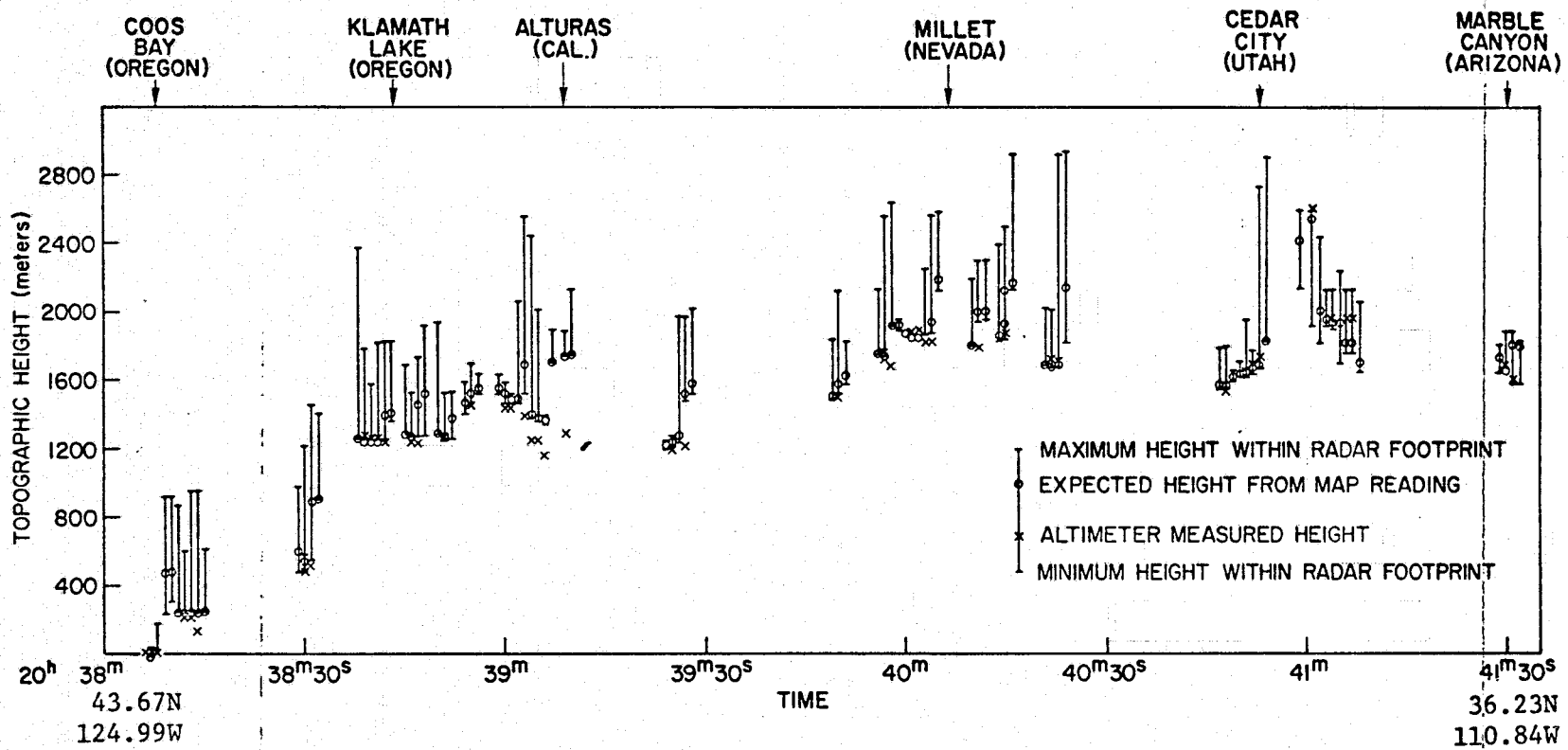

FIGURE 21. COMPARISON OF SKYLAB ALTIMETRY GROUND HEIGHTS AND TOPOGRAPHIC MAP ELEVATIONS (SL-2, PASS GT20).

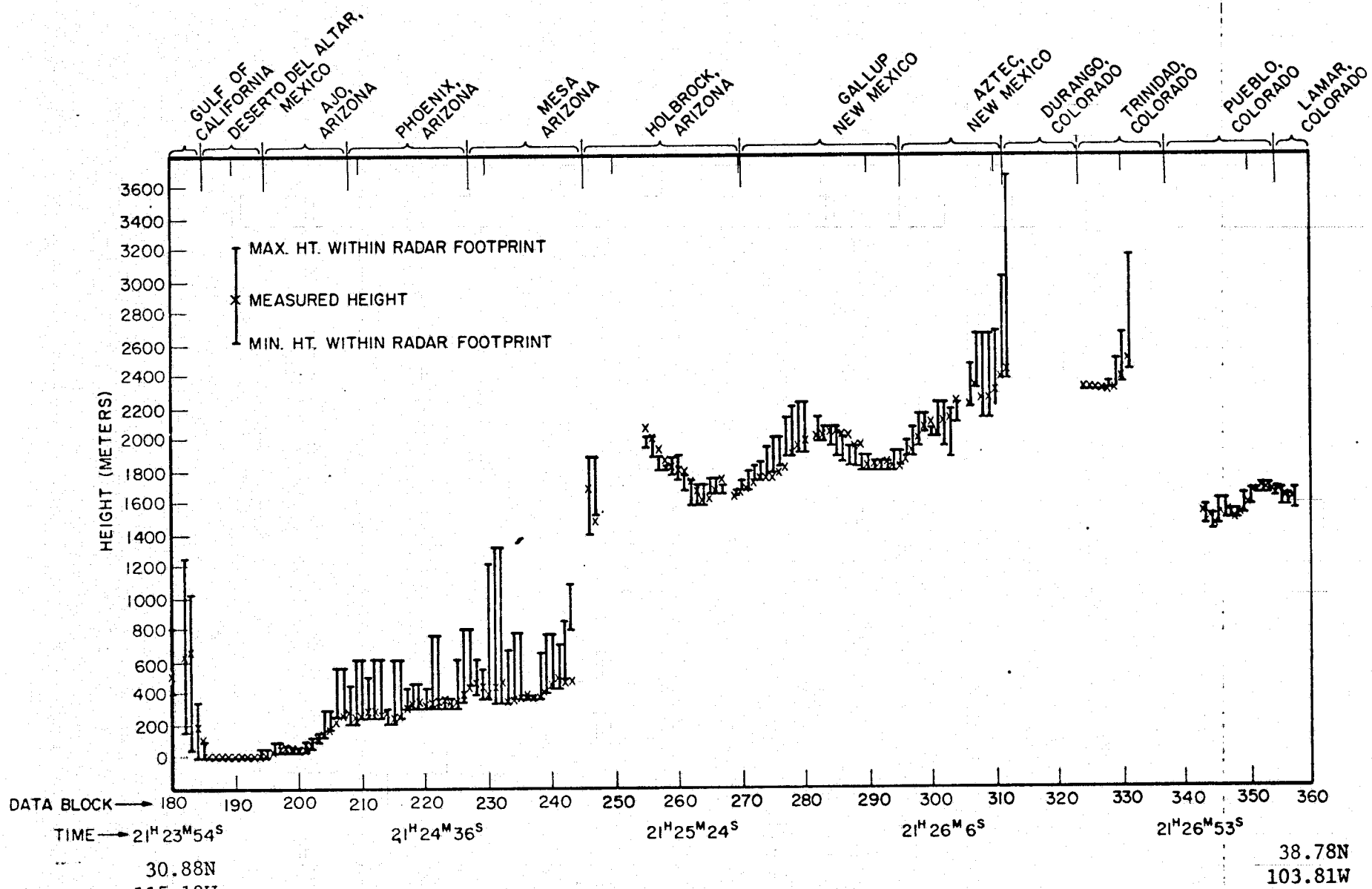

FIGURE 22. COMPARISON OF SKYLAB ALTIMETRY GROUND HEIGHTS AND TOPOGRAPHIC MAP ELEVATIONS (SL-3, PASS 16).

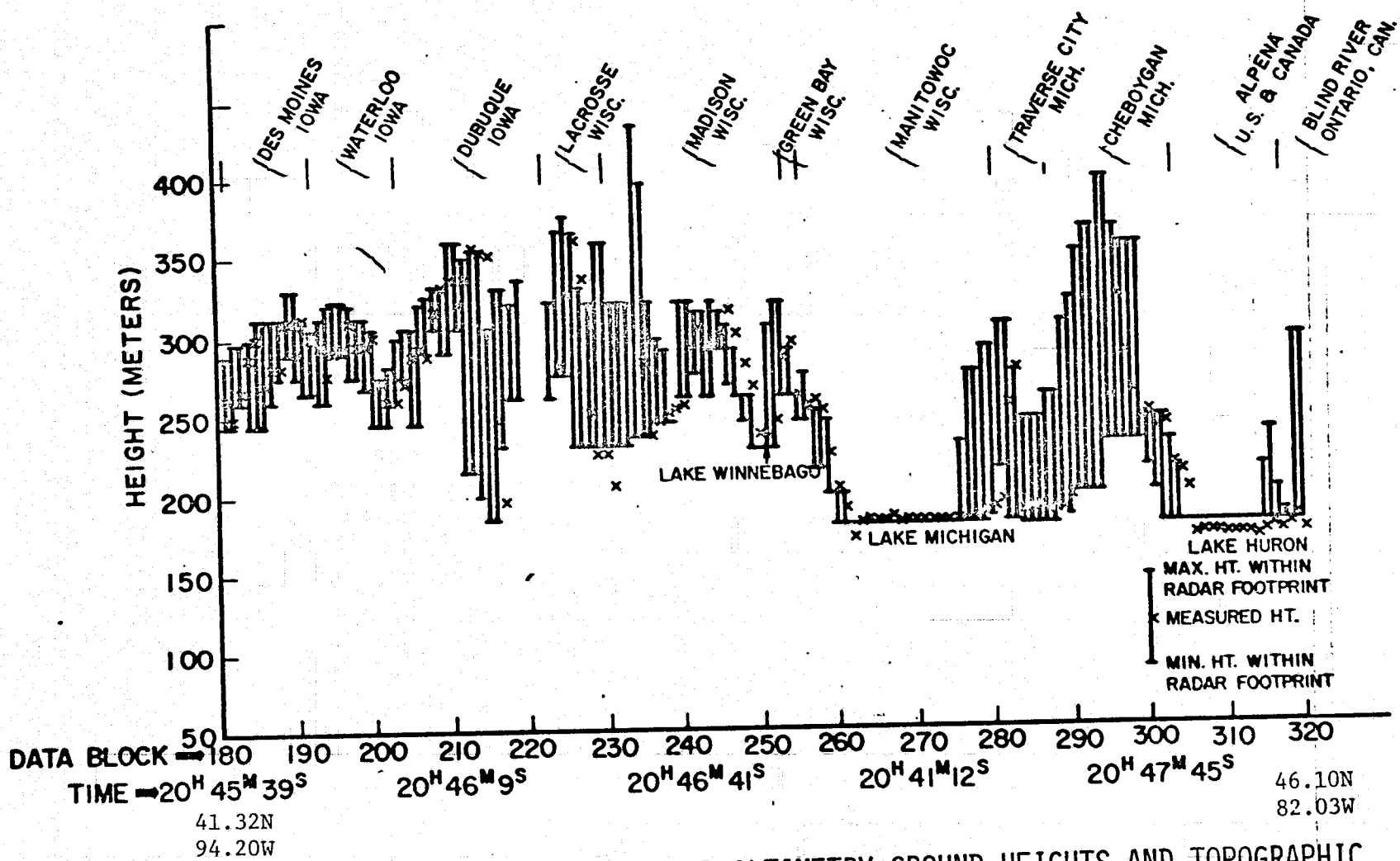

FIGURE 23. COMPARISON OF SKYLAB ALTIMETRY GROUND HEIGHTS AND TOPOGRAPHIC MAP ELEVATIONS (SL-3, PASS 17).

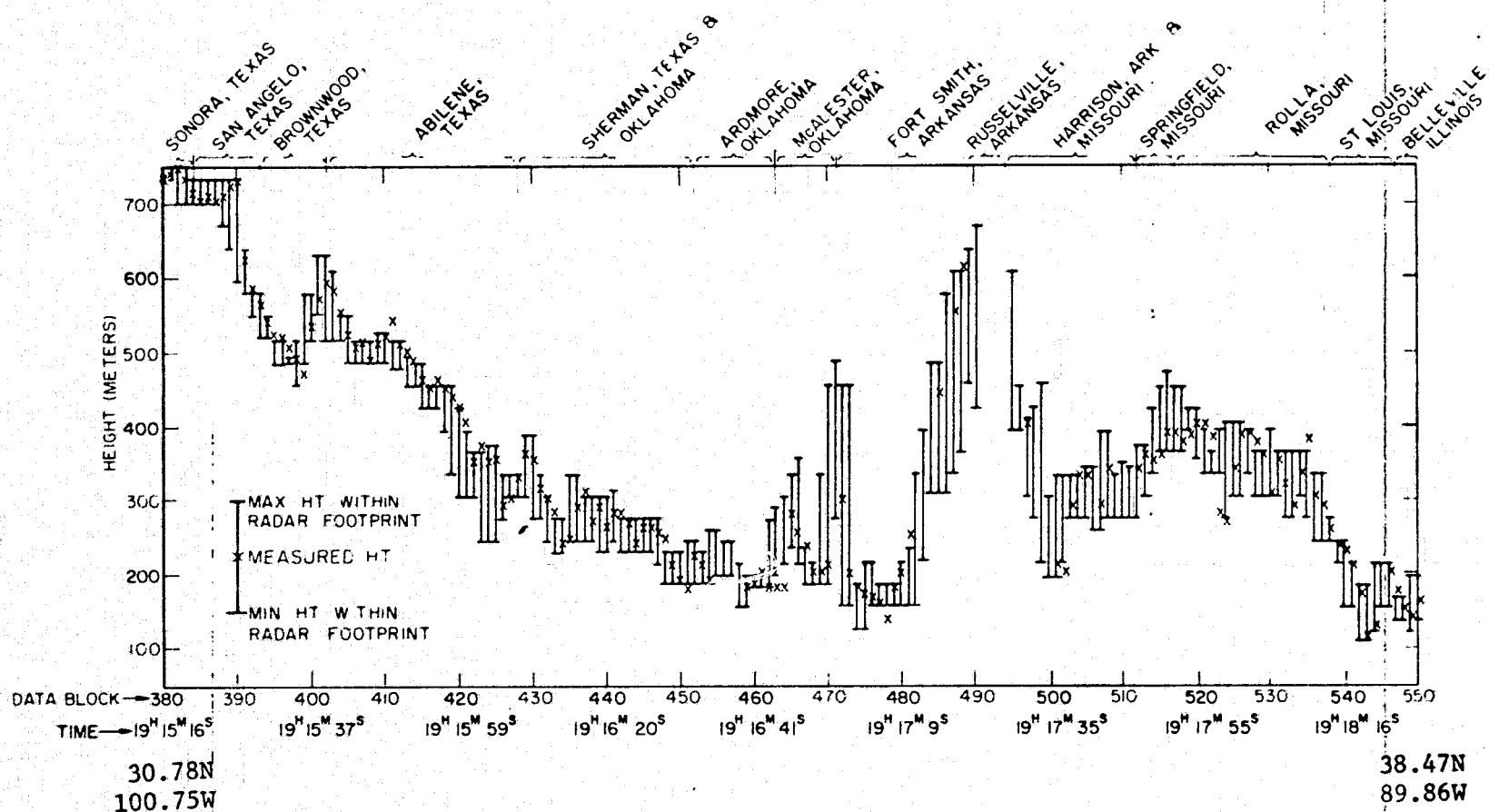

FIGURE 24. COMPARISON OF SKYLAB ALTIMETRY GROUND HEIGHTS AND TOPOGRAPHIC MAP ELEVATIONS (SL-3, PASS 18).

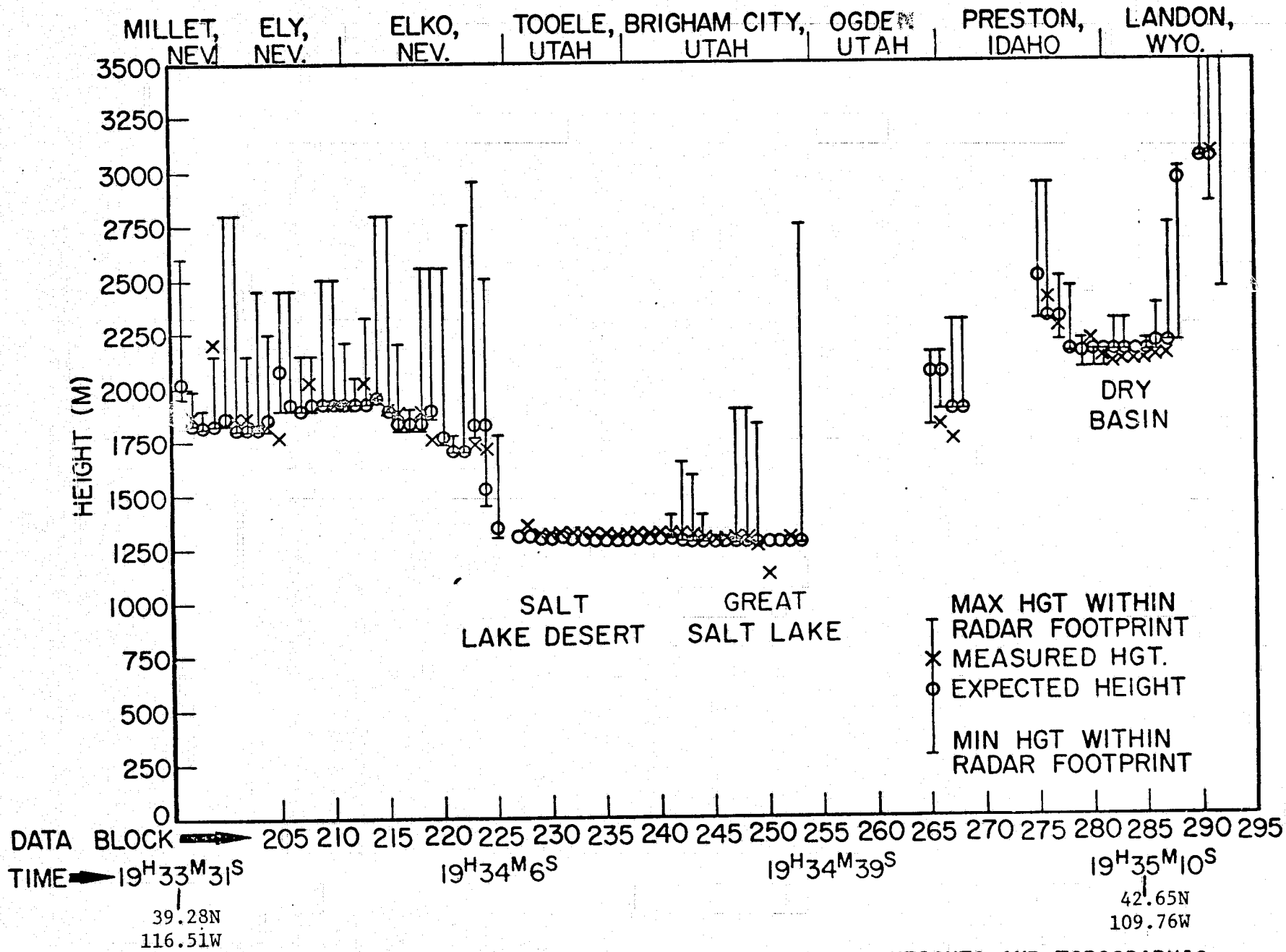

FIGURE 25. COMPARISON OF SKYLAB ALTIMETRY GROUND HEIGHTS AND TOPOGRAPHIC MAP ELEVATIONS (SL-3, PASS 28).

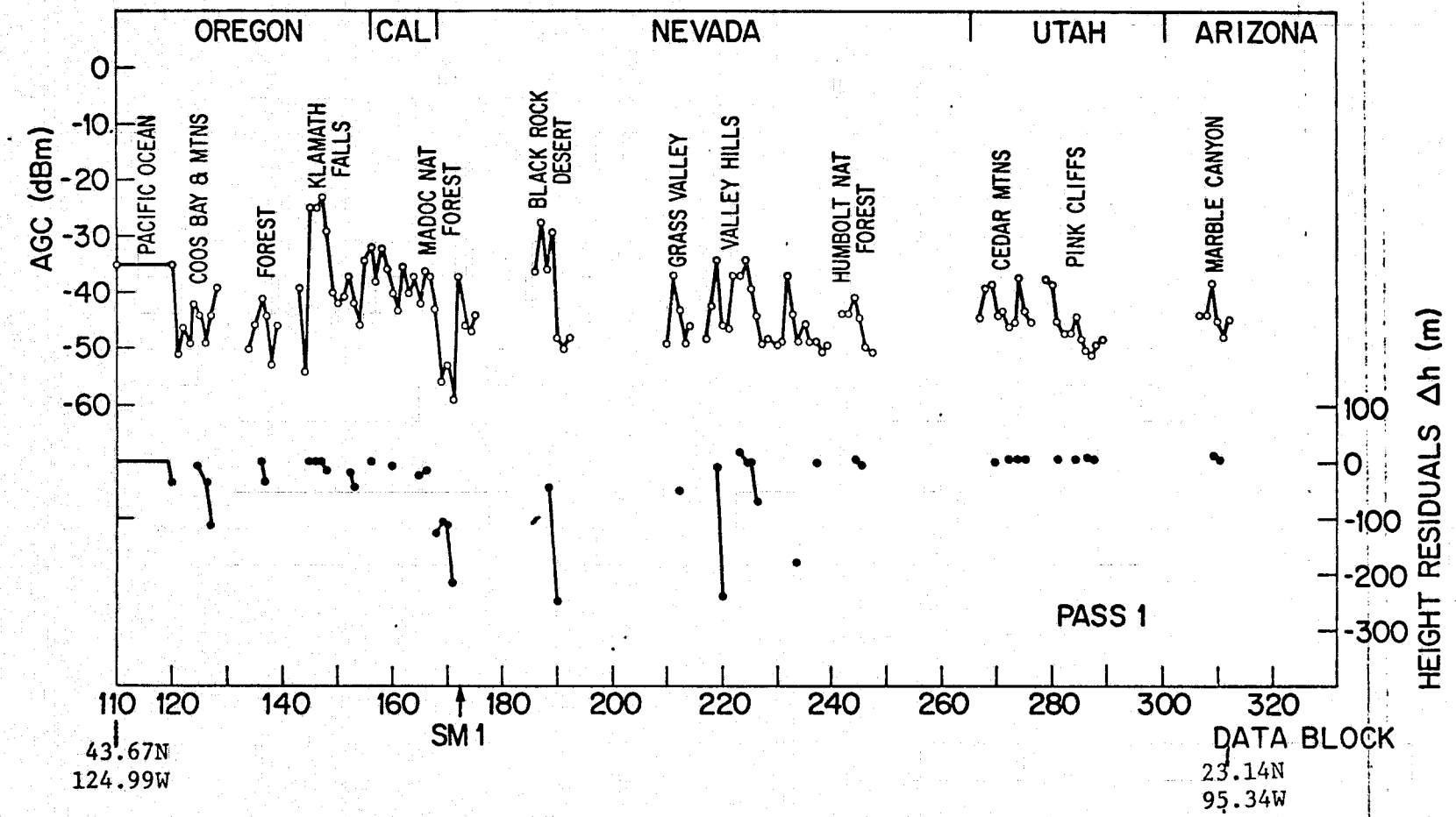

FIGURE 26. AGC AND TOPOGRAPHIC HEIGHT RESIDUALS (SL-2, PASS 1).

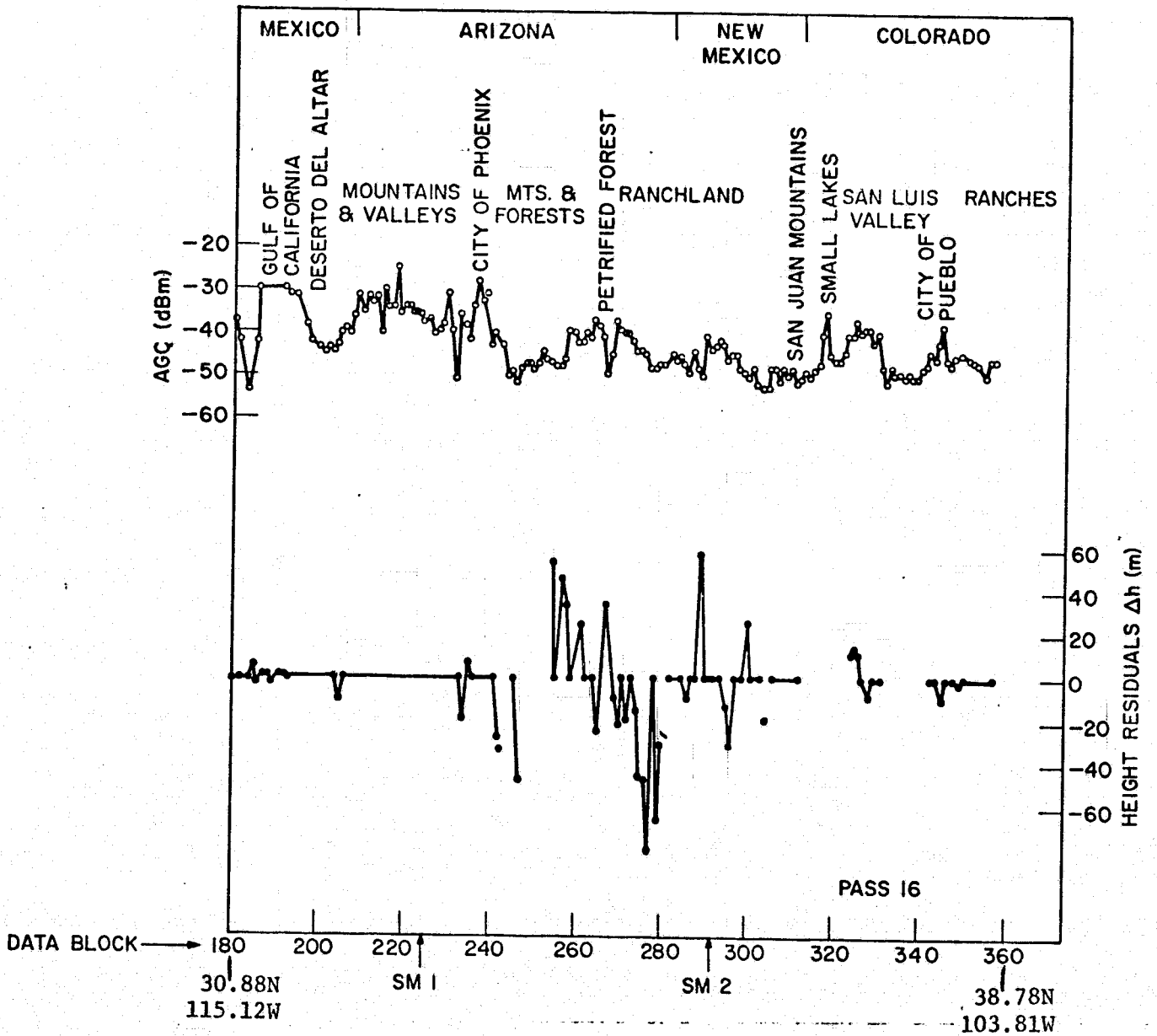

FIGURE 27. AGC AND TOPOGRAPHIC HEIGHT RESIDUALS (SL-3, PASS 16).

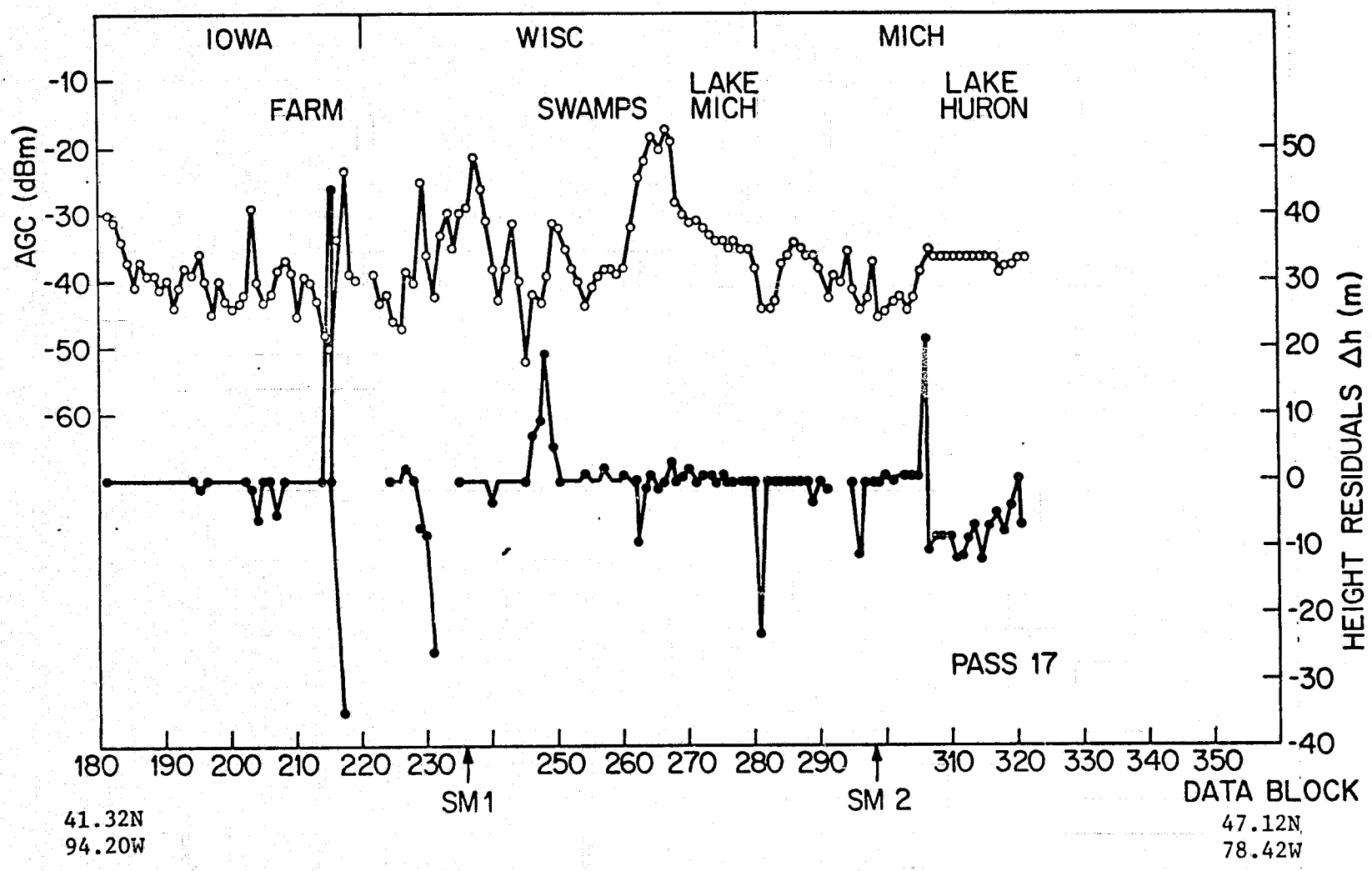

FIGURE 28. AGC AND TOPOGRAPHIC HEIGHT RESIDUALS (SL-3, PASS 17).

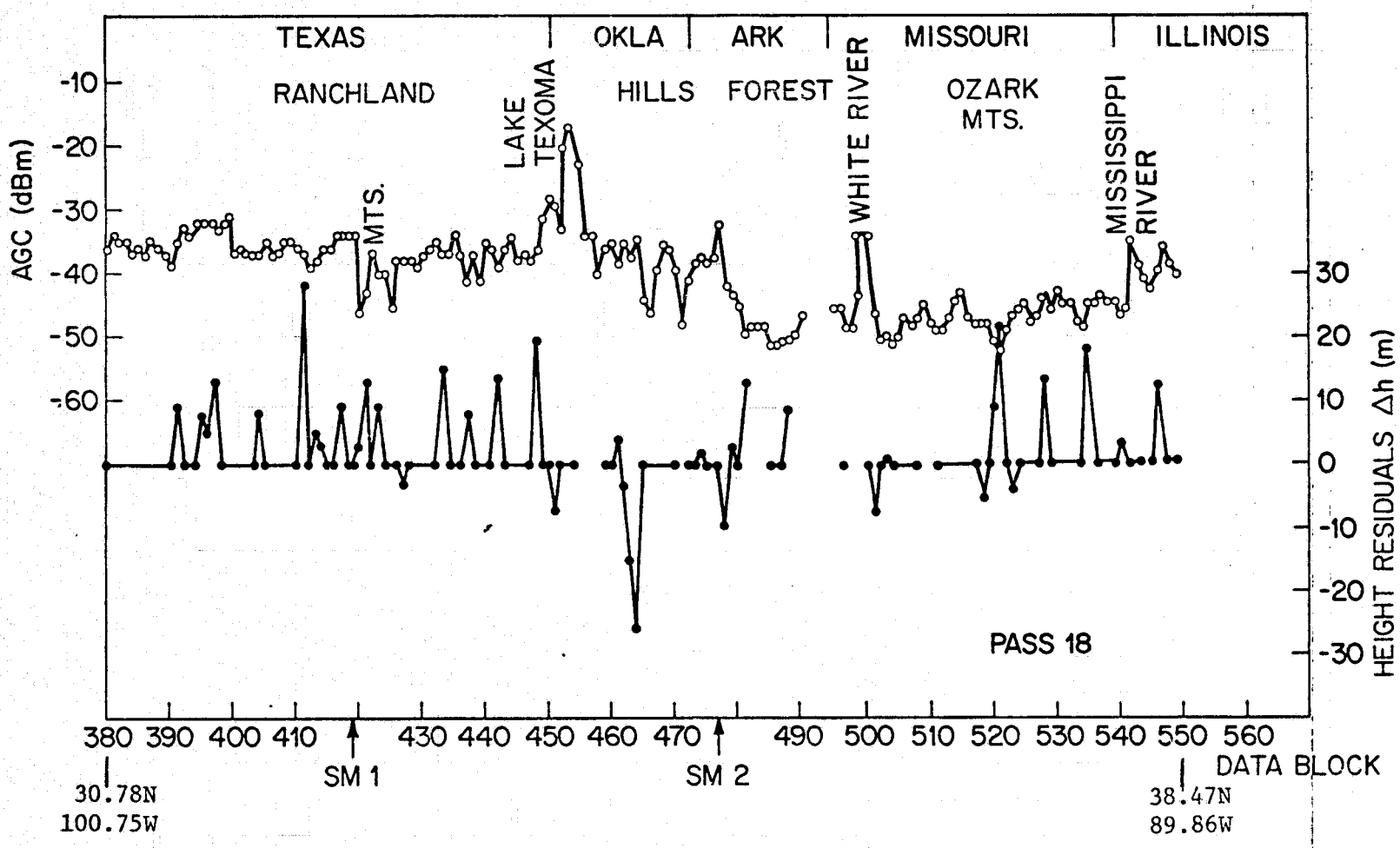

FIGURE 29. AGC AND TOPOGRAPHIC HEIGHT RESIDUALS (SL-3, PASS 18).

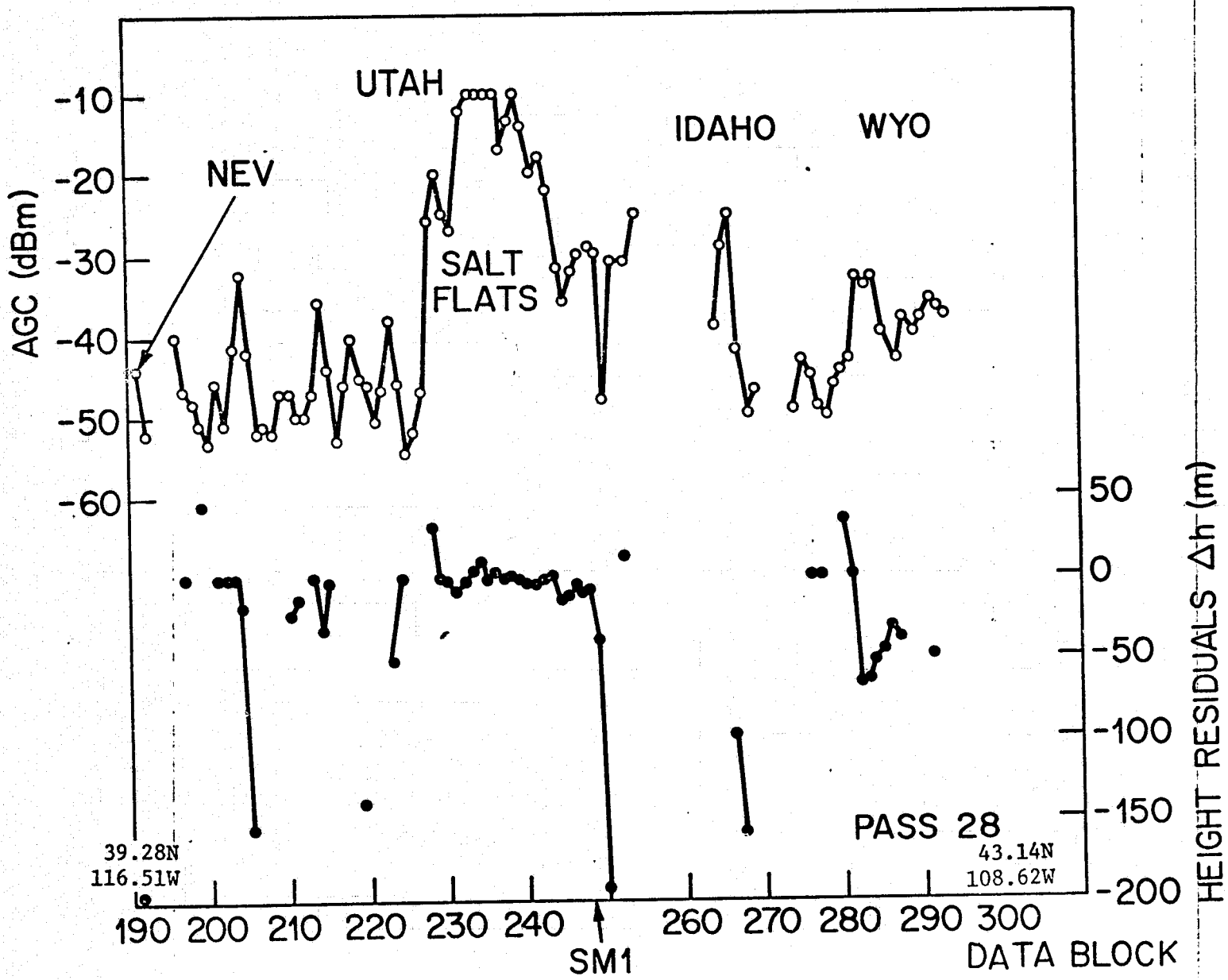

FIGURE 30. AGC AND TOPOGRAPHIC HEIGHT RESIDUALS (SL-3, PASS 28).

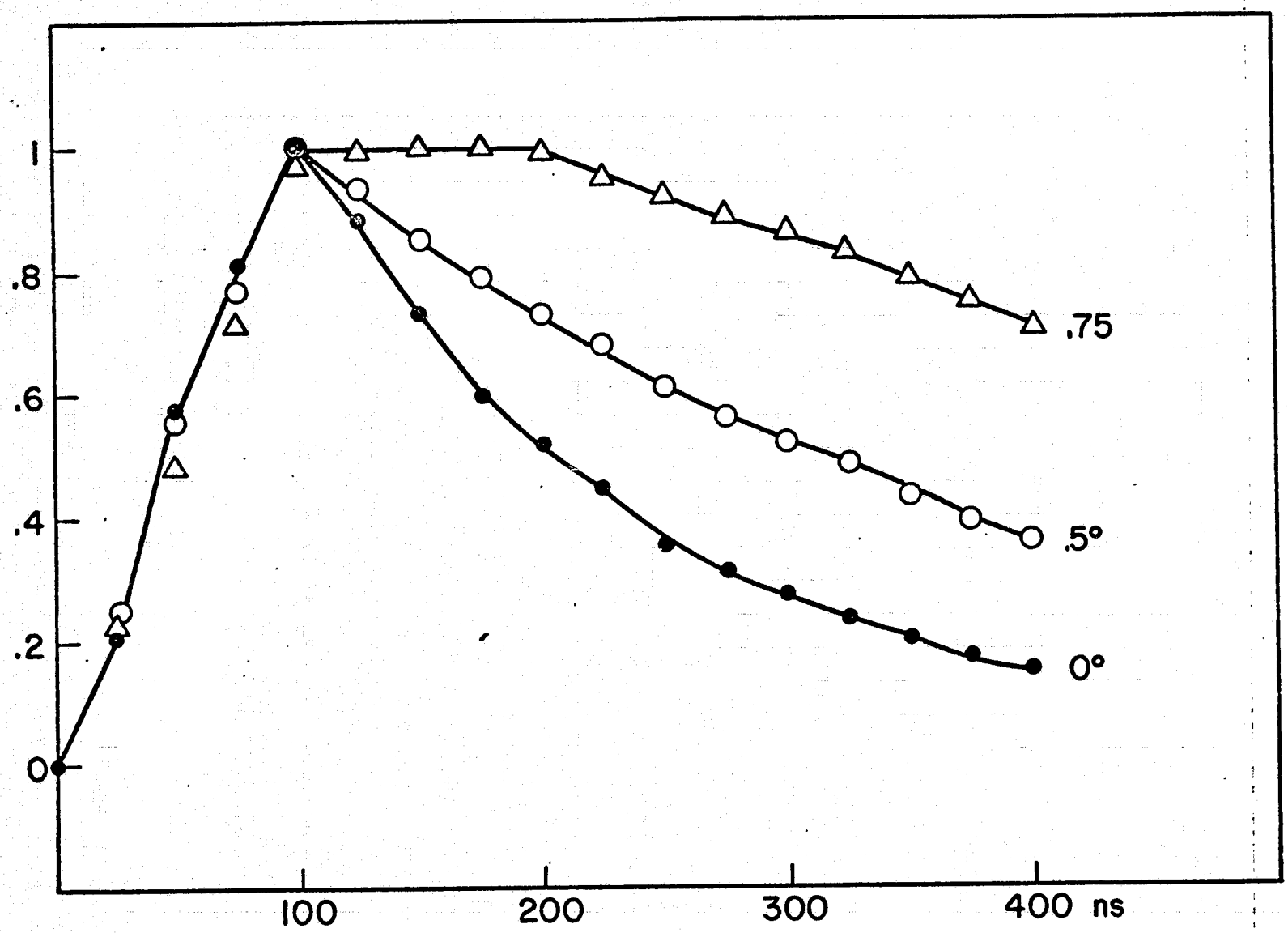

FIGURE 31. THEORETICAL OCEAN RADAR RETURN FOR OFF-NADIR ANGLE OF 0°, .5° AND .75°.

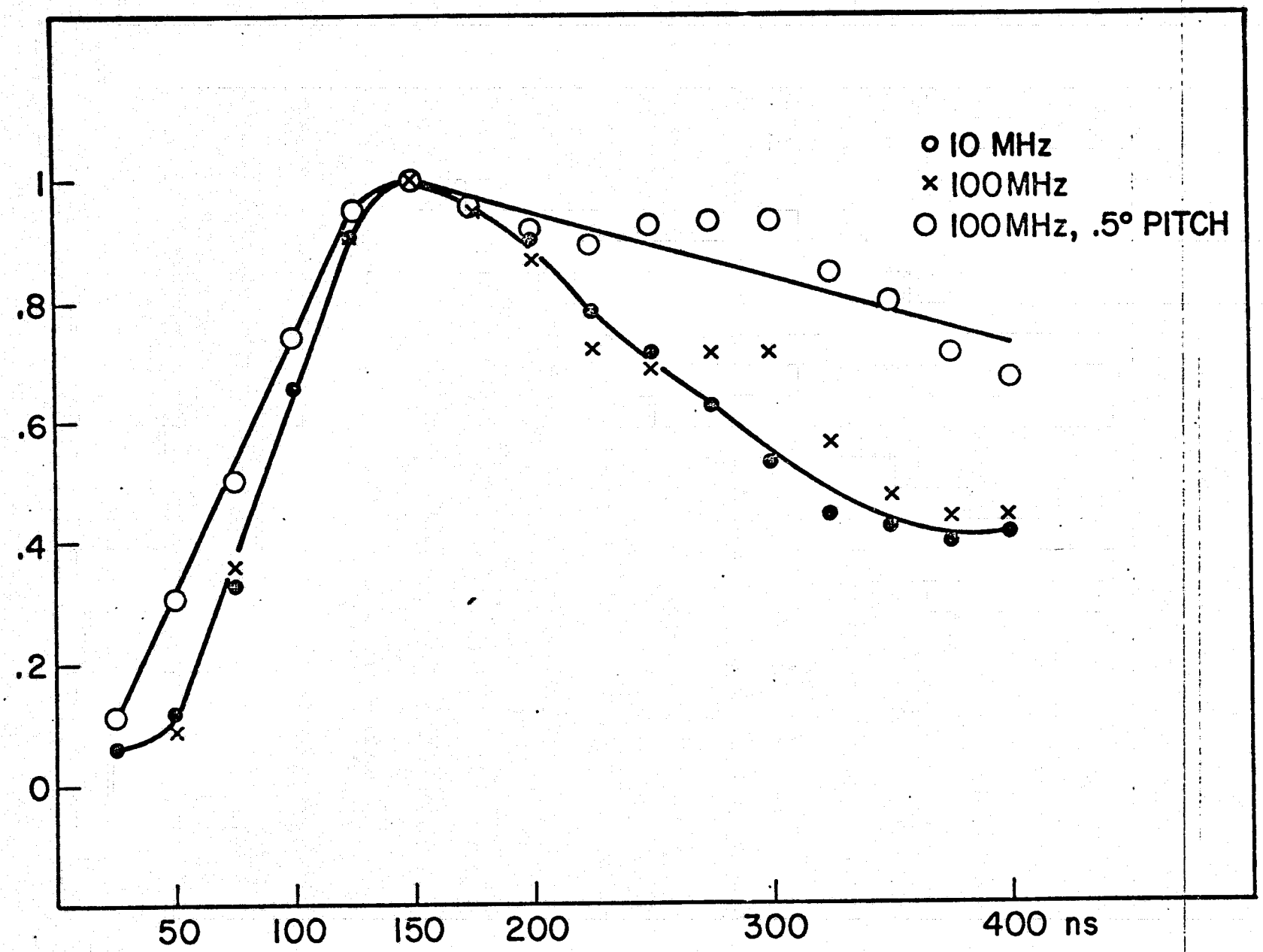

FIGURE 32. OCEAN RADAR RETURN PASS 11 (SL-3) DB 707-708, 759-760, 815-816.

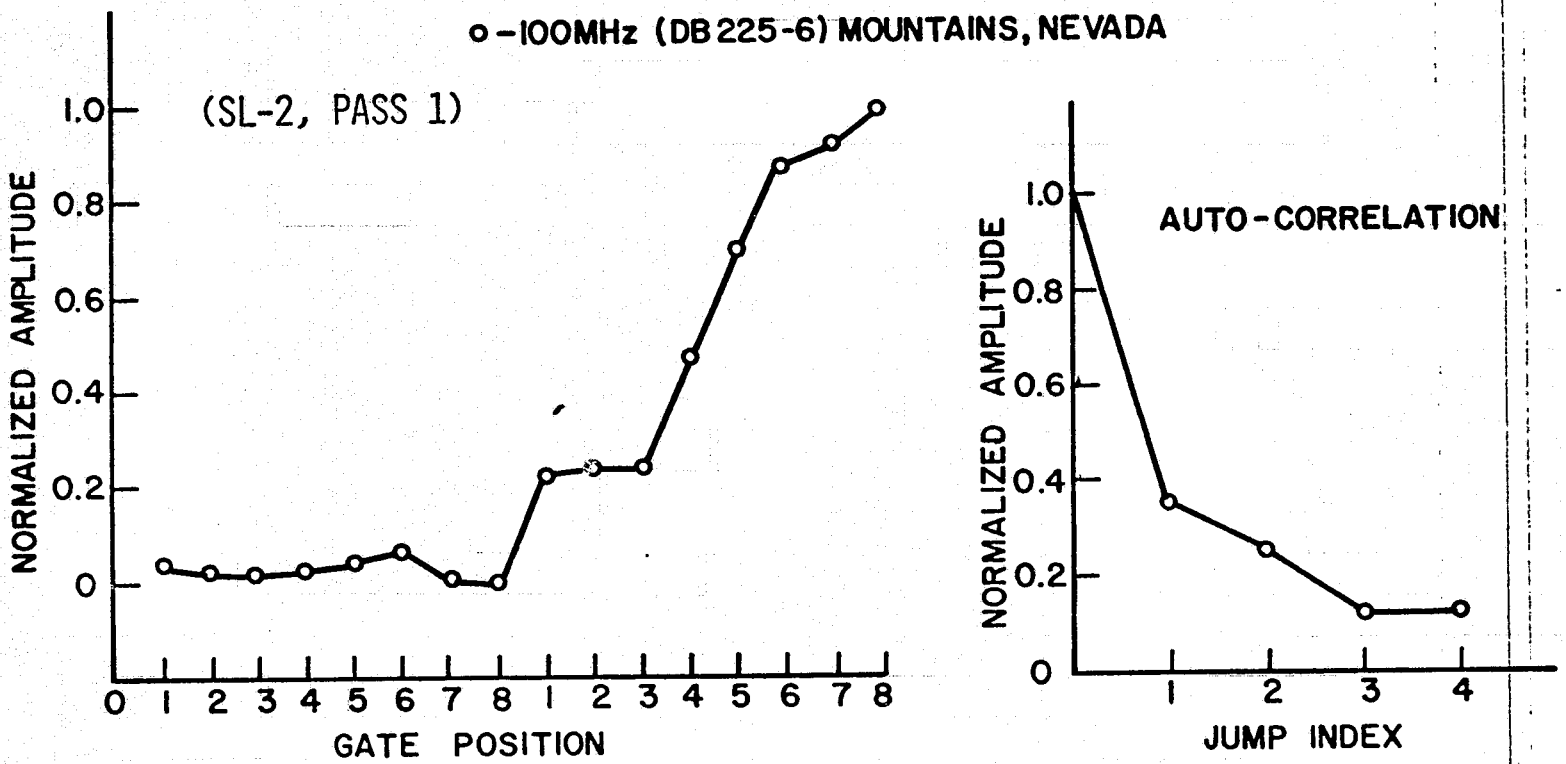

FIGURE 33. TERRAIN WAVEFORMS, NOISE AND RAMP GATES (SL-2, PASS 1).

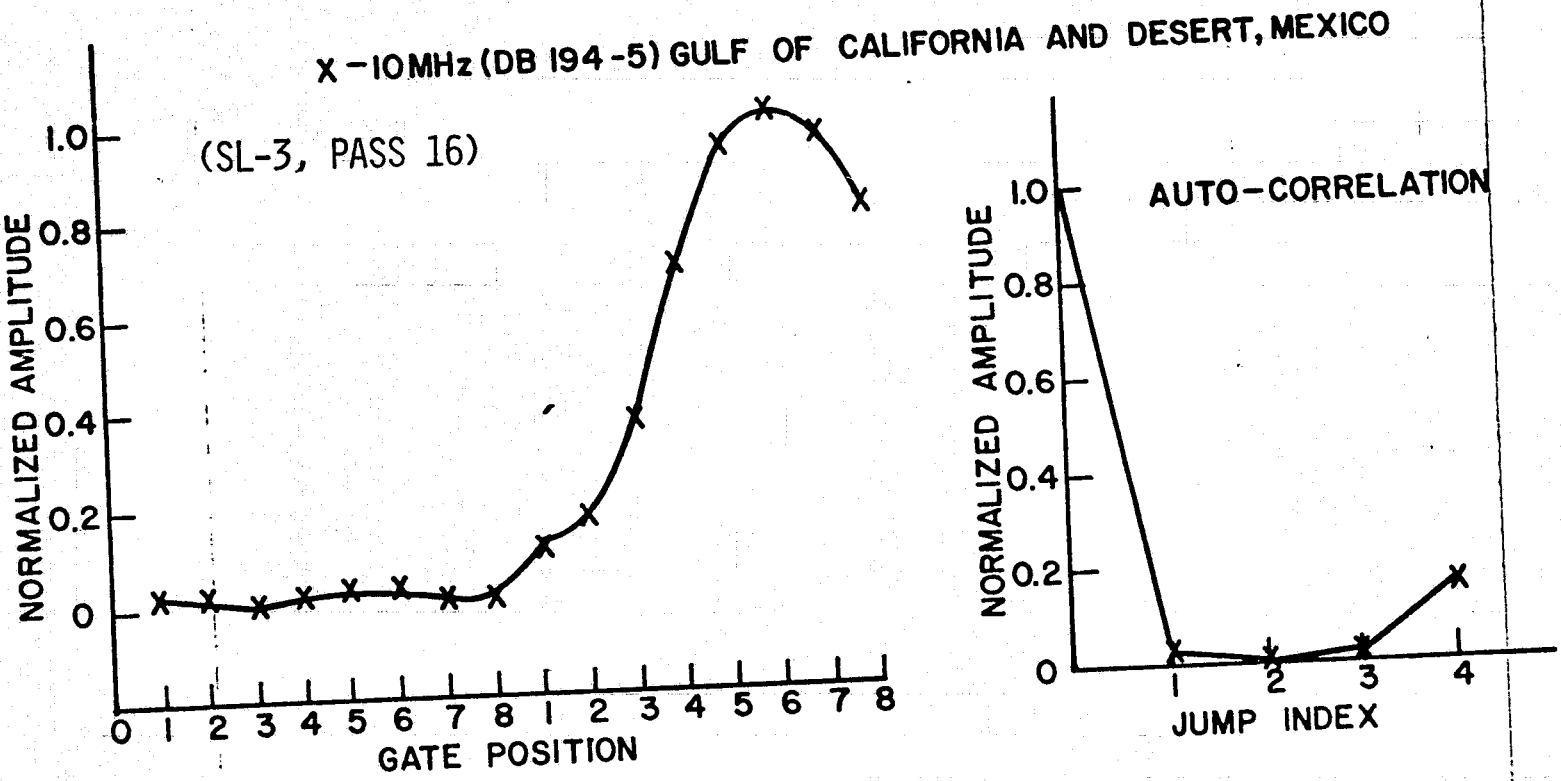

FIGURE 34. TERRAIN WAVEFORMS, NOISE AND RAMP GATES (SL-3, PASS 16).

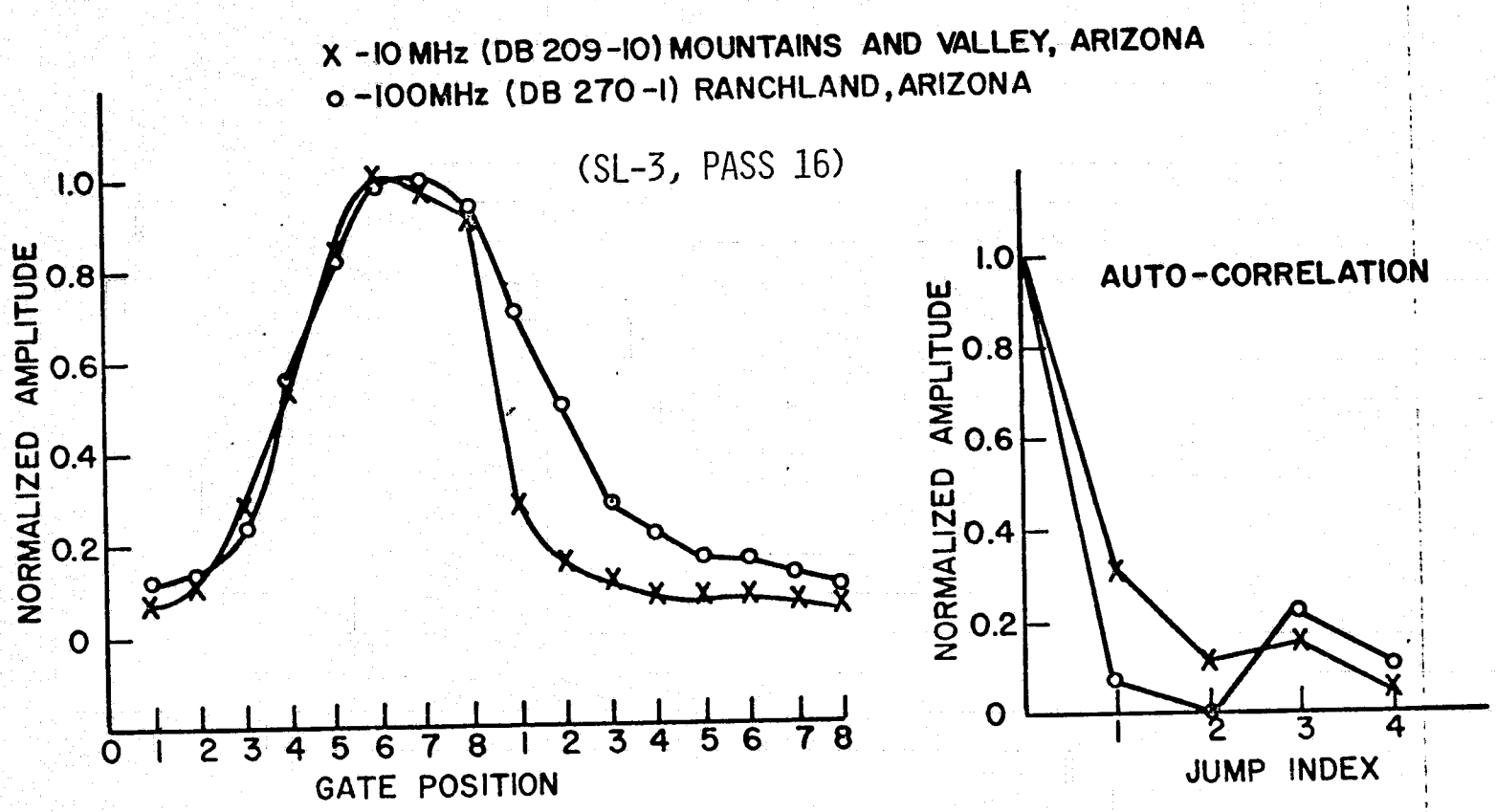

FIGURE 35. TERRAIN WAVEFORMS, RAMP AND PLATEAU GATES (SL-3, PASS 16).

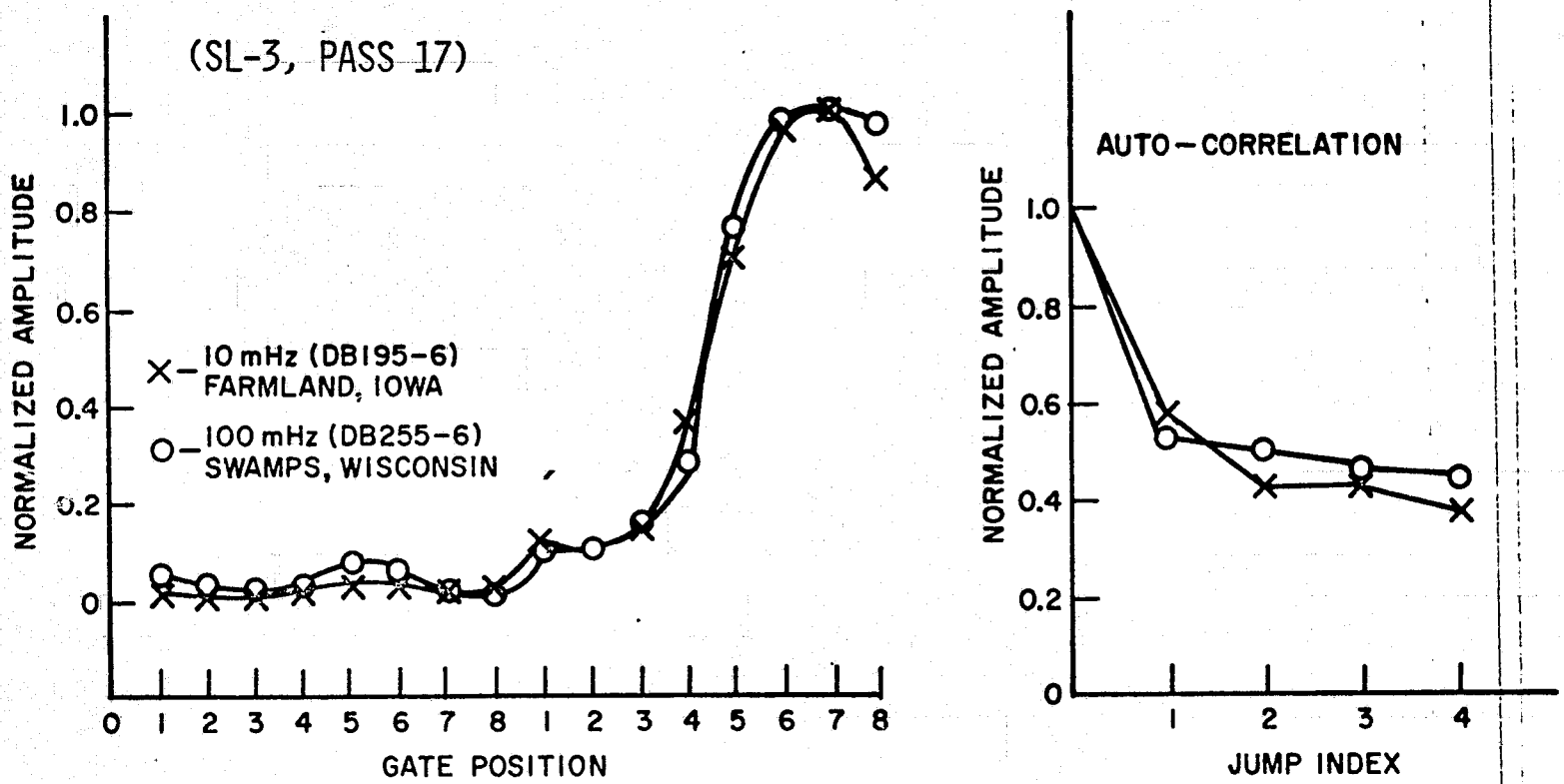

FIGURE 36. TERRAIN WAVEFORMS, NOISE AND RAMP GATES (SL-3, PASS 17).

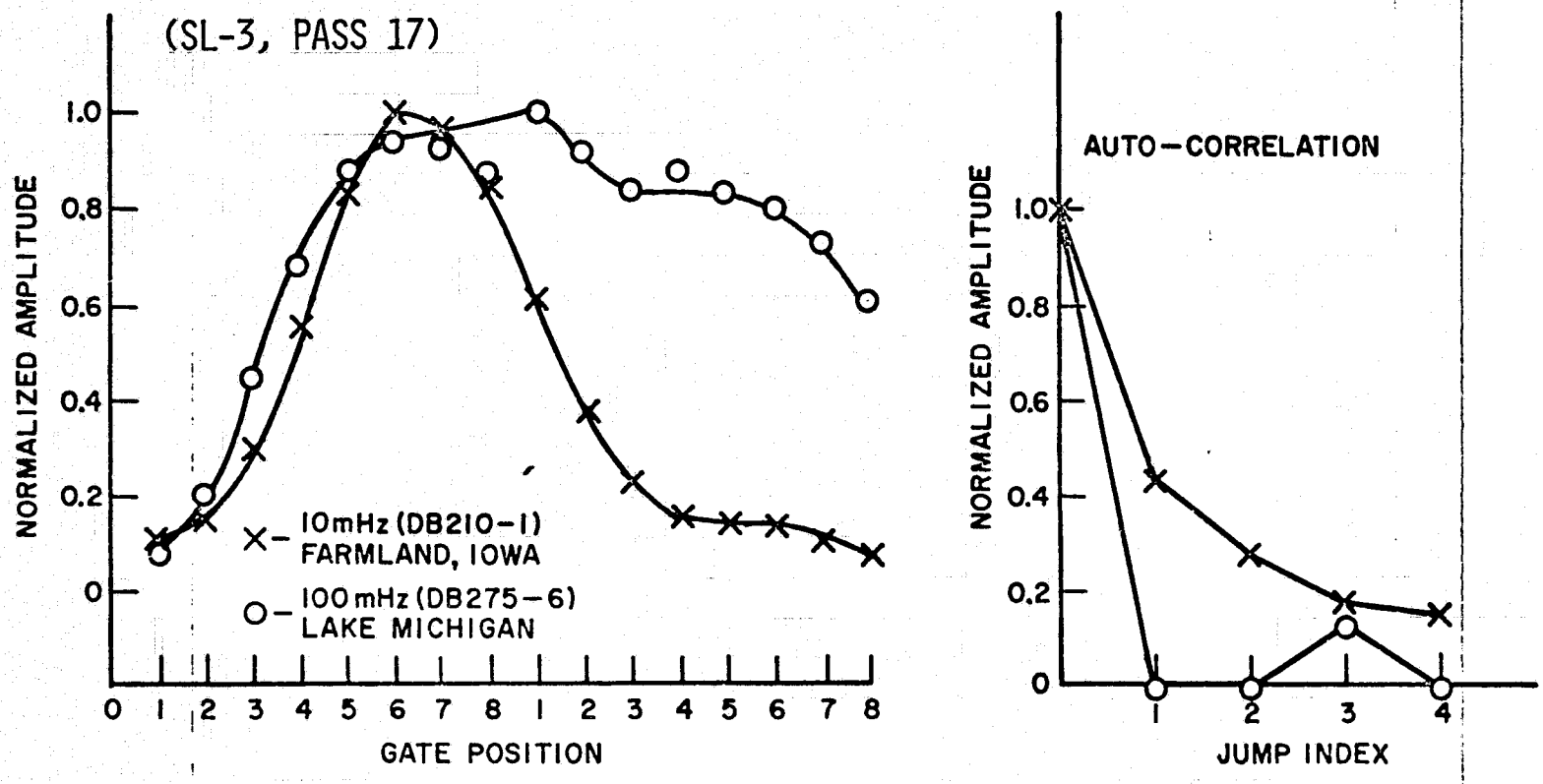

FIGURE 37. TERRAIN WAVEFORMS, RAMP AND PLATEAU GATES (SL-3, PASS 17).

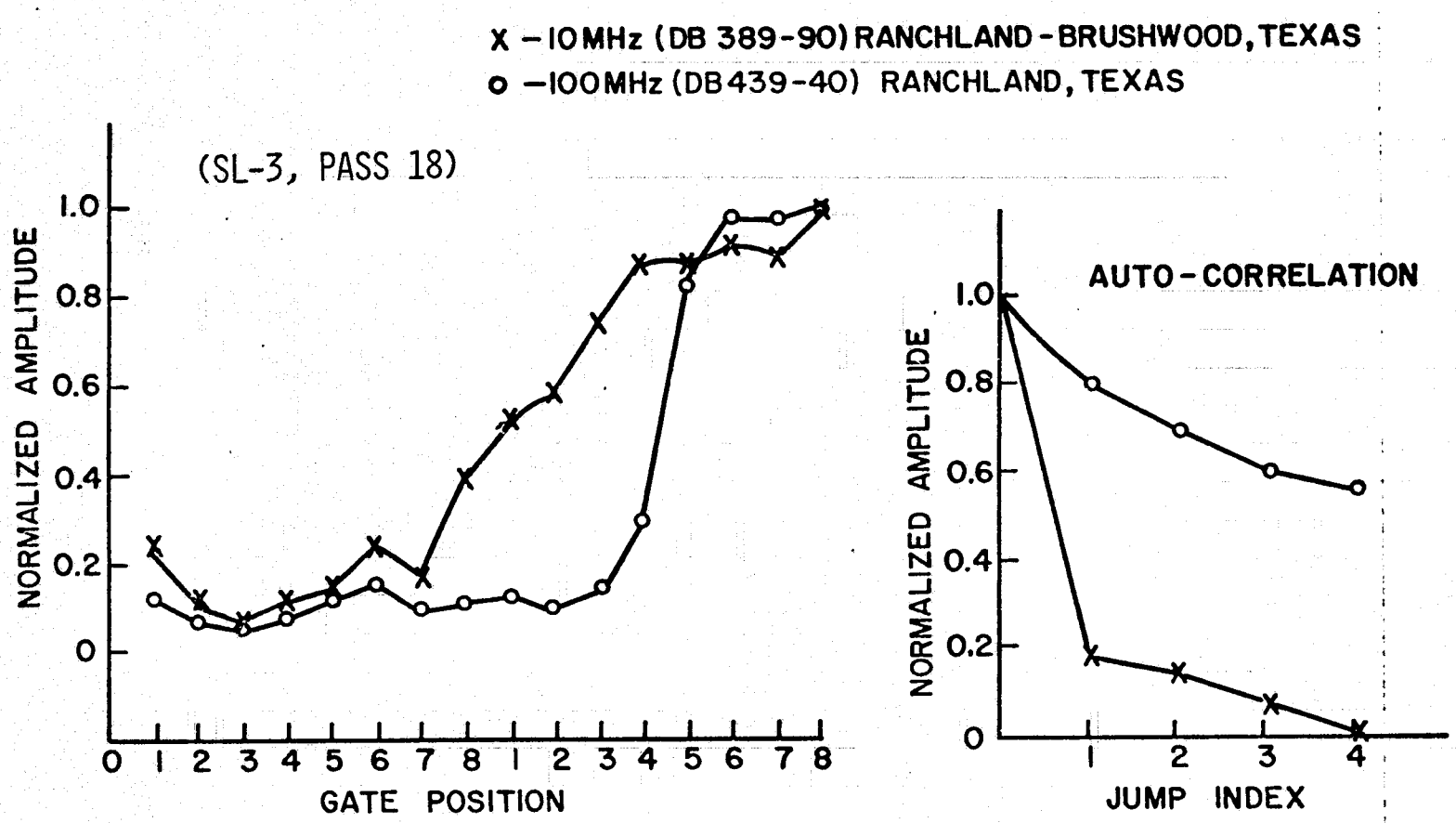

FIGURE 38. TERRAIN WAVEFORMS, NOISE AND RAMP GATES (SL-3, PASS 18).

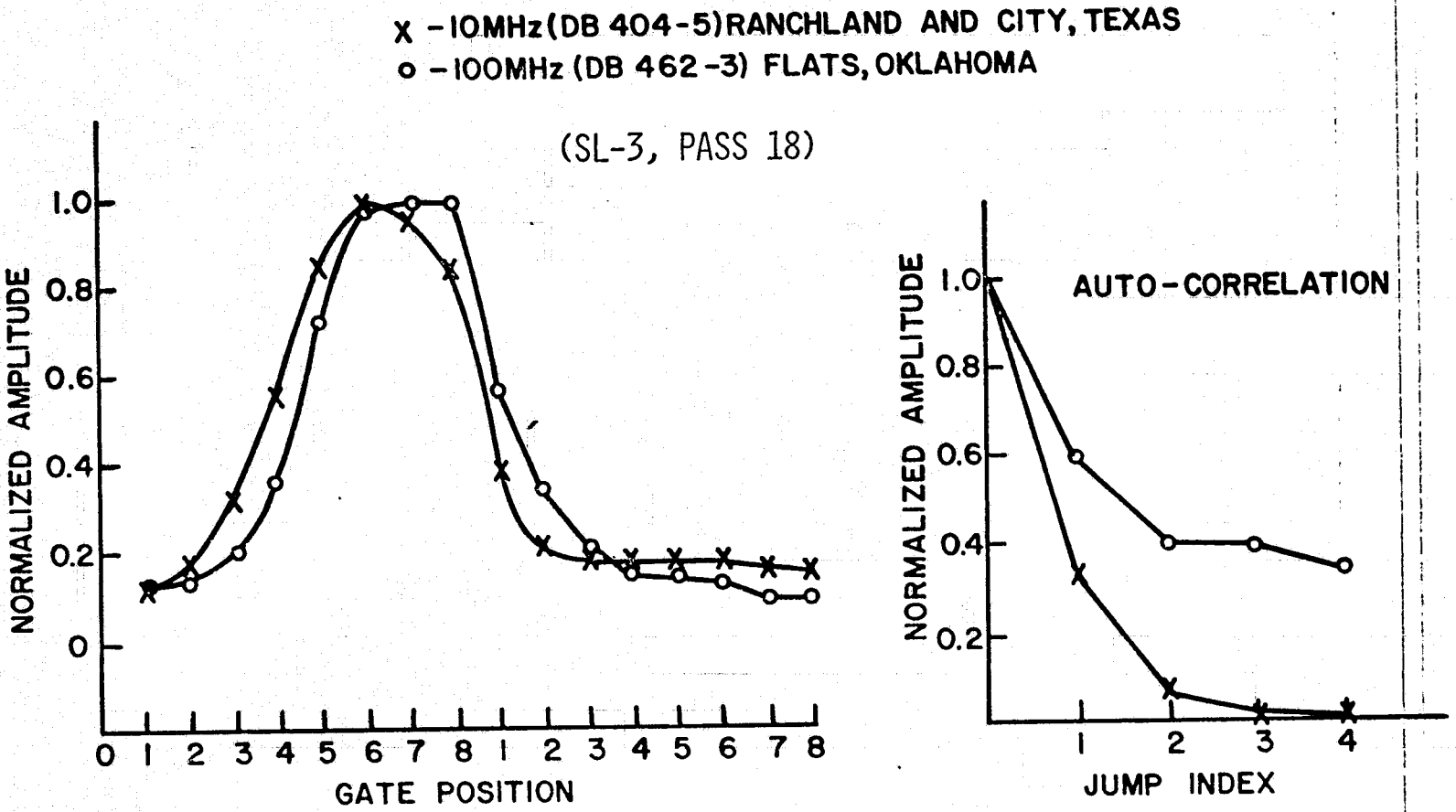

FIGURE 39. TERRAIN WAVEFORMS, RAMP AND PLATEAU GATES (SL-3, PASS 18).

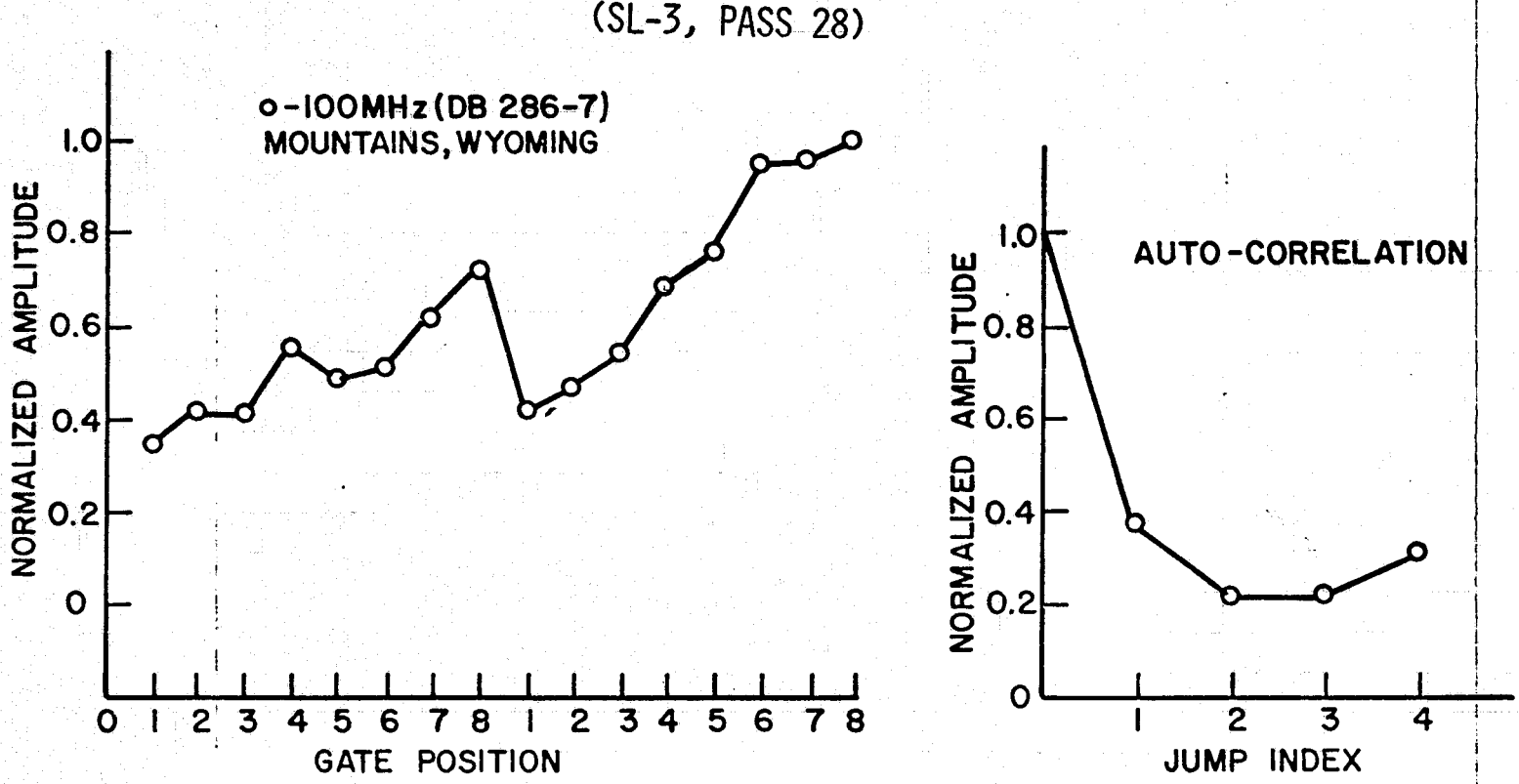

FIGURE 40. TERRAIN WAVEFORMS, NOISE AND RAMP GATES (SL-3, PASS 28).

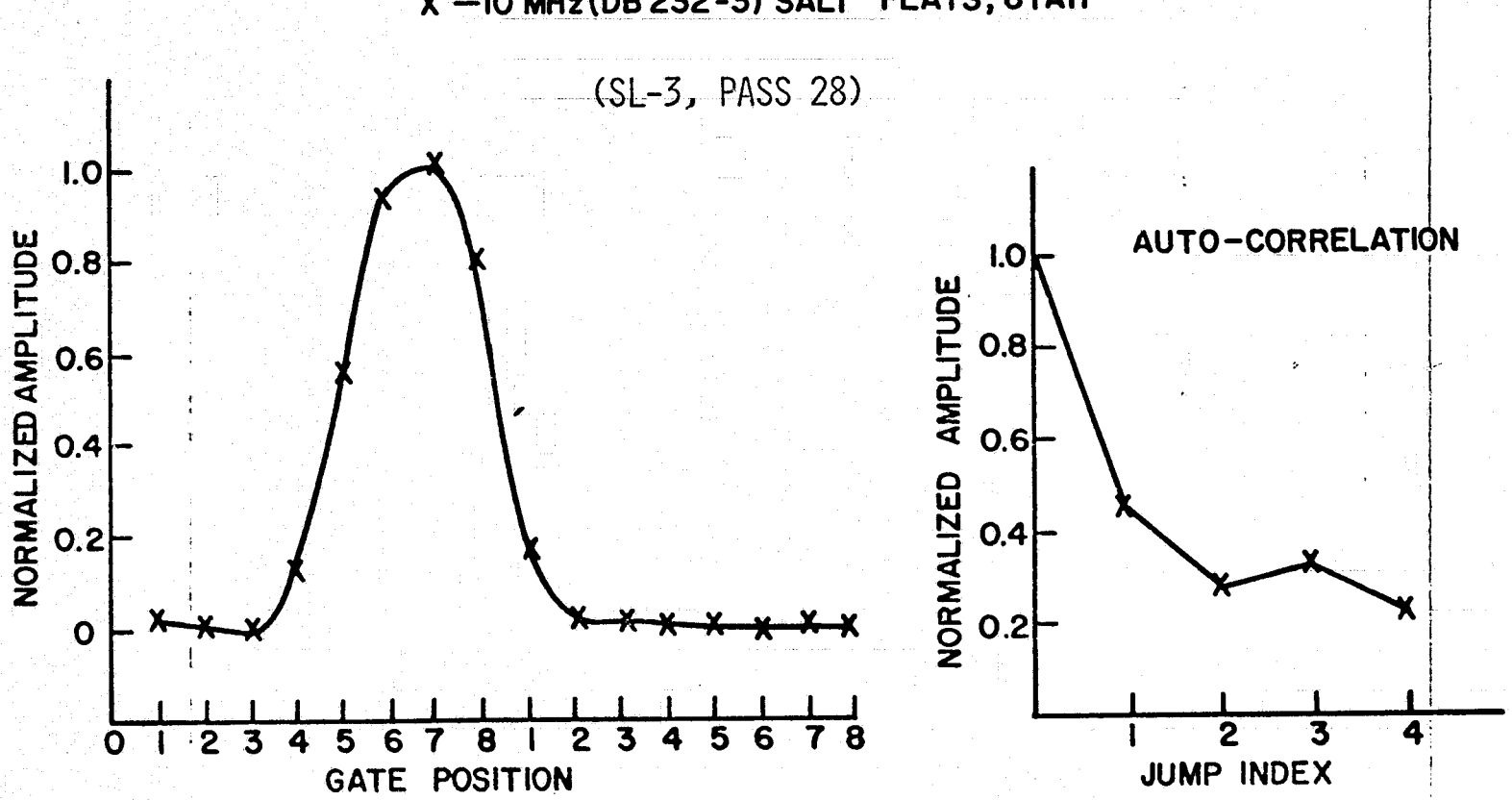

FIGURE 41. TERRAIN WAVEFORMS, RAMP AND PLATEAU GATES (SL-3, PASS 28).

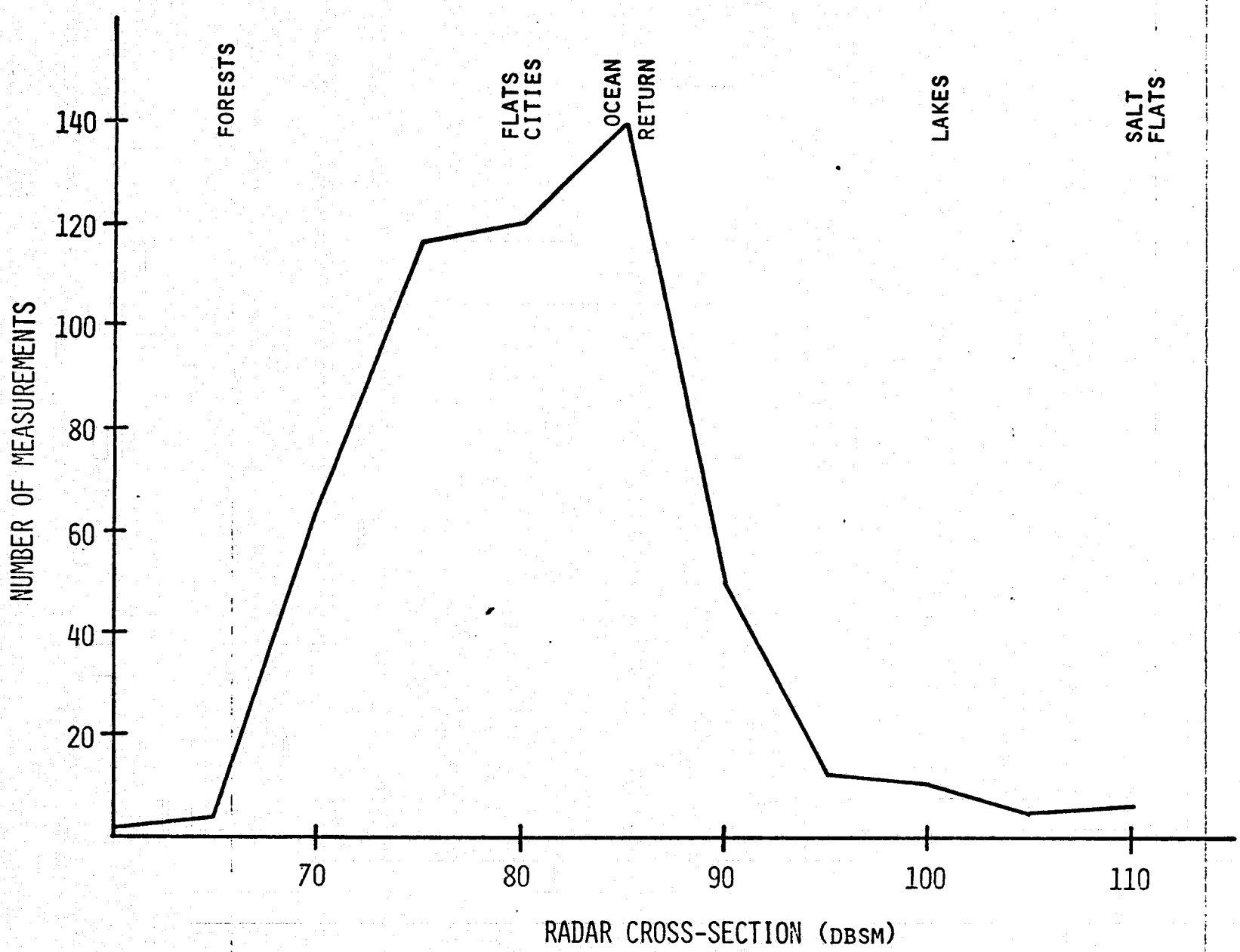

FIGURE 42. DISTRIBUTION OF RADAR CROSS-SECTION.

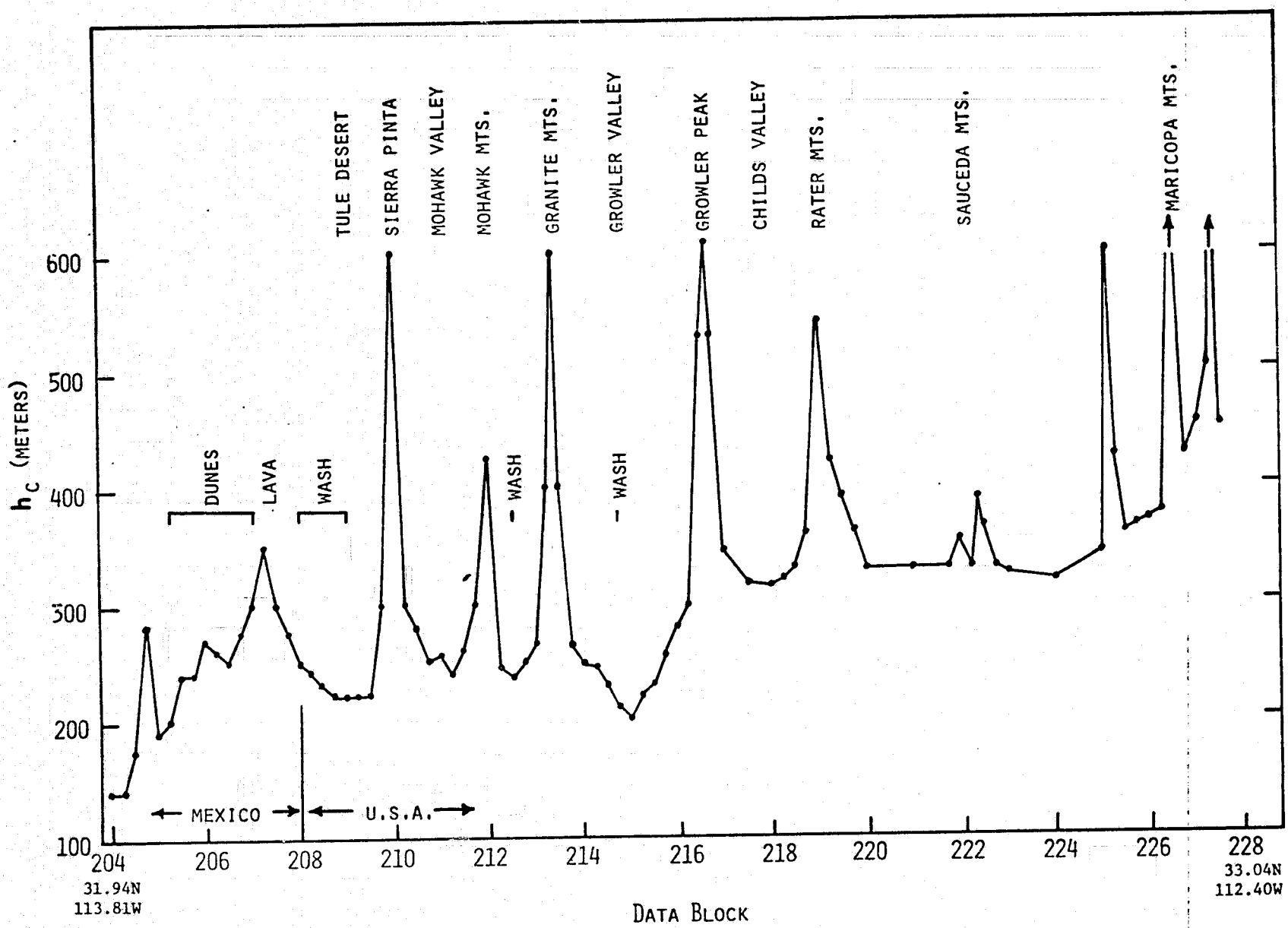

FIGURE 43. EXAMPLE OF TOPOGRAPHIC MAP PROFILE (SL-3, PASS 16).

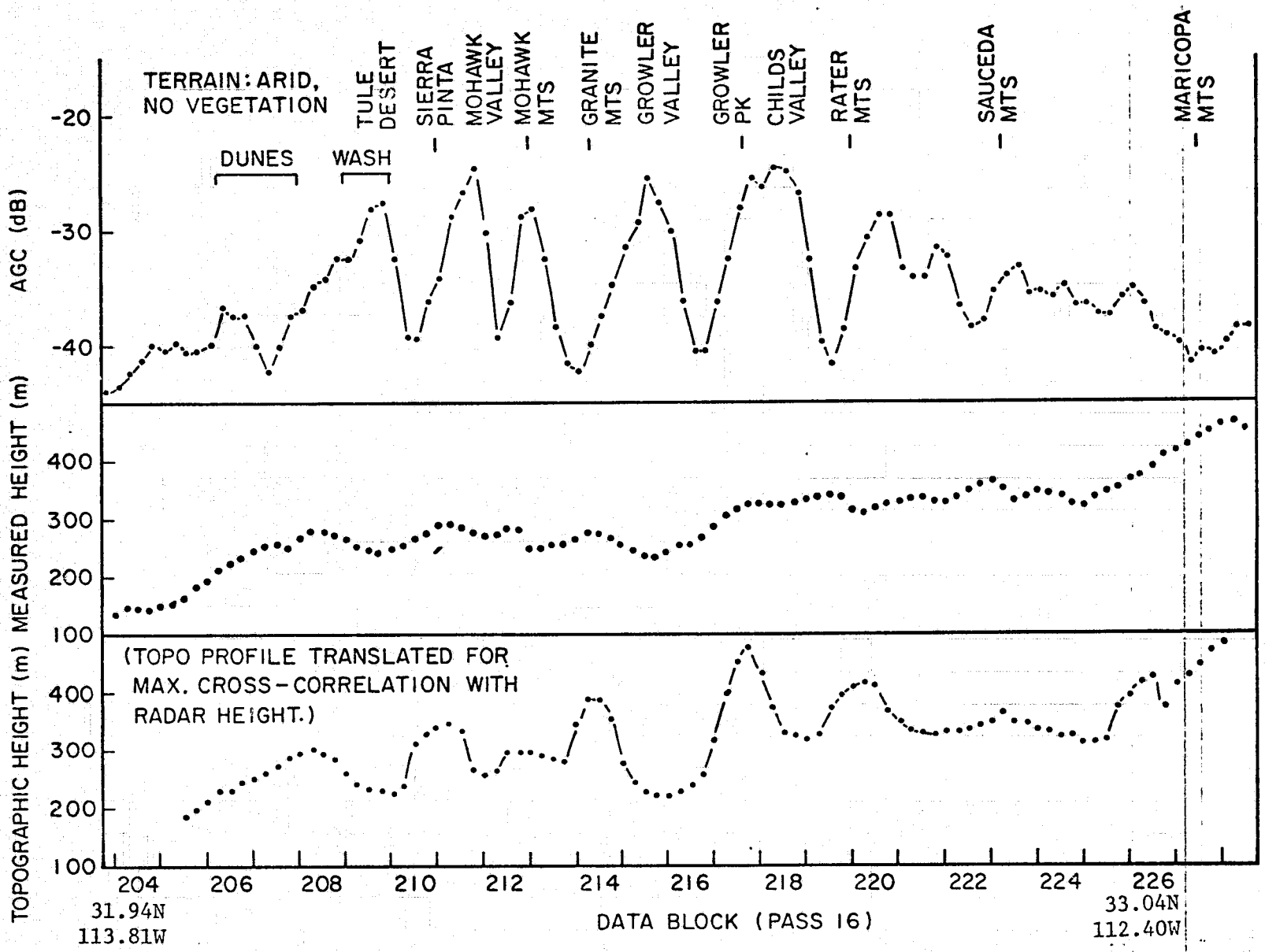

FIGURE 44. SKYLAB ALTIMETER OUTPUT AND TOPOGRAPHIC MAP PROFILE (SL-3, PASS 16, DB 204-228).

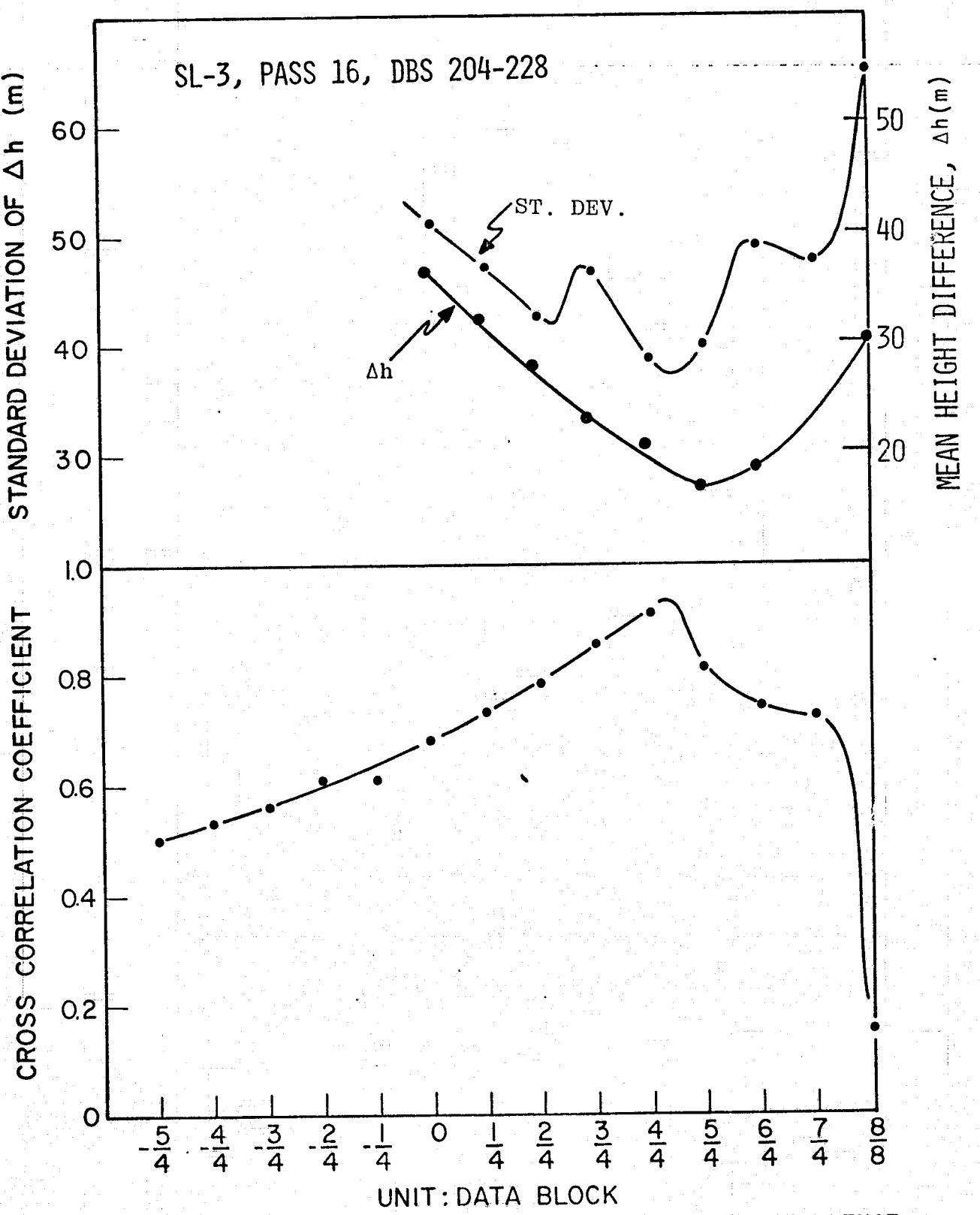

FIGURE 45. MEAN AND STANDARD DEVIATION OF HEIGHT DIFFERENCE AND CROSS-CORRELATION OF ALTIMETRY GROUND HEIGHT VERSUS MAP ELEVATION (SL-3, PASS 16, DB 204-228).

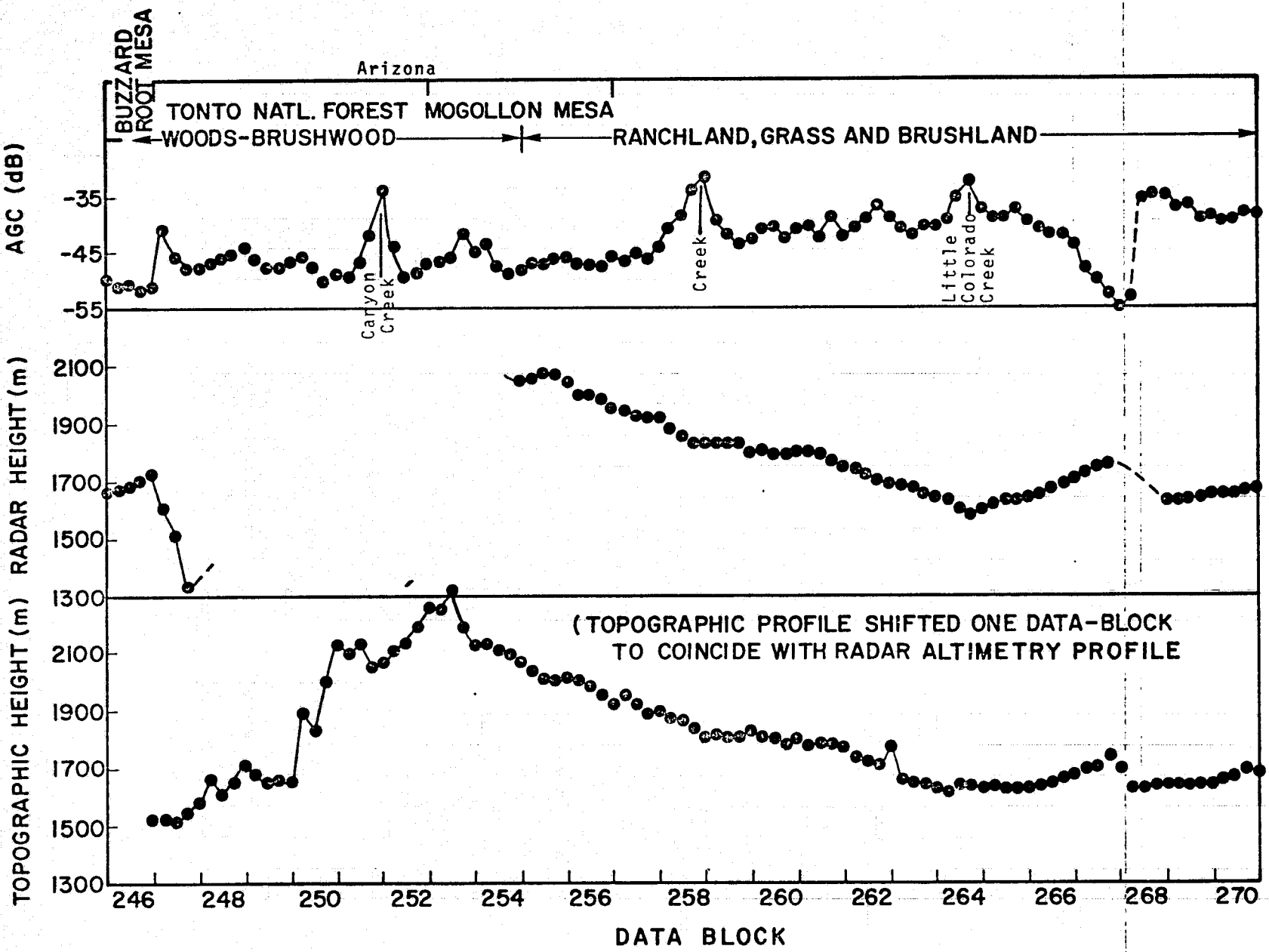

FIGURE 46. SKYLAB ALTIMETER OUTPUT AND TOPOGRAPHIC MAP PROFILE (SL-3, PASS 16, DB 246-270).

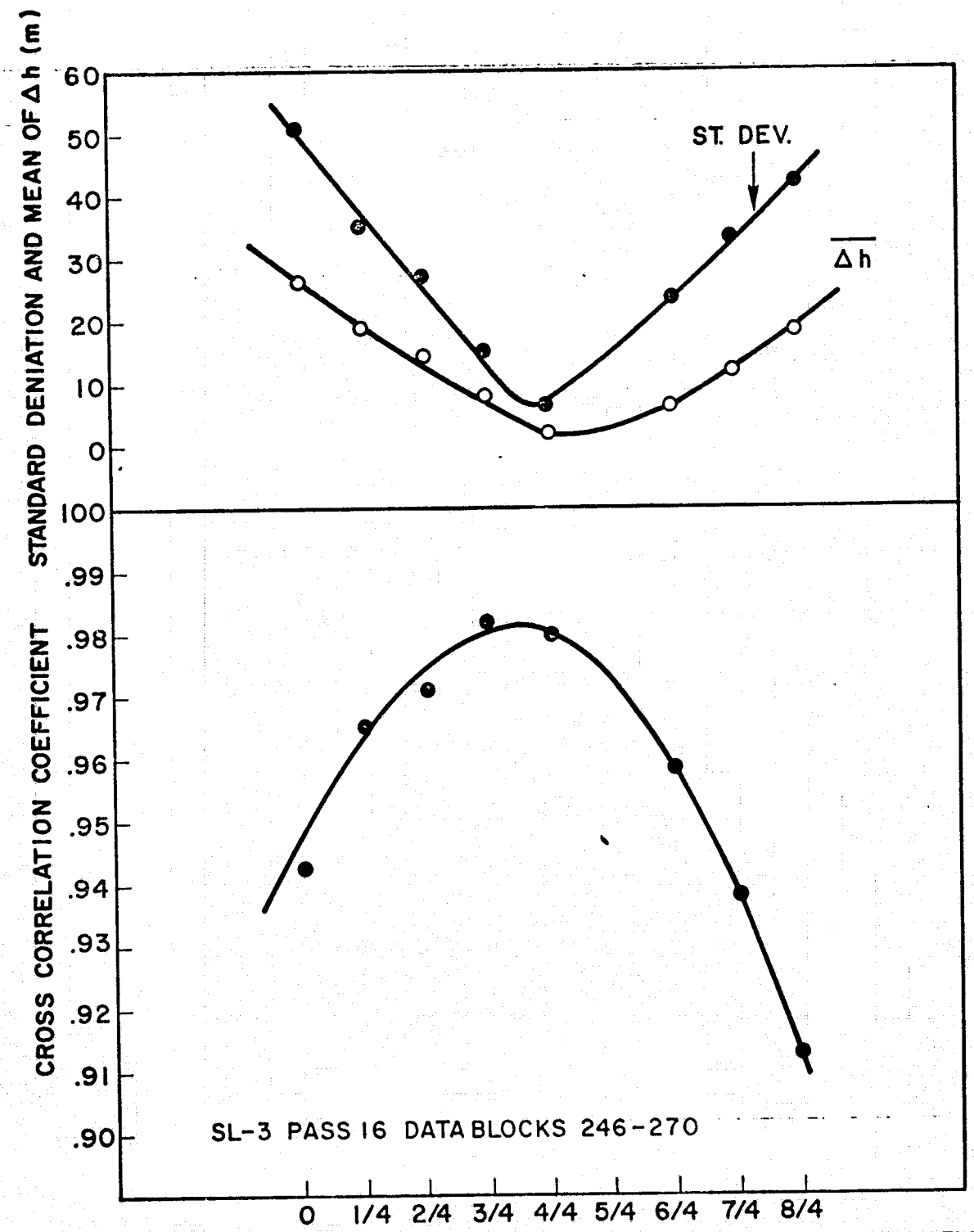

FIGURE 47. MEAN AND STANDARD DEVIATION OF HEIGHT DIFFERENCE, AND CROSS-CORRELATION OF ALTIMETRY HEIGHT VERSUS MAP ELEVATION (SL-3, PASS 16, DB 246-270).

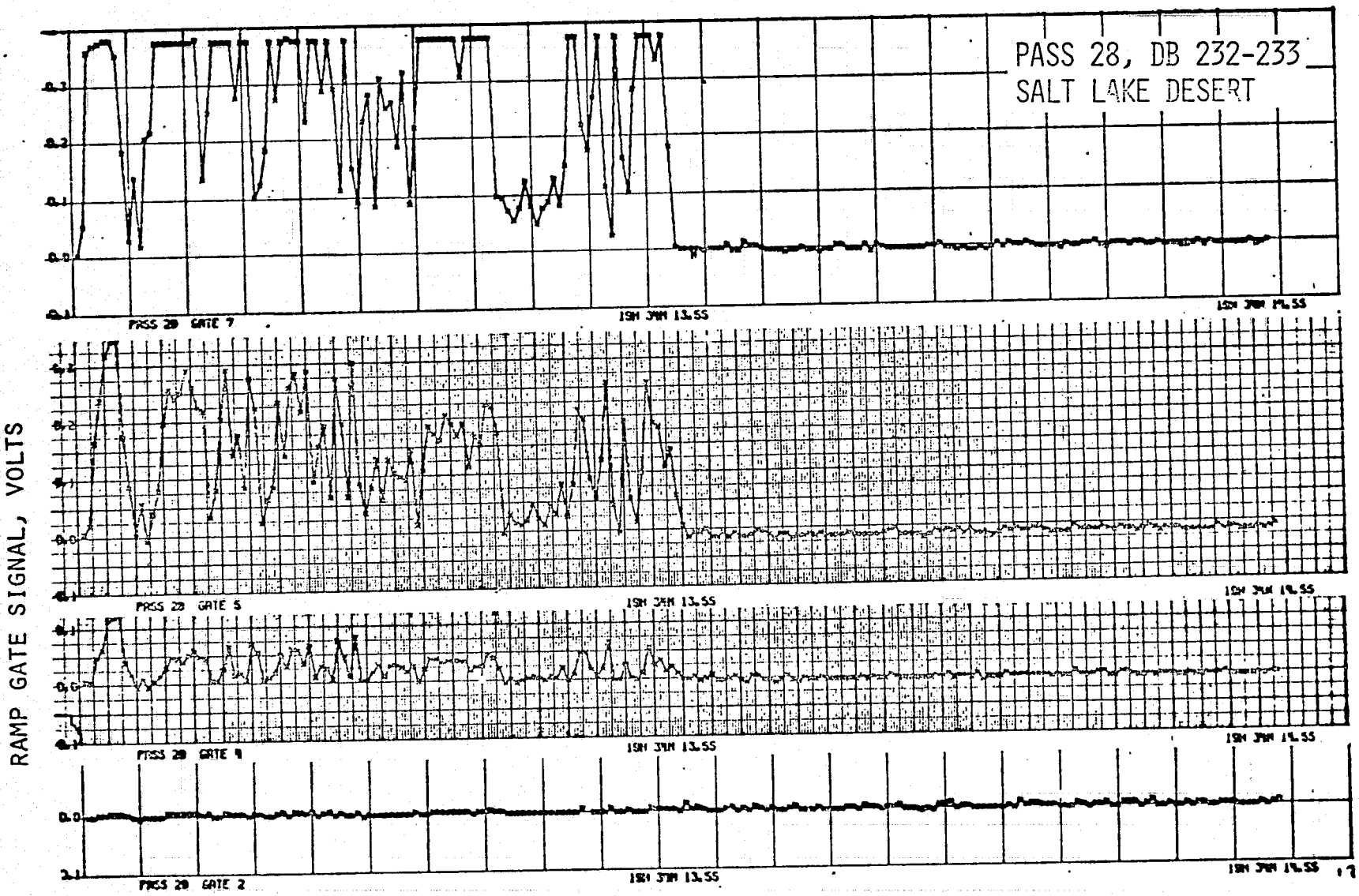

FIGURE 48. WAVEFORM AND STATISTICAL CHARACTERISTICS OF RADAR RETURN.

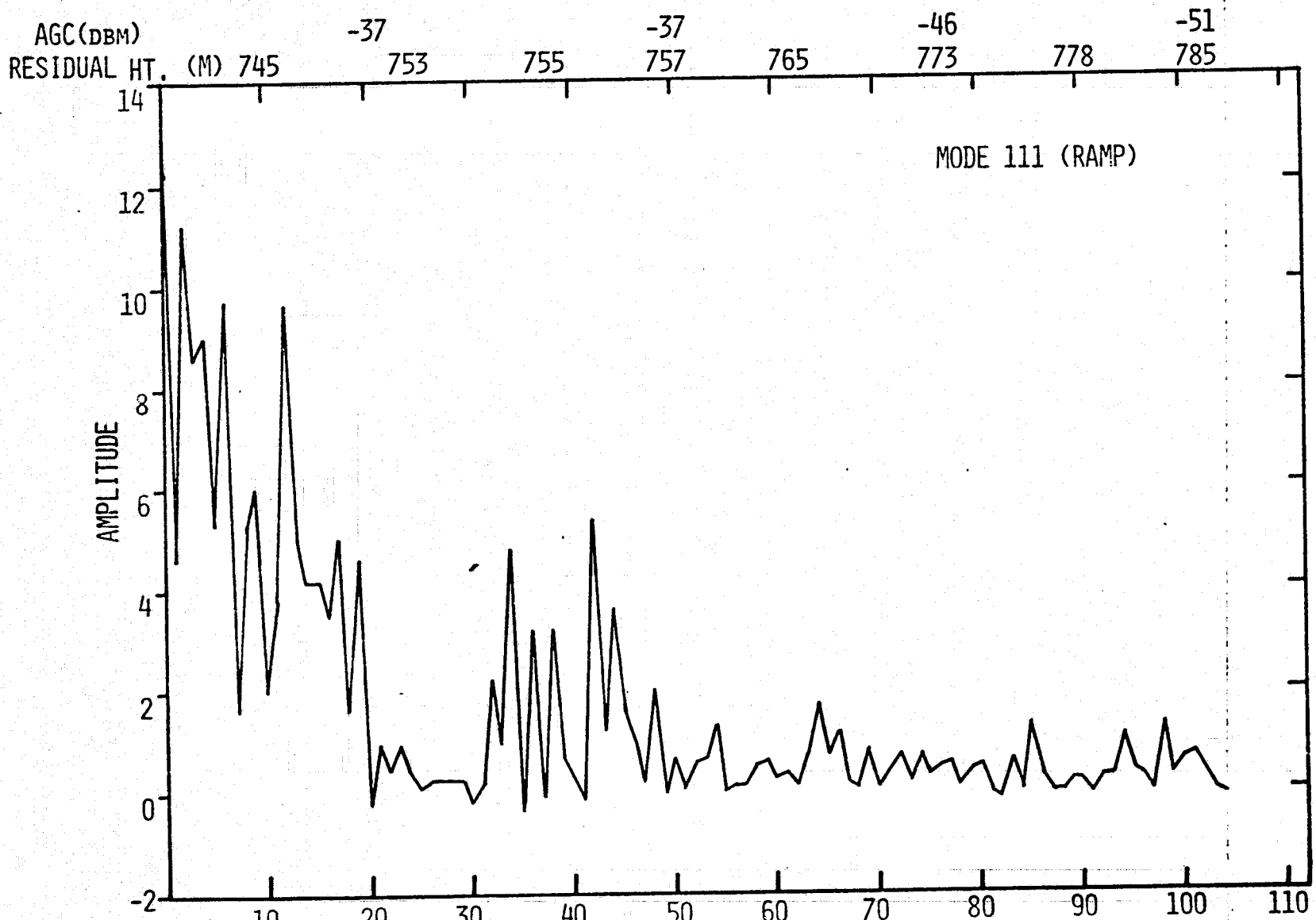

FIGURE 49. RAMP GATE (NO. 7) OUTPUT BEFORE RANGE-TRACK LOSS (DB 243).

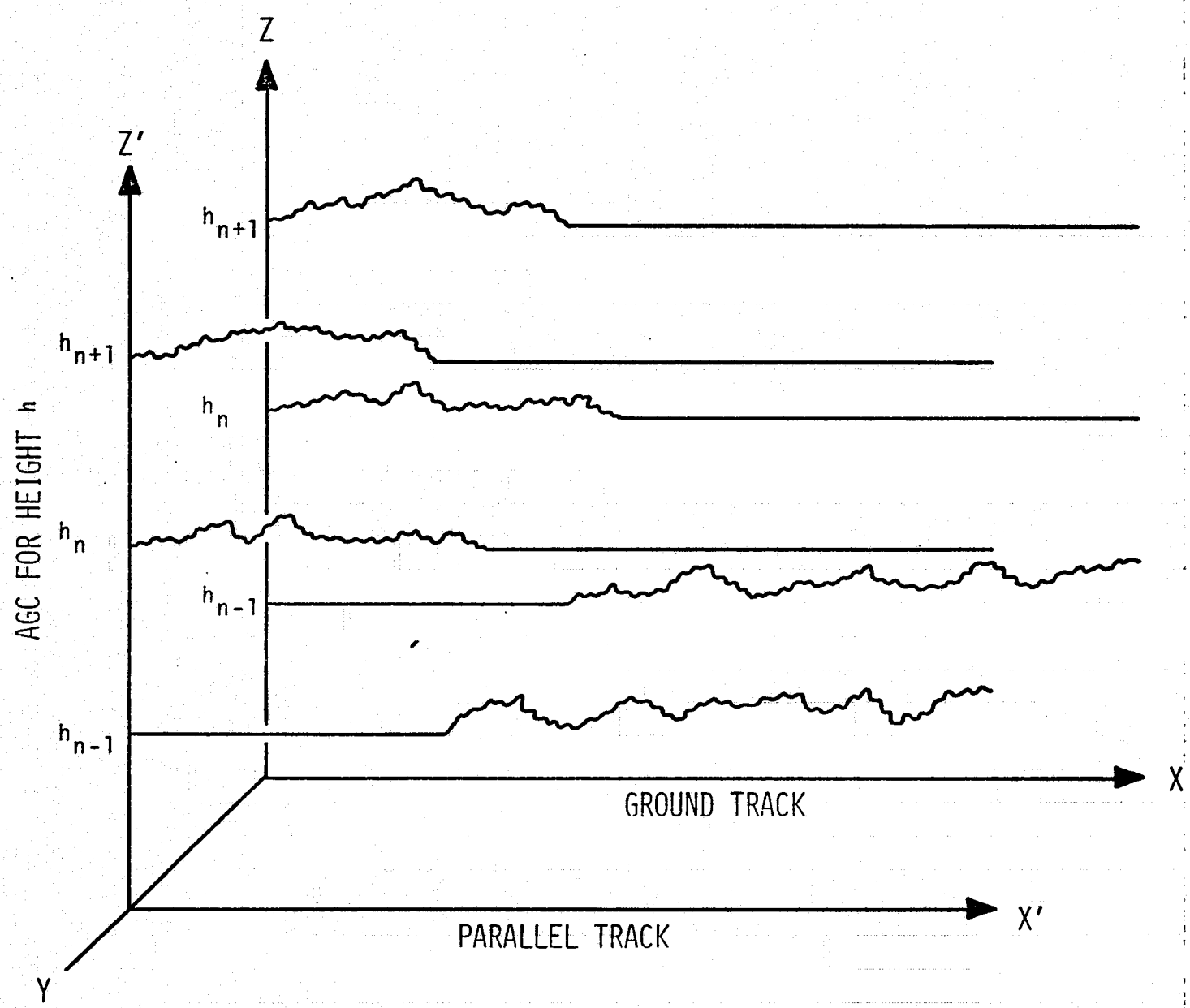

FIGURE 50. TERRAIN PROFILING BY SATELLITE ALTIMETER.

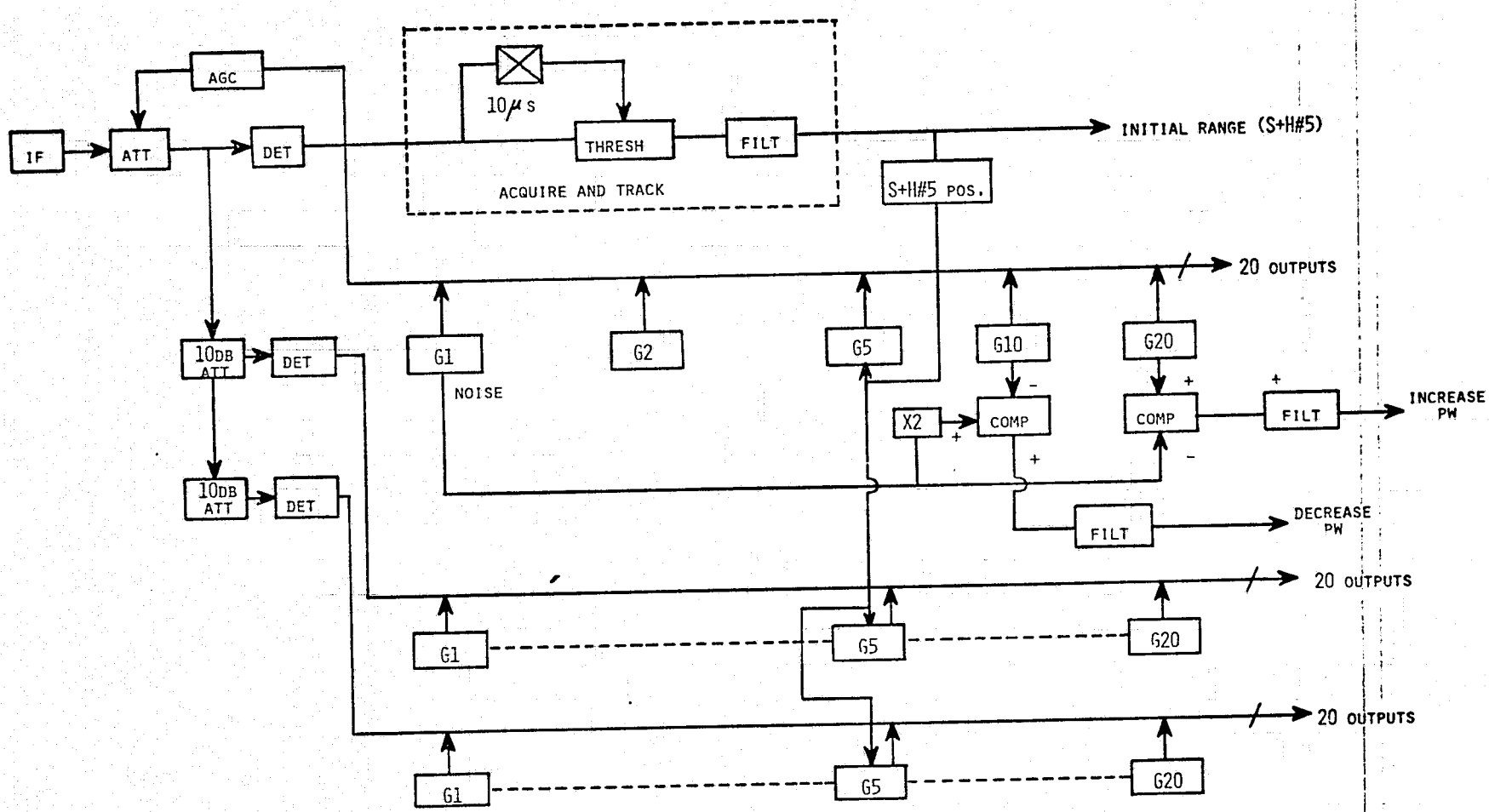

FIGURE 51. ACQUISITION AND TRACKING SYSTEM FOR A DEDICATED TERRAIN SATELLITE RADAR ALTIMETER.

APPENDIX A

CATALOGUE OF TERRAIN SIGNATURES

KEY TO COLUMN HEADINGS

Column

1. Data Block
2. SM and S^2M - sub-mode and sub-sub-mode of operation (see Section 1.7).
3. AGC (dBm)-AGC signal level in dB above mW, calibrated.
4. Rise-Time (Gates) - Number of S&H gates required to cover 10%-90% rise of amplitude of ramp portion of signal. Note S^2M-1 operation. When the signal does not rise from the noise level, the number in parentheses indicates the amplitude of the signal in the first gate as a percentage of the maximum amplitude. This is an indicator of the slope of the signal ramp, a long rise-time signifying complex terrain and reflectivity characteristics.
5. Auto-Corr. - Normalized auto-correlation function value for 100 samples of No. 4 S&H gate signal with jump index or lag of 0.01 seconds (72 meters).
6. h_m^* (m)- Reduced altimetry ground height, corrected for bias for each pass. In general, this correction is obtained from a water surface or a large homogeneous terrain area such as a desert, where absolute height can be easily derived from a topographic map.

7. h_{mid}(m) - Average of maximum and minimum map elevations in a footprint of a data block.

8. $\Delta h/2$(m) - Absolute value of one-half of the difference between the maximum and minimum elevations within a footprint of a data block.

9. Min. Res (m) - Defined as MIN.RES. = $h_m^* - (h_{mid} + \Delta_{h/2}) \geq 0$ or MIN.RES. = $h_m^* - (h_{mid} - \Delta_{h/2}) \leq 0$.

10. Type of Terrain - Self-explanatory.

11. Location - Self-explanatory.

Table A-1

Catalogue of Terrain Radar Signatures, SL-2, Pass 1, 30 May 1973

DATA BLOCK	SM S^2M	AGC (dbm)	TIME (#Gates)	AUTO CORR.	h^*_m (m)	h_{mid} (m)	$\Delta h/2$ (m)	MIN RES (m)	TYPE OF TERRAIN	LOCATION
110	00	-36			0	0	0	0	Pacific Ocean	
111	00	-36			-1	0	0	-1		
112	00	-36			0	0	0	0		
113	00	-36			-1	0	0	-1		
114	00	-36			1	0	0	1		
115	00	-36			0	0	0	0		
116	00	-36			0	0	0	0		
117	00	-36			1	0	0	1		
118	00	-35			0	0	0	0	Bay	Coos Bay, Ore.
119	00	-35			3	15	15	0	City	
120	00	-35			-3	39	39	-3		Oregon
Time	Skip									
124	01	-42	2.7	.4	236	427	183	-8	Mts. & Vegetation	
125	01	-44	2.4	.4	210	604	360	-34		
126	01	-49	4.5(36%)	.2	133	604	360	-111		
136	01	-41	3.0	.5	506	854	367	0	Mts. & Forest	
137	01	-44	4.0(32%)	.2	512	1006	458	-36		
145	01	-25	2.1	.5	1287	1522	260	0	Mts., Upper Klamath Lake	
146	01	-25	3.9	.1	1265	1423	161	0		
147	01	-23	5.0(37%)	.5	1266	1540	278	4	Swamp	

* Referenced to ocean mean measured height (+18 m)

Table A-1 (continued)

DATA BLOCK	S^2_M	AGC (dbm)	RISE TIME (#Gates)	AUTO CORR.	h^*_m (m)	h_{mid} (m)	$\Delta h/2$ (m)	MIN RES (m)	TYPE OF TERRAIN	LOCATION
148	01	-29	4.8	.1	1247	1546	284	-15	Mts. & Valley	Oregon
152	02	-37			1261	1405	125	-19	Valley	
153	02	-42			1238	1508	228	-42	Mts.	
156	02	-32			1271	1387	137	0	Valley	California
160	02	-40			1455	1585	122	-8	Ridges & Vegetation	
165	02	-42			1439	1524	61	-24	Mt. Small Lake	
166	02	-36			1447	1494	31	-16	Valley Small Lake	
168	02	-43			1398	2022	498	-126	Forest & Mts.	
169	02	-56			1264	1906	534	-108	Middle Alkali Lake	
170	02	-53			1252	1686	326	-108	Dry Valley	
171	02	-59			1147	1366	6	-213		
173	10	-46			1290	1814	76	-448	Dry Lake	Nevada
188	10	-36			1171	1250	30	-49	Desert	
190	10	-48			1213	1725	262	-250	Mts.	
212	10	-43			1474	1829	305	-50	Mts.	
219	10	-34			1735	2150	412	-3	Mts. & Park	

Table A-1 (continued)

DATA BLOCK	S^2_M	AGC (dbm)	RISE TIME (#Gates)	AUTO CORR.	h^*_m (m)	h_{mid} (m)	$\Delta h/2$ (m)	MIN RES (m)	TYPE OF TERRAIN	LOCATION
220	10	-46			1678	2272	351	-243	Mts. & Valley	Nevada
223	10	-37			1880	1857	3	20	Dry Valley	
224	10	-34			1870	1872	18	0		
225	10	-39			1821	2058	198	-39	Mts. & Vetetation	
226	11	-44	5.5(23%)	.4	1819	2226	336	-71		
232	11	-44	3.8(40%)	.4	1769	2123	172	-182	Range	
236	11	-49	4.3(80%)	0	1856	2180	320	-4	Range, Forest	
243	11	-41	1.9	.1	1716	1845	168	0	Valley	
244	11	-45	3.1(31%)	.3	1668	2302	625	-9	Mts.	
268	11	-39	3.2	.2	1550	896	119	-5	Mts., Desert	Utah
271	11	-47	3.7	.3	1633	1786	170	0	Valley, Mts.	
272	11	-46	1.3	.6	1674	1707	61	0	Valley	
273	11	-38	2.5	.4	1709	2211	534	0	Mts., City	
280	11	-46	4.6(29%)	.1	2581	1294	335	2200	Forest, Cliffs	
283	12	-45			1935	2012	122	0	Cliffs & Terraces	
285	12	-51			1947	1951	183	0		
286	12	-52			1938	1951	183	0		

Table A-1 (continued)

DATA BLOCK	S^2_M	AGC (dbm)	RISE TIME (#Gates)	AUTO CORR.	h^*_m (m)	h_{mid} (m)	$\Delta h/2$ (m)	MIN RES (m)	TYPE OF TERRAIN	LOCATION
308	12	-39			1679	945	107	0	Valley & Mesa	Arizona
309	12	-46			1582	1738	153	-3	↓	↓

Table A-2

Catalogue of Terrain Radar Signatures, SL-3, Pass 16, 6 September 1973

DATA BLOCK	S^2_M	AGC (dbm)	RISE TIME (#Gates)	AUTO CORR.	h^*_m (m)	h_{mid} (m)	$\Delta h/2$ (m)	MIN RES (m)	TYPE OF TERRAIN	LOCATION
180	00	-37			457	605	205	0	Valley	Lower California, Mexico
182	00	-47			629	709	558	0	Mountains	
183	00	-53			650	539	514	0		
184	00	-48			177	175	175	0	Gulf of California	
185	00	-42			106	50	50	6		
186	00	-30			-2	0	0	-2		Gulf of California
187	00	-30			1	0	0	1		
188	00	-30			1	0	0	1		
189	00	-29			-1	0	0	-1		
190	00	-30			0	0	0	0		
191	00	-30			1	0	0	1		
192	00	-30			1	0	0	1		
193	00	-31			0	0	0	0		
194	00	-31			0	25	25	0		Mexico
195	01	-31	2.7	0.0	1	25	25	0	Desert	
196	01	-35	5.3(31%)	.2	34	57	31	0		
197	01	-38	2.7	.3	44	57	31	0		
198	01	-42	3.7(25%)	0.0	56	48	43	0		
199	01	-42	4.2	0.0	50	38	12	0		
200	01	-44	3.4	.1	45	38	12	0		
201	01	-44	3.0	.1	42	73	28	0		

* Referenced to Gulf of California (-33 m)

Table A-2 (continued)

DATA BLOCK	S^2_M	AGC (dbm)	RISE TIME (#Gates)	AUTO CORR.	h^*_m (m)	h_{mid} (m)	$\Delta h/2$ (m)	MIN RES (m)	TYPE OF TERRAIN	LOCATION
202	01	-44	4.3(25%)	.1	68	88	38	0	Desert	Mexico
203	01	-44	4.0(23%)	0.0	116	125	25	0		
204	01	-43	3.4	.2	141	207	82	0		
205	01	-40	4.1(34%)	.1	165	232	57	-10		
206	01	-39	3.4	.2	213	379	179	0	Mountains	
207	01	-40	4.4	.3	252	404	154	0		
208	01	-36	2.3	.1	271	332	16	-45	Wash & Tule Desrt	Arizona
209	01	-31	2.8	.3	252	412	199	0		
210	02	-35			260	427	183	0	Sierra Pinta Mountains	
211	02	-32			285	374	130	0	Valley	
212	02	-33			278	427	183	0	Mountains, Wash	
213	02	-32			253	427	183	0		
214	02	-40			270	259	46	0	Wash	
215	02	-30			244	412	199	0	Mountains	
216	02	-34			253	427	183	0		
217	02	-34			304	366	61	-1	Mountains	
218	02	-25			326	385	80	0		
219	02	-35			337	385	80	0		
220	02	-33			317	366	61	0		
221	02	-33			328	534	229	0	Mountains	
222	02	-35			340	534	229	0	Washes	
223	02	-35			352	336	31	0		
224	02	-35			338	336	31	0		
Time	Skip									
225	10	-37			337	458	153	0		
226	10	-37			382	570	224	0	Mountains	
227	10	-40			430	610	273	0	Valley	

Table A-2 (continued)

DATA BLOCK	SM	AGC (dbm)	RISE TIME (#Gates)	AUTO CORR.	h^*_m (m)	h_{mid} (m)	$\Delta h/2$ (m)	MIN RES (m)	TYPE OF TERRAIN	LOCATION
228	10	-39			457	503	107	0	Valley, Washes, Mountains, populated, River, Mts.	Arizona
229	10	-38			431	458	92	0		
230	10	-31			391	793	427	0		
231	10	-39			429	829	494	0		
232	10	-51			460	829	494	0		
233	10	-36			335	503	168	0		
234	10	-39			348	570	204	-18		
235	10	-42			359	570	204	7		
236	10	-34			376	366	8	0		
237	10	-28			363	366	8	0		
238	10	-33			371	508	142	0		
239	10	-31			400	584	188	0		
240	10	-43			445	599	172	0		
241	10	-40			479	566	139	0		
242	10	-43			460	671	183	-28		
Time Skip 243	11	-43	3.3(40%)	.4	764	943	150	-29	Vegetation, Mts.	
246	11	-52	1.5(63%)	.05	1682	1646	244	0	Forest, Mts.	
247	11	-48	3.9(31%)	.4	1477	1707	183	-47		
255	11	-48	1.9(40%)	.05	2066	1982	31	54	Ranches, Vegetation	
256	11	-47	5.8(45%)	.2	2000	1949	59	0		
257	11	-46	5.2(46%)	.1	1934	1845	46	46		
258	11	-40	2.6	.5	1863	1814	15	34		
259	11	-40	1.9	.4	1822	1833	57	0		
260	11	-42	2.6(26%)	.2	1796	1818	80	0		

Table A-2 (continued)

DATA BLOCK	S^2_M	AGC (dbm)	RISE TIME (#Gates)	AUTO CORR.	h^*_m (m)	h_{mid} (m)	$\Delta h/2$ (m)	MIN RES (m)	TYPE OF TERRAIN	LOCATION
261	11	-42	4.5	.2	1791	1723	46	25	Ranches - Dry	Arizona
262	11	-40	3.8	.4	1725	1662	77	0		
263	11	-41	1.9	.3	1671	1646	61	0		
264	11	-37	4.8(31%)	.5	1611	1646	61	0		
265	11	-38	6.6(32%)	0.0	1621	1701	55	-25		
266	11	-41	3.8(39%)	.2	1665	1701	55	0		
267	11	-49	2.5(38%)	.3	1741	1677	31	34	Petrified Forest	
269	11	-37	2.3	.4	1637	1662	16	-9	Dry Ranchland	
270	11	-39	2.7	.1	1656	1708	31	-21		
271	12	-40			1684	1738	61	0		
272	12	-40			1719	1784	46	-19		
273	12	-42			1749	1799	61	0		
274	12	-44			1753	1859	92	-15		
275	12	-44			1753	1906	107	-46	Brushwood	
276	12	-45			1782	1921	92	-47		
277	12	-48			1811	2012	122	-49		
278	12	-48			1894	2043	153	0		
279	12	-47			1946	2119	107	-66		
280	12	-47			1981	2119	107	-31		
282	12	-45			2009	2058	26	0		New Mexico
283	12	-46			2021	2028	46	0		
284	12	-45			2038	2012	61	0		
285	12	-47			2040	1982	92	0		
286	12	-49			2021	1936	76	9		

Table A-2 (continued)

DATA BLOCK	S^2_M	AGC (dbm)	RISE TIME (#Gates)	AUTO CORR.	h^*_m (m)	h_{mid} (m)	$\Delta h/2$ (m)	MIN RES (m)	TYPE OF TERRAIN	LOCATION
287	12	-44			1919	1890	61	0	Dry Ranchland	New Mexico
288	12	-48			1949	1887	65	0		
289	12	-50			1954	1848	49	58		
290	12	-41			1932	1848	49	0		
291	12	-44			1839	1830	31	0		
Time Skip										
292	20	-43			1837	1830	31	0		
293	20	-42			1855	1830	31	0		
294	20	-43			1823	1860	61	0		
295	20	-46			1816	1875	46	-13		
296	20	-45			1860	1936	46	-30		
297	20	-45			1926	1982	92	0		
298	20	-48			2002	2053	102	0		
299	20	-49			2067	2099	56	0		
300	20	-50			2099	2042	31	26		
301	20	-48			2026	2109	97	0		
302	20	-52			2108	2079	128	0	Ranches, Vegetation	
303	20	-52			2126	2035	145	0	Canyon	
Time Skip										
304	20	-52			2235	2165	61	9	Forest	
306	20	-48			2202	2333	138	0	Ranches	
307	21	-51			2331	2490	173	0		
308	21	-48			2246	2398	264	0	Mts. & Canyons	
309	21	-49			2252	2398	264	0		
310	21	-48			2297	2439	244	0		

Table A-2 (continued)

DATA BLOCK	S^2_M	AGC (dbm)	RISE TIME (#Gates)	AUTO CORR.	h^*_m (m)	h_{mid} (m)	$\Delta h/2$ (m)	MIN RES (m)	TYPE OF TERRAIN	LOCATION
311	21	-51			2388	2702	324	0	Mts. & Canyons	New Mexico
312	21	-51			2432	3023	645	0	↓	Colorado
324	21	-40			2314	2302	2	11	Dry San Luis Valley	
325	21	-37			2315	2301	0	14		
326	21	-39			2311	2300	0	11		
327	21	-39			2300	2304	4	0		
328	21	-39			2299	2328	20	-9	Lake	
329	21	-41			2309	2404	96	0		
330	21	-40			2378	2507	159	0		
331	21	-48			2500	2801	362	0	Mountains & Forest	
343	21	-46			1542	1521	58	0	City of Pueblo	
344	21	-42			1507	1479	46	0		
345	21	-38			1453	1540	77	-10		
346	21	-46			1531	1525	31	0	Dry Ranchland	
347	21	-47			1546	1525	31	0		
348	22	-45			1496	1525	31	0		
349	22	-45			1522	1585	61	-2		
350	22	-46			1588	1631	46	0		
351	22	-46			1666	1662	16	0		
352	22	-46			1689	1677	31	0		
353	22	-47			1678	1677	31	0		
354	22	-48			1672	1662	31	0		
355	22	-49			1670	1624	54	0		
356	22	-46			1632	1608	38	0		
357	22	-46			1622	1616	61	0	↓	↓

TABLE A-3

Catalogue of Terrain Radar Signatures, SL-3, Pass 17, 7 September 1973

DATA BLOCK	SM S^2M	AGC (dBm)	RISE TIME (#Gates)	AUTO CORR.	h_m* (m)	h_{mid} (m)	$\Delta h/2$ (m)	MIN RES (m)	TYPE OF TERRAIN	LOCATION
181	00	-30			262	267	23	0	City of Des Doines	Iowa
182	00	-31			252	271	27	0	↓	↓
183	00	-34			267	278	19	0	Farmland	↓
184	00	-37			287	272	28	0	↓	↓
185	00	-41			302	279	35	0	Skunk River	↓
186	00	-37			267	279	35	0	↓	↓
187	00	-39			279	286	27	0	↓	↓
188	00	-39			278	294	20	0	↓	↓
189	00	-41			309	310	20	0	↓	↓
190	00	-40			291	302	28	0	↓	↓
191	00	-44			313	289	24	0	↓	↓
192	00	-41			300	285	20	0	↓	↓
193	00	-38			295	286	27	0	Iowa River	↓
194	00	-39			276	290	31	0	↓	↓
195	00	-36			292	307	17	0	↓	↓
196	01	-40	2.5	.6	293	307	17	0	↓	↓
197	01	-45	3.6	.1	311	297	23	0	↓	↓
198	01	-40	2.7	.5	295	294	20	0	↓	↓
199	01	-43	2.8	.3	294	290	23	0	↓	↓
200	01	-44	4.5(30%)	.2	299	275	31	0	↓	↓
201	01	-43	5.0 (23%)	.2	272	259	15	0	↓	↓
202	01	-42	2.8	.4	262	263	19	0	Cedar River	↓
203	01	-29	2.0	.6	261	279	20	0	↓	↓
204	01	-40	3.9	.2	271	290	16	-3	↓	↓
205	01	-43	2.9	.7	288	275	32	0	↓	↓

* Referenced to Lake Michigan (-30 m)

TABLE A-3 (continued)

DATA BLOCK	SM S^2M.	AGC (dBm)	RISE TIME (#Gates)	AUTO CORR.	h_m* (m)	h_{mid} (m)	$\Delta h/2$ (m)	MIN RES (m)	TYPE OF TERRAIN	LOCATION
206	01	-42	2.6	.4	298	282	38	0	Farmland	
									Wapsipinicon R.	Iowa
207	01	-38	2.6	.5	288	308	18	-2		
208	01	-37	2.6	.6	315	319	14	0		
209	01	-39	2.2	.4	329	311	22	0		
210	01	-45	3.2	.4	335	326	36	0		
211	02	-39			318	333	28	0		
212	02	-40			335	282	69	0	Hills	
213	02	-43			355	284	72	1		
214	02	-48			353	276	78	0		
215	02	-50			352	244	61	47		
216	02	-33			243	256	73	0	Mississippi River	
217	02	-23			197	279	50	-32		
224	02	-42			281	320	46	0	Hills	Wisconsin
225	02	-46			324	325	53	0		
226	02	-47			361	298	69	0		
227	02	-38			334	279	50	5		
228	02	-40			250	275	46	0	Wisconsin River Valley	
229	02	-25			225	294	65	-4		
230	02	-36			224	294	65	-5		
231	02	-42			206	275	46	-23		
235	02	-30			283	316	80	0	Parks & Lake Wisconsin	
236	10	-29			246	278	42	0		
237	10	-21			251	270	26	0	Wisconsin River & Swamp	
238	10	-26			254	267	23	0	Small Lakes & Swamp	
239	10	-31			257	282	38	0		
240	10	-38			259	290	31	0		

TABLE A-3 (continued)

DATA BLOCK	SM S^2M	AGC (dBm)	RISE TIME (#Gates)	AUTO CORR.	h_m* (m)	h_{mid} (m)	$\Delta h/2$ (m)	MIN RES (m)	TYPE OF TERRAIN	LOCATION
241	10	-43			291	290	31	0		Wisconsin
242	10	-38			303	294	20	0	Small Lake	
243	10	-31			292	286	27	0		
244	10	-40			294	290	31	0		
245	10	-52			302	302	12	0	Swamp	
246	10	-42			315	286	19	10		
247	10	-43			302	275	16	11		
248	10	-39			281	252	8	21		
249	10	-31			267	230	16	21	Lake Winnebago	
250	10	-32			237	229	.5	18		
251	10	-35			235	267	39	0		
252	10	-38			246	274	46	0		
253	10	-40			286	290	31	0		
254	10	-44			294	275	16	4	Swamp	
255	10	-41			259	252	8	0	Manitowoc R.	
256	11	-39	2.3	.5	255	259	15	0		
257	11	-38	1.9	.5	257	233	20	5		
258	11	-38	2.5	.5	252	253	20	0		
259	11	-39	2.5	.5	226	221	23	0	Manitowoc R. (Swamp)	
260	11	-38	2.6	.7	202	188	11	4		
261	11	-32	4.6(26%)	.3	190	188	11	0	Lake Michigan	
262	11	-24	2.9	.2	171	177	0	-6		
263	11	-22	4.(22%)	.1	179	177	0	2		
264	11	-18	2.8	.25	181	177	0	4		
265	11	-20	6.(27%)	.5	179	177	0	2		
266	11	-17	3.2	.2	180	177	0	3		
267	11	-19	3.2	.4	183	177	0	6		
268	11	-28	3.7	.2	180	177	0	3		
269	11	-30	2.9	0	181	177	0	4		

TABLE A-3 (continued)

DATA BLOCK	SM S^2M	AGC (dBm)	RISE TIME (#Gates)	AUTO CORR.	h_m* (m)	h_{mid} (m)	$\Delta h/2$ (m)	MIN RES (m)	TYPE OF TERRAIN	LOCATION
270	11	-31	3.2	0	182	177	0	5	Lake Michigan	Wisconsin
271	11	-31	3.5	0	180	177	0	3		Michigan
272	11	-32	2.8	.1	181	177	0	4		
273	11	-33	3.6	.1	181	177	0	4		
274	11	-34	3.9	.2	180	177	0	3		
275	11	-34	2.9	0	181	177	0	4		
276	12	-35			181	203	26	0		
277	12	-34			180	226	49	0	Platte Bay	
278	12	-35			186	226	49	0		
279	12	-35			185	234	57	0		
280	12	-38			188	237	54	0		
281	12	-44			193	259	46	-20	Fife Lake State Forest	
282	12	-44			252	243	63	0		
283	12	-43			275	227	47	1	Lakes	
284	12	-37			186	211	34	0		
285	12	-36			186	211	34	0		
286	12	-34			188	211	34	0		
287	12	-35			184	218	41	0		
288	12	-36			185	218	41	0		
289	12	-36			186	246	60	-1	Pigeon River State Forest	
290	12	-38			186	252	69	0		
291	12	-42			200	275	77	0		
295	12	-41			256	263	34	0		
296	12	-44			221	298	54	-8		
297	12	-42			287	267	38	0	Hardwood State Forest	
298	12	-37			260	267	38	0	Swamp	
299	20	-45			244	267	38	0		

TABLE A-3 (continued)

DATA BLOCK	SM S^2M	AGC (dBm)	RISE TIME (#Gates)	AUTO CORR.	h_m* (m)	h_{mid} (m)	$\Delta h/2$ (m)	MIN RES (m)	TYPE OF TERRAIN	LOCATION
300	20	-44			248	229	16	4	Black Lake State Forest	Michigan
301	20	-43			237	221	23	0		
302	20	-45			240	211	34	0		
303	20	-43			216	203	26	0		
304	20	-39			210	195	18	0	Lake Huron	
305	20	-36			201	177	0	24		
306	20	-36			169	177	0	-8		
307	20	-36			171	177	0	-6		
308	20	-36			171	177	0	-6		
309	20	-36			171	177	0	-6		
310	20	-36			168	177	0	-9		
311	20	-37			168	177	0	-9		
312	20	-37			171	177	0	-6		Canada
313	20	-37			173	177	0	-4		
314	20	-37			168	177	0	-9		
315	20	-37			171	195	18	-4		
316	21	-39			175	207	30	-2	Islands	
317	21	-38			172	188	11	-5		
318	21	-38			176	180	3	-1		
319	21	-37			180	237	60	0		
320	21	-37			173	237	60	-4		

Table A-4

Catalogue of Terrain Radar Signatures, SL-3, Pass 18, 9 September 1973

DATA BLOCK	S^2_M	AGC (dbm)	RISE TIME (#Gates)	AUTO CORR.	h^*_m (m)	h_{mid} (m)	$\Delta h/2$ (m)	MIN RES (m)	TYPE OF TERRAIN	LOCATION
380	00	-36			736	736	4	0	Dry Ranchland	Texas
381	00	-34			742	740	8	0		
382	00	-35			749	726	25	0	Ranchland w/brushwood	
383	00	-35			734	726	25	0		
384	00	-37			716	717	16	0		
385	00	-36			706	717	16	0		
386	00	-37			710	717	16	0		
387	00	-35			704	717	16	0		
388	00	-36			710	702	31	0		
389	00	-37			726	686	41	0		
390	01	-39	4.5(52%)	.2	730	664	69	0		
391	01	-35	4.2(24%)	.3	623	610	31	0		
392	01	-33	4.3	.2	588	564	15	9		
393	01	-34	3.2(23%)	.1	564	549	31	0		
394	01	-32	5.0(22%)	.2	539	536	16	0		
395	01	-32	3.0	.2	526	503	15	8		
396	01	-32	3.2	.3	523	503	15	5		
397	01	-33	5.4(22%)	.5	508	490	5	13		
398	01	-32	2.2	.8	493	488	31	0		
399	01	-31	1.9	.7	476	534	46	0		

* Referenced to Data Block 380 (-19 m)

Table A-4 (continued)

DATA BLOCK	S^2_M	AGC (dbm)	RISE TIME (#Gates)	AUTO CORR.	h^*_m (m)	h_{mid} (m)	$\Delta h/2$ (m)	MIN RES (m)	TYPE OF TERRAIN	LOCATION
400	01	-37	4.8(26%)	.1	538	549	31	0	Ranchland w/brushwood	Texas
401	01	-36	4.4(21%)	.3	573	590	42	0		
402	01	-37	4.6	.3	594	574	56	0		
403	01	-37	3.1	.3	584	564	46	0	Small City	
404	01	-37	3.2	.3	557	534	16	8		
405	02	-35			528	519	31	0		
406	02	-37			508	503	15	0		
407	02	-37			515	503	15	0		
408	02	-35			491	503	15	0		
409	02	-35			513	507	19	0		
410	02	-36			526	507	19	0		
411	02	-37			546	499	19	28		
412	02	-39			511	499	19	0		
413	02	-33			500	476	19	5		
414	02	-36			491	473	16	3		
415	02	-36			463	458	32	0		
416	02	-34			454	442	15	0		
417	02	-34			466	442	15	9	Small City	
418	02	-34			453	427	32	0		
419	02	-34			444	396	61	0		
420	10	-46			430	366	61	3		
421	10	-43			409	351	46	13		
422	10	-37			354	336	31	0		
423	10	-40			375	305	61	9	Mountains	
424	10	-40			353	309	65	0		

Table A-4 (continued)

DATA BLOCK	S^2_M	AGC (dbm)	RISE TIME (#Gates)	AUTO CORR.	h^*_m (m)	h_{mid} (m)	$\Delta h/2$ (m)	MIN RES (m)	TYPE OF TERRAIN	LOCATION
425	10	-45			355	309	65	0	Ranchland w/brushwood	Texas
426	10	-38			297	305	31	0		
427	10	-38			302	320	15	-3		
428	10	-38			335	320	15	0		
429	10	-39			364	347	42	0		
430	10	-37			361	332	58	0		
431	10	-36			319	305	31	0		
432	10	-35			304	275	31	0		
433	10	-37			289	252	23	15		
434	10	-37			243	252	23	0		
435	10	-34			249	290	46	0		
436	10	-37			292	290	46	0	Dry Ranchland	
437	10	-41			313	275	31	8		
438	10	-37			273	275	31	0		
439	10	-41			297	267	38	0		
440	11	-35	2.0	.8	258	267	38	0		
441	11	-36	3.3	.5	282	279	35	0		
442	11	-39	2.4	.5	288	252	23	14		
443	11	-36	1.9	.3	270	252	23	0	City of Gainesville	
444	11	-34	3.5	.3	245	252	23	0		
445	11	-38	2.7	.3	264	252	23	0	Ranchland w/brushwood & oil wells	
446	11	-37	3.0	.4	265	252	23	0		
447	11	-38	2.1	.4	260	244	31	0		
448	11	-36	2.3	.6	249	209	21	20	Lake Texoma	
449	11	-31	2.8	.2	216	209	21	0		
450	11	-28	4.3	.3	193	209	21	0		Oklahoma

Table A-4 (continued)

DATA BLOCK	S^2_M	AGC (dbm)	RISE TIME (#Gates)	AUTO CORR.	h^*_m (m)	h_{mid} (m)	$\Delta h/2$ (m)	MIN RES (m)	TYPE OF TERRAIN	LOCATION
451	11	-29	4.1(51%)	.3	181	216	28	-7	Ranchland w/brushwood	Oklahoma
452	11	-33	2.3	.6	229	216	28	0	& oil wells (Lake Texoma)	
453	11	-20	2.4	.3	214	209	21	0		
454	11	-17	2.1	.4	196	224	36	0		
459	11	-36	1.3	.8	186	175	23	0	Brushwood	
460	11	-35	2.0	.4	189	189	9	0	Small City	
461	11	-38	2.6	.4	202	189	9	4		
462	11	-35	2.8	.6	183	227	47	-3		
463	12	-37			183	244	46	-15		
464	12	-34			187	259	46	-26	Mountains	
465	12	-44			285	290	46	0		
>time skip										
466	12	-46			260	290	77	0		
467	12	-39			240	214	32	0	Valley	
468	12	-35			205	198	15	0		
469	12	-36			205	259	76	0	Small City	
470	12	-39			216	320	137	0	Mountains	
472	12	-42			303	305	153	0	Mountains	Arkansas
473	12	-38			204	305	153	0		
474	12	-37			185	153	31	2	Valley	
475	12	-38			177	168	46	0		
476	12	-37			172	183	31	0	Small City	
477	12	-32			164	168	16	0		
478	20	-42			143	168	16	-9	Arkansas River	

Table A-4 (continued)

DATA BLOCK	S^2_M	AGC (dbm)	RISE TIME (#Gates)	AUTO CORR.	h^*_m (m)	h_{mid} (m)	$\Delta h/2$ (m)	MIN RES (m)	TYPE OF TERRAIN	LOCATION
479	20	-43			186	168	16	3	Valley Arkansas River	Arkansas
480	20	-45			204	183	31	0		
481	20	-49			257	198	46	13		
485	20	-51			488	397	92	0	Ozark Mts. National Forest	
487	20	-50			553	473	138	0		
488	20	-50			619	488	122	9		
497	20	-48			405	358	53	0	Mountains	
501	20	-34			212	267	69	0	Bull Shoals Lake	Missouri
502	20	-46			206	274	61	-7	Mark Twain Natl. Forest	
503	20	-50			295	305	31	0		
504	20	-50			336	305	31	1		
505	20	-51			335	309	35	0		
506	20	-50			331	301	42	0		
507	21	-47			299	328	69	0		
508	21	-48			345	335	61	0		
512	21	-49			343	325	51	0		
513	21	-49			364	340	35	0		
514	21	-47			353	381	46	0		
515	21	-44			366	412	46	0		
516	21	-43			397	420	54	0		

Table A-4 (continued)

DATA BLOCK	S^2_M	AGC (dbm)	RISE TIME (#Gates)	AUTO CORR.	h^*_m (m)	h_{mid} (m)	$\Delta h/2$ (m)	MIN RES (m)	TYPE OF TERRAIN	LOCATION
517	21	-47			395	412	46	0	Ozark Mts. & Clark Natl. Forest	Missouri
518	21	-48			378	412	46	0		
519	21	-48			391	412	16	-5		
520	21	-48			407	366	61	0		
521	21	-51			405	335	61	9		
522	21	-52			388	320	46	22		
523	21	-49			285	320	76	0		
524	21	-47			270	339	65	-4		
525	21	-46			343	355	50	0		
526	21	-45			392	355	50	0		
527	21	-48			392	366	31	0		
528	21	-47			379	336	31	13		
529	21	-44			363	336	31	0		
530	22	-46			311	351	50	0		
531	22	-43			358	336	31	0		
532	22	-45			328	320	46	0		
533	22	-45			292	320	46	0		
534	22	-48			339	336	31	0		
535	22	-49			384	320	46	18		
536	22	-45			307	290	46	0	Vegetation	
537	22	-45			293	290	46	0		
538	22	-44			262	259	15	0		
539	22	-45			240	229	16	0		
540	22	-45			233	198	46	0		
541	22	-47			216	183	31	3		

Table A-4 (continued)

DATA BLOCK	S_M^2	AGC (dbm)	RISE TIME (#Gates)	AUTO CORR.	h_m^* (m)	h_{mid} (m)	$\Delta h/2$ (m)	MIN RES (m)	TYPE OF TERRAIN	LOCATION
542	22	- 46			172	147	37	0	Vegetation ↓ Mississippi River ↓	Missouri Illinois ↓
543	22	- 35			119	147	37	0		
544	22	- 39			130	168	46	0		
546	22	-43			207	183	31	0		
547	22	-40			180	153	16	12		
548	22	-36			154	153	16	0	Small Cities ↓	
549	22	-39			145	160	38	0		
550	22	-41			166	153	16	0		

Table A-5

Catalogue of Terrain Radar Signatures, SL-3, Pass 28, 13 September 1973

DATA BLOCK	S^2_M	AGC (dbm)	RISE TIME (#Gates)	AUTO CORR.	h^*_m (m)	h_{mid} (m)	$h_{(m)/2}$	MIN RES (m)	TYPE OF TERRAIN	LOCATION
191	00	-44			1934	2561	427	-200	Mts. and Forest	Nevada
197	00	-47			1843	1906	77	0	Mts. and Valley	
199	00	-51			2177	1982	153	43	Valley	
201	00	-46			1844	2302	503	0	Mts. and Valley	
202	00	-51			1832	1967	168	0	Valley	
203	00	-41			1800	2119	320	0	Mts. and Valley	
204	00	-32			1778	2028	229	-21	↓	
205	00	-42			1732	2168	278	-158	Mts. and Ridges	
208	00	-52			2000	2012	122	0	Valley	
210	00	-47			1896	2216	295	-25	Mts. and Valley	
211	00	-50			1906	2119	198	-15	↓	
213	01	-47	3.4(55%)	.1	1991	2119	198	0	Dry Valley	
214	01	-36	2.0	.5	1916	2378	427	-35	Valley and Mts.	
215	01	-44	6.6(32%)	.2	1884	2348	458	-6	Mts.	
216	01	-53	2.2(70%)	0	1864	1997	198	0	Valley and Mts.	

* Referenced to Salt Lake Desert (-28 m)

Table A-5 (continued)

DATA BLOCK	S^2_M	AGC (dbm)	RISE TIME (#Gates)	AUTO CORR.	h^*_m (m)	h_{mid} (m)	$\Delta h'^2$ (m)	MIN RES (m)	TYPE OF TERRAIN	LOCATION
218	01	-40	6.1(30%)	.1	1850	2180	381	0	Valley	Nevada
219	01	-45	6.2(37%)	.4	1720	2211	351	-140	Valley and Mts.	
223	01	-38	5.1	.4	1715	2348	580	-53	Mts. and Valley	
224	01	-46	3.8(32%)	.3	1669	1982	519	0		
228	01	-26	2.0	.5	1327	1288	8	31	Salt Flats	Utah
229	01	-20	1.7	.5	1282	1288	8	0		
230	01	-25	2.9	.1	1280	1288	8	0		
231	01	-27	1.9	.5	1282	1288	8	0		
232	01	-12	1.7	.5	1288	1288	8	0	Salt Lake Desert	
233	02	-10			1288	1288	8	0		
234	02	-10			1288	1288	8	0		
235	02	-10			1287	1288	8	0		
236	02	-10			1286	1288	8	0		
237	02	-17			1284	1288	8	0		
238	02	-13			1287	1288	8	0		
239	02	-10			1287	1288	8	0		
240	02	-14			1286	1288	8	0		
241	02	-20			1284	1346	56	-6	Hills	
242	02	-18			1286	1468	178	-4		
243	02	-22			1283	1432	153	0		Great Salt Lake
244	02	-32			1260	1341	62	-19		
245	02	-36			1264	1279	0	-15		
246	02	-32			1271	1279	0	-8		

Table A-5 (continued)

DATA BLOCK	S^2_M	AGC (dbm)	RISE TIME (#Gates)	AUTO CORR.	h^*_m (m)	h_{mid} (m)	$\Delta h/2$ (m)	MIN RES (m)	TYPE OF TERRAIN	LOCATION
247	02	-30			1267	1707	428	-12	Mts.	Utah
248	10	-29			1270	1707	427	-10		
249	10	-30			1238	1555	275	-42	Mud Flats	
250	10	-48			1083	1280	1	-196		
252	10	-31			1282	1280	4	0	Swamp, dry valley	
266	10	-25			1789	2012	122	-101	Plateau and Ridge	Idaho
267	10	-42			1726	2088	198	-164		
276	10	-45			2373	2623	305	0	Forest and Mts.	Wyoming
277	10	-49			2230	2348	153	0	Ridges	
280	10	-44			2165	2104	31	31	Dry Basin	
281	10	-43			2096	2104	31	0		
282	10	-33			2064	2211	77	-70		
283	10	-34			2067	2211	77	-67		
284	10	-33			2080	2134	0	-54		
285	10	-40			2086	2165	31	-48		
286	10	-43			2100	2256	122	-34		
287	11	-43	4.7(43%)	.1	2129	2470	275	-66	Mts.	
291	11	-36	3.3	.4	3030	3320	454	0	Mts.	